8-20-2013 12:00 AM

Topological properties of modular networks, with a focus on networks of functional connections in the human brain

Estefania Ruiz Vargas
The University of Western Ontario

Supervisor
Lindi M. Wahl
The University of Western Ontario

Graduate Program in Applied Mathematics
A thesis submitted in partial fulfillment of the requirements for the degree in Doctor of Philosophy
© Estefania Ruiz Vargas 2013

Topological properties of modular networks, with a focus on networks of functional connections in the human brain.

(Thesis format: Integrated Article)

by

Estefanía Ruiz Vargas

Graduate Program in Applied Mathematics

A thesis submitted in partial fulfillment
of the requirements for the degree of
Doctor of Philosophy

School of Graduate and Postdoctoral Studies
The University of Western Ontario
London, Ontario, Canada

Abstract

Complex network theory offers useful approaches to analyze the structural and functional properties of real life networks. In this work, we explore some of the mathematical concepts of network theory and study real life systems from a complex network perspective. We pay particular attention to networks of connections within the human brain.

We analyze weighted networks calculated from full functional magnetic resonance imaging (fMRI) data acquired during task performance. The first novelty of this study is the fact that we retain all of the connections between all of the voxels in the full brain fMRI data. We then evaluate the extent to which this rich dataset can be described by existing models of scale-free or exponentially truncated scale-free topology, comparing results across a large number of more complex topological models as well. Our results suggest that the novel model presented in this dissertation offers a significantly better fit at the voxel level.

Structural characterization of the brain can also give insights into the effects of traumatic injuries. For our second study, we used brain networks to explore the topological consequences of brain damage in computational models. By simulating the effects of several traumatic brain injury (TBI) models we find a variety of disruptions in the modular structure and connectivity of the post-injury networks. In particular, we focused on the effects of focalized injuries, axonal degeneration and

diffuse microlesions. Our results suggest that mathematical models can predict, to some extent, the structural and functional effects of TBIs based on the analysis of specific topological measures. Furthermore, these results may be correlated to known cognitive sequelae of TBI.

In order to complement the set of topological properties studied, we review the concept of participation of a node in a modular network. The participation coefficient is often used to provide a ranking of the "importance" of a node; however, we propose a new measure, called the gateway coefficient, to assess the involvement of a node. Our results suggest that the gateway coefficient has a superior ranking power than the participation coefficient since it takes into account a variety of modular properties of the network. These results are illustrated with examples of simulations and real life datasets, such as the air transportation network and the human brain network.

Keywords: Networks; fMRI; Topology; Degree-distribution; Scale-Free; Traumatic Brain Injury; Participation Coefficient; Gateway Coefficient.

Co-Authorship

This thesis was completed under the supervision of Dr. Lindi Wahl. The article versions of Chapters 3, 4 and 5 are co-authored with Lindi Wahl.

All the fMRI data used for the analysis of brain networks in Chapters 3, 4 and 5 were provided by Steven G. Greening, who is a co-author on the article version of Chapters 3 and 4. Data were collected as approved by the University of Western Ontario Human Research Ethics Board.

Suggestions for the study design, interpretation of the data and the editing of the manuscript of Chapter 4 were carried out by Dr. Lindi Wahl and Dr. Derek Mitchell. Derek Mitchell is a co-author on the article version of Chapters 3 and 4.

The candidate performed the data analysis for all chapters, wrote the drafts of the manuscripts and revised the final manuscripts.

Acknowledgements

First and foremost, I would like to thank my supervisor, Lindi Wahl, for her advice, encouragement and support throughout these years. I would also like to thank Derek Mitchell for many helpful discussions. Thanks to all my professors and the wonderful staff at the Deparment of Applied Mathematics.

Thanks to my friends, their laughs, company and support helped me enormously. Each one of you is extremely special to me. A special thanks goes to my boyfriend, Abe, for being my best friend and my rock. Thank you for your patience and encouragement during good and bad times, it truly meant the world to me.

I am deeply grateful to my parents for their unconditional love, their kindness and support made all of this possible. I also need to thank my sister for her support and invaluable advices. Muchas gracias por todo, los quiero mucho.

Thank you

To my parents.

Table of Contents

List of Tables

List of Figures

Acronyms

ADHD	*Attention Deficit-Hyperactivity Disorder*
AIC	*Akaike Information Criterion*
BOLD	*Blood Oxygen Level Dependent*
BTS	*Bureau of Transportation Statistics*
DMN	*Default Mode Network*
DW-MRI	*Diffusion-weighted Magnetic Resonance Imaging*
EEG	*Electroencephalography*
fMR	*Functional Magnetic Resonance Imaging*
ICA	*Independent Component Analysis*
LCG	*Left Cingulate Gyrus*
LI	*Left Insula*
LIFG	*Left Inferior Frontal Gyrus*
LMeFG	*Left Medial Frontal Gyrus*
LMFG	*Left Middle Frontal Gyrus*
LP	*Left Precuneus*
LPaG	*Left Parahippocampal Gyrus*
LPG	*Left Precentral Gyrus*
LSFG	*Left Superior Frontal Gyrus*
MEG	*Magnetoencephalography*
MNI	*Montreal Neurological Institute*
PET	*Positron Emission Tomography*
RCG	*Right Cingulate Gyrus*
RI	*Right Insula*
RIFG	*Right Inferior Frontal Gyrus*
RMeFG	*Right Medial Frontal Gyrus*
RMFG	*Right Middle Frontal Gyrus*

ROI	*Regions Of Interest*
RP	*Right Precuneus*
RPG	*Right Precentral Gyrus*
RSFG	*Right Superior Frontal Gyrus*
RSTG	*Right Superior Temporal Gyrus*
rsfMRI	*Resting-state Functional Magnetic Resonance Imaging*
TBI	*Traumatic Brain Injury*
WGCNA	*Weighted Gene Coexpression Network Analysis*
WVCNA	*Weighted Voxel Coactivation Network Analysis*

Table of Symbols

a_{ij}	*Entries of the adjacency matrix*
β	*Soft-threshold power*
C	*Clustering coefficient*
$c(i)$	*Betweenness centrality of node i*
c_{iS}	*Sum of the centralities of the nodes in V_{iS}*
c_n	*Sum of the centralities of the nodes in module n*
$\overline{c_{iS}}$	*$c_{iS}/max(c_n)$*
d_{ij}	*Euclidean distance between node i and node j*
G_i	*Gateway coefficient of node i*
g_{iS}	*Gateway coefficient weights*
k_i	*Degree of node i*
k_{nn}^w	*Degree-dependent average nearest-neighbours degree for weighted networks*
k_{iS_i}	*Degree of node i within the module S_i*
k_{iS}	*Number of connections between node i and nodes in module S*
$\overline{k_{iS}}$	*Fraction of the overall connections between node i's module and module S that belong to node i*
$\overline{k}_{S_i}$	*Average of k over all the nodes in S_i*
L	*Average path length*
$P(k)$	*Probability mass function for node degree*
P_i	*Participation coefficient of node i*
Q	*Modularity*

r_{ij}	*Pearson correlation coefficient*
s_i	*Strength of node i*
s_{ij}	*Entries of the similarity matrix*
$\sigma_{k_{S_i}}$	*Standard deviation of node degree in module S_i*
σ_{jk}	*Number of shortest paths from node j to node k*
$\sigma_{jk}(i)$	*Number of shortest paths from node j to node k that pass through node i*
T	*Number of time points in the time series*
V_{iS}	*Set of neighbours of node i within module S*
w_{ij}	*Weight of the connection between nodes i and j*
W_{ij}	*Topological overlap between nodes i and j*
$x_i(t)$	*Time series of node i*
$\overline{x_i}$	*Average time series of node i*
z_i	*Within-module degree*

Chapter 1

Introduction

1.1   Background

Many communication and life sciences systems can be effectively modelled by networks [Erdös and Rényi, 1959]. Examples of such systems include metabolic networks [Sales-Pardo et al., 2007], transportation systems [Guimerà et al., 2005, Sales-Pardo et al., 2007], the spread of disease [Eubank et al., 2004], social networks [Newman, 2001] and brain functional networks [Barabási and Albert, 1999]. A network consists of elements called nodes that are connected by edges. The degree of the node is the number of edges connected to it. The elements of many real life systems tend to cluster together and form modules [Pastor-Satorras and Vespignani, 2001, Ravasz et al., 2002, Zhou et al., 2006]. This modular structure can be used to further classify the nodes into specific topological roles according to their intra- and inter-modular connectivity [Guimerà and Amaral, 2005]. Another characteristic that has attracted much interest is the degree distribution of complex networks; it has been shown that it can provide insight into the error tolerance and attack vulnerability of the system begin modelled [Barabási et al., 2000].

There are important computational limitations when constructing and analyzing real life networks. In the particular case of brain network studies, the large functional magnetic resonance imaging (fMRI) data sets obtained are computationally expensive to analyze. Special methods are required to overcome such limitations [Vincent et al., 2006, Achard et al., 2006, He et al., 2007, Iturria-Medina et al.,

2008, Castellanos et al., 2011, Slobounov et al., 2011] often resulting in an under-characterization of the system.

Network theory methodologies can also serve as an aid in clinical diagnosis. An average of 1.4 million traumatic brain injuries (TBI) are estimated to occur each year in the United States [Langlois and Rutland-Brown, 2006], making TBI a major health concern. Studies have shown that abnormal topological properties can be efficient markers of certain brain disorders and TBI sequelae [Honey and Sporns, 2008, Stam et al., 2009, Cho and Choi, 2010, Bullmore and Sporns, 2012]. Further research in this area can be of great benefit.

1.2 Research Objectives

The purpose of this research consists of three main objectives that are presented in detail below:

1. To apply network theory methodologies to fMRI data sets:
   - Analyze complete fMRI data sets without possible biases introduced by the use of seed voxels and the restriction to specific areas of the brain.
   - Build functional connectivity networks retaining all of the connections between all of the voxels in full brain fMRI data, and evaluate the extent to which this dataset can be described by existing topological models.
   - Explore the differences between soft and hard thresholding analyses.

2. To investigate clinical implications:
   - Develop accurate mathematical models of traumatic brain injuries.
   - Provide information regarding potential effects of traumatic brain injuries on the network structure of the brain.

3. To present novel quantities to asses topological properties:
   - Explore, and if needed improve, topological measures used to build cartographic representations of real life networks.
   - Assess the accuracy of these measures in real life complex systems.

1.3   Thesis Outline

This thesis has been written in an integrated-article format, following the guidelines of the Faculty of Graduate and Postdoctoral Studies at Western University.

Chapter 2 introduces general network concepts and their topological properties. It also contains a description of different neuroimaging techniques to better understand the data used in the subsequent chapters. Furthermore, this chapter reviews the relevant literature on network theory and its applications to fMRI data analyses, discussing in detail the role of modularity. Finally, it provides an outline of the potential clinical implications of brain network research.

Chapter 3 presents an analysis of weighted networks calculated from functional magnetic resonance imaging (fMRI) data acquired during task performance. In this chapter, a very rich fMRI data set is used to expand previous work in brain network theory. The degree distribution predicted by existing models is evaluated and a novel "log quadratic" model is presented. It is shown that this model offers a significantly better fit to networks of functional connections in the human brain.

In Chapter 4 functional modular networks were generated for a sample of control subjects. Mathematical models of traumatic brain injuries were further explored to examine in detail the effects of TBI at the network level, in particular, effects on the network's modular structure. The effects on the network of three potential TBI models were examined: a) whole brain diffuse axonal degeneration; b) destruction of specific cortical sites at the point of impact; c) diffuse microlesions.

Chapter 5 focuses on the concept of participation in the network. A generalization of the participation coefficient, that depends not only on the node's particular properties but also on the network's modular structure, is proposed. The cartographic implications of this new definition are analyzed in the U.S. air transportation network

and in the human brain.

Chapter 6 summarizes the research findings, discusses the overall implications of the studies presented and suggests directions for future work in the area.

Bibliography

Achard, S., Salvador, R., Whitcher, B., Suckling, J., and Bullmore, E. (2006). A resilient, low-frequency, small-world human brain functional network with highly connected association cortical hubs. *J Neurosci*, 26(1):63–72.

Barabási, A.-L. and Albert, R. (1999). Emergence of scaling in random networks. *Science*, 286(5439):509–512.

Barabási, A.-L., Jeong, H., and Albert, R. (2000). Error and attack tolerance of complex networks. *Nature*, 406(6794):378–382.

Bullmore, E. and Sporns, O. (2012). The economy of brain network organization. *Nat Rev Neurosci*, 13(5):336–349.

Castellanos, N., Leyva, I., Buldú, J., Bajo, R., Paul, N., Cuesta, P., Ordóñez, V., Pascua, C., Boccaletti, S., Maestú, F., and del Pozo, F. (2011). Principles of recovery from traumatic brain injury: Reorganization of functional networks. *NeuroImage*, 55(3):1189–1199.

Cho, M. W. and Choi, M. Y. (2010). Brain networks: Graph theoretical analysis and development models. *Int J Imaging Syst Technol*, 20(2):108–116.

Erdös, P. and Rényi, A. (1959). On random graphs i. *Publ Math Debrecen*, 6:290.

Eubank, S., Guclu, H., Kumar, V. A., Marathe, M. V., Srinivasan, A., Toroczkai, Z., and Wang, N. (2004). Modelling disease outbreaks in realistic urban social networks. *Nature*, 429(6988):180–184.

Guimerà, R. and Amaral, L. (2005). Functional cartography of complex metabolic networks. *Nature*, 433:895–900.

Guimerà, R., Mossa, S., Turtschi, A., and Amaral, L. (2005). The worldwide air transportation network: Anomalous centrality, community structure, and cities' global roles. *Proc Natl Acad Sci U S A*, 102(22):7794.

He, Y., Chen, Z. J., and Evans, A. C. (2007). Small-world anatomical networks in the human brain revealed by cortical thickness from MRI. *Cereb Cortex*, 17(10):2407–2419.

Honey, C. J. and Sporns, O. (2008). Dynamical consequences of lesions in cortical networks. *Hum Brain Mapp*, 29(7):802–809.

Iturria-Medina, Y., Sotero, R. C., Canales-Rodríguez, E. J., Alemán-Gómez, Y., and Melie-García, L. (2008). Studying the human brain anatomical network via diffusion-weighted MRI and graph theory. *NeuroImage*, 40(3):1064–1076.

Langlois, J. and Rutland-Brown, W.and Wald, M. (2006). The epidemiology and impact of traumatic brain injury: A brief overview. *J Head Trauma Rehab*, 21(5):375–378.

Newman, M. E. J. (2001). Scientific collaboration networks. ii. shortest paths, weighted networks, and centrality. *Phys Rev E*, 64:016132+.

Pastor-Satorras, R. and Vespignani, A. (2001). Epidemic spreading in scale-free networks. *Phys Rev Lett*, 86(14):3200–3203.

Ravasz, E., Somera, A., Mongru, D., Oltvai, Z., and Barabási, A. (2002). Hierarchical organization of modularity in metabolic networks. *Science*, 297(5586):1551.

Sales-Pardo, M., Guimerà, R., Moreira, A., and Amaral, L. (2007). Extracting the hierarchical organization of complex systems. *Proc Natl Acad Sci U S A*, 104:15224–15229.

Slobounov, S., Gay, M., Zhang, K., J., B., Pennell, D., Sebastianelli, W., Horovitz, S. G., and Hallett, M. (2011). Alteration of brain functional network at rest and in response to YMCA physical stress test in concussed athletes: RsfMRI study. *NeuroImage*, 55(4):1716–1727.

Stam, C., de Haan, W., Daffertshofer, A., Jones, B., Manshanden, I., van Cappellen van Walsum, A., Montez, T., Verbunt, J., de Munck, J., van Dijk, B., Berendse, H., and Scheltens, P. (2009). Graph theoretical analysis of magnetoencephalographic functional connectivity in alzheimer's disease. *Brain*, 132(Pt 1):213–24.

Vincent, J., Snyder, A., Fox, M., Shannon, B., Andrews, J., Raichle, M., and Buckner, R. (2006). Coherent spontaneous activity identifies a hippocampal-parietal memory network. *J Neurophysiol*, 96(6):3517–3531.

Zhou, C., Zemanová, L., Zamora, G., Hilgetag, C. C., and Kurths, J. (2006). Hierarchical organization unveiled by functional connectivity in complex brain networks. *Phys Rev Lett*, 97:238103.

Chapter 2

Literature Review

2.1   Introduction to networks and basic notation

Networks consist of a set of nodes (also called vertices), and a set of edges (also called connections or links), which connect the nodes. Networks can be represented graphically as a set of dots representing the nodes, and dot-connecting lines representing edges between the nodes.

Nodes connected by edges are called neighbours. A network is connected if there is a path from any node to any other node in the graph, otherwise it is disconnected. If the edges have an associated direction the graph is called directed, otherwise it is an undirected graph. Direction is represented graphically by an arrow (Figure 2.1). Air transportation is an example of a directed graph in which nodes represent airports, and a flight from airport i to airport j is represented by a directed edge from node i towards node j.
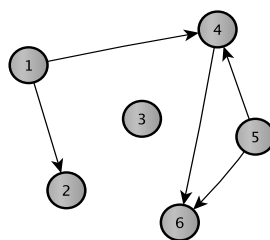
Figure 2.1: Example of a directed network. Dots numbered $1 - 5$ represent the nodes, and the lines represent the connections between them.

Nodes	1	2	3	4	5	6
1	0	1	0	1	0	0
2	0	0	0	0	0	0
3	0	0	0	0	0	0
4	0	0	0	0	0	1
5	0	0	0	1	0	1
6	0	0	0	0	0	0

Table 2.1: Adjacency matrix of the directed unweighted graph given in Figure 2.1

A weight w_{ij} can also be assigned to each edge; the weights may represent, for instance, the strength of the connection between two nodes or the physical length of the edges. If a graph has weights assigned it is called a weighted graph, otherwise it is unweighted. A road network is an example of weighted graph in which the weight associated to the edges could be the length of the streets.

The complete topology of the network is encapsulated in the adjacency matrix A, where each entry a_{ij} indicates which voxels are connected and the strength of each connection. For an unweighted network, the entry equals one, $a_{ij} = 1$, if there is a connection from node i to node j, and 0 if there is no connection (see Table 2.1 for an example). If the network is weighted then $a_{ij} = w_{ij}$ represents a connection from i to j. For undirected graphs the adjacency matrix will be symmetric.

For an unweighted network the number of edges connected to a node is called its degree k; it is defined in terms of the adjacency matrix as

$$k_i = \sum_{j=1}^{N} a_{ij}$$

where N is the number of nodes in the network. If the network is directed, nodes have an in-degree (incoming edges) $k_i^{in} = \sum_{j=1}^{N} a_{ij}$, and an out-degree (outgoing edges) $k_i^{out} = \sum_{j=1}^{N} a_{ji}$. The degree of a node can be generalized to weighted networks, it is

often called strength and denoted s_i

$$s_i = \sum_j^N w_{ij} \ .$$

The probability that a randomly chosen node will have degree k is given by the degree distribution $P(k)$. This concept can be generalized for weighted networks with a continuous probability density function, $P(s)$.

Clusters are formed if a node's nearest neighbours are also connected to each other [Bullmore and Sporns, 2009]. The tendency to form cliques or clusters is quantified by the clustering coefficient [Watts and Strogatz, 1998], defined as

$$C = \frac{3 \times \text{number of triangles on the graph}}{\text{number of connected triples of vertices}} \ .$$

We note that each complete triangle (three vertices) contributes three connected triples; the factor 3 in the numerator compensates for this and ensures $C = 1$ for fully connected graphs [Newman, 2001].

2.2 Topological properties of networks

Many physical, biological, social, and communication systems can be described as complex networks, in which their elements are represented by nodes and the interactions between them by edges. In the late 1950's, two mathematicians, Paul Erdös and Alfred Rényi suggested that communication and life sciences systems could be modelled by networks with randomly connected nodes [Erdös and Rényi, 1959]. These networks are called random networks or random graphs. The full degree distribution of a random graph was analyzed and derived later by Bollobás [Bollobás, 1980, Bollobás, 2001]. The degree distribution of a random graph is a binomial distribution, which converges to a Poisson distribution for a large number of nodes.

For many years, complex networks were typically modelled using random network theory. That started to change in the late 1990's, when Watts and Strogatz explored a type of network that lies between regular and random networks [Watts and Strogatz, 1998]. These networks are called "small-world", in analogy to the small-world phenomenon observed in 1967 by the psychologist S. Milgram [Milgram, 1967]. Small-world networks are characterized by small path lengths and high clustering coefficients, the former measuring separation between nodes, and the latter, neighbourhoods' cliquishness.

In 1999 Barabási and Albert identified a particular algorithm for generating networks: networks expand continuously by the addition of new vertices that will preferentially attach to well connected vertices [Barabási and Albert, 1999]. This behaviour results in a scale-free power-law distribution for the vertex connectivities. These networks are therefore called "scale-free" networks; their probability distribution follows $P(k) \propto k^{-\gamma}$, where γ is the degree exponent. Scale-free networks have been shown to exhibit both error tolerance and attack vulnerability [Barabási et al., 2000]. An example of a real life system that has been found to exhibit a scale-free topology is the world-wide web; this system can be modelled as a large directed network in which the nodes represent web pages or documents and the edges represent hyperlinks [Albert and Barabási, 1999, Faloutsos et al., 1999, Barabási et al., 2000]. Another example of a system with scale-fee topology is the air transportation system, in which the nodes are areas (towns, cities, etc.) with at least one airport, and edges are nonstop passenger flights [Guimerà et al., 2005]. Metabolic networks also display this type of topology [Jeong et al., 2000]. A variation of the scale-free power law has gained recent attention in the study of brain networks [Achard et al., 2006, Iturria-Medina et al., 2008]. In these "exponentially truncated scale-free" networks the probability $P(k)$ is proportional to $k^{-\gamma} \exp\left(-\alpha k\right)$ for constants α and γ.

Another characteristic of real life systems is their modular structure [Pastor-Satorras and Vespignani, 2001, Ravasz et al., 2002, Zhou et al., 2006], which is defined as the division of network nodes into groups within which the network connections are

dense but between which they are more sparse [Newman, 2004, Newman and Girvan, 2004]. Modules deeply influence the systems' behaviour. For example, each module can perform different tasks resulting in different topological properties, therefore a global characterization is not enough to model the network's structure [Guimerà et al., 2007]. Modular organization can be critical for the network's functionality, making the network especially vulnerable to failure and attacks [Bagrow et al., 2011].

Many algorithms have been suggested for identifying a network's modular structure; the most relevant to this research will be presented in Section 2.4.3. Once the functional modules are found, nodes can be classified according to their intra- and inter-modular connectivity giving rise to a "cartographic representation" of the network [Guimerà and Amaral, 2005]. The within-module degree z_i and the participation coefficient P_i are often used to define the roles of specific nodes [Guimerà and Amaral, 2005] and will be discussed in detail in Section 2.4.4.

The modular structure is thought to be responsible for some of the degree-degree correlations that have recently attracted the interest of researchers [Guimerà et al., 2007]. For some networks, high-degree nodes tend to be connected to other high-degree (low-degree) nodes, this property is known as assortative (disassortative) mixing [Newman, 2002]. Assortative mixing has important implications in real life networks, for example, as pointed out by Miller the reduction of the epidemic threshold is an effect of assortative mixing [Miller, 2009].

2.3   Functional neuroimaging methods

One particular network that has been the subject of much scientific interest is the brain. Non-invasive tools to analyze the human brain's functionality are essential. Functional neuroimaging methods have been widely used to shed light on the neuroanatomy of cognitive functions [Horowitz et al., 1999, Frackowiak et al., 2003].

Methods that detect and measure magnetic or electrical activity of the brain over time include electroencephalography (EEG) and magnetoencephalography (MEG) [Horowitz et al., 1999]. EEG uses electrodes to record the brain's electrical activity along the scalp over a period of time; it is a relatively safe method since there are no strong magnetic fields or radiation. MEG is closely related to EEG, its difference being that MEG measures magnetic fields. EEG and MEG methods have been used in a number of studies (for review, see Stam, 2007). One of the main advantages of electrophysiological techniques is their high temporal resolution, however, they lack spatial resolution [Horowitz et al., 1999, Cho and Choi, 2010]. Another drawback of MEG or EEG is that, compared to functional magnetic resonance imaging data, they perform poorly when detecting activity below the cortical surface [Bullmore and Sporns, 2009].

Methods that measure the metabolic or hemodynamic responses of the brain include positron emission tomography (PET) and functional magnetic resonance imaging (fMRI) [Horowitz et al., 1999, Cho and Choi, 2010]. PET scans are especially helpful for oncologic imaging; their superiority over other methods lies in the fact that PET images biochemical phenomena, providing detailed information at the molecular level. The disadvantages of PET are not only the fact that it uses radiation, but also that it is a very expensive modality [Griffeth, 2005].

fMRI measures hemodynamic responses, i.e. changes in blood oxygen level dependent (BOLD) signals, identifying areas in the brain that show activation in response to certain stimuli. fMRI has been widely used to study the functionality of the human brain (for review, see Horowitz, 1999; Bullmore, 2009). Advantages of fMRI over electrophysiological techniques are good spatial resolution and superior anatomical coverage, however the technique offers poor temporal resolution [Horowitz et al., 1999, Cho and Choi, 2010]. fMRI is capable of detecting localized activity in the brain resulting from stimuli or cognitive functions, making it a suitable method for the study of brain functionality [Smith, 2004].

2.3.1   fMRI data acquisition

The usual setup for an fMRI study consists of a subject lying supine in the scanner; head motion is often limited with forehead straps or foam padding. A consensus on whether keeping the eyes open or closed makes a significant impact on the results has not been reached [Marx et al., 2004, Bianciardi et al., 2009]. Data acquired through fMRI can be either resting-state or task-state data. Resting state, as the name implies, refers to data taken while the subject is at rest. Task-state refers to data taken while the subject is carrying out physical or cognitive activity, causing specialized brain areas relevant to the task in turn to activate in response to stimuli [Smith, 2004, Alonso et al., 2011]. The resultant functional network will depend on the experimental task (or the lack of it).

Resting-state fMRI (rsfMRI) data allows the analysis of brain function in the absence of direct input, focusing only on endogenous neurophysiological processes [Achard et al., 2006]. Spontaneous BOLD signal modulations that occur during the resting state can be used to define a "default network" [Greicius et al., 2003] that has been the subject of many studies [Mason et al., 2007, Damoiseaux et al., 2008, Vanhaudenhuyse et al., 2010]. rsfMRI data sensitivity to neurological abnormalities is considered one of its main advantages [Slobounov et al., 2010]; however, task data has been shown to serve as a better discriminant than rsfMRI data for certain brain disorders [Du et al., 2012]. Task fMRI data are important for understanding the response of the brain to cognitive and emotional stimuli.

An fMRI data set consists of a number of volumes taken every few seconds, or equivalently, a number of voxels along with their associated time series (Figure 2.2). Some research studies are mainly interested in regions composed of many voxels; in this case, a regional mean time series is estimated by averaging the time series over all voxels in each of the regions [Smith, 2004, Achard et al., 2006, Wang et al., 2010c].

In order for the data set to be used for statistical analysis, it first has to undergo
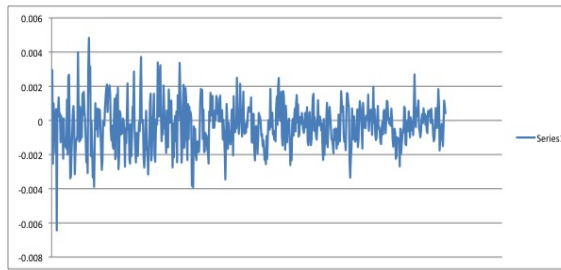
Figure 2.2: Signal intensity versus time for a representative voxel. fMRI data consist of a time series such as the one illustrated here, for each voxel in the recorded volume.

pre-processing. The pre-processing differs from study to study; usually, a series of adjustments are made to correct for noise, slice-timing differences, alignment and head movements [Smith, 2004]. For multi-subject analysis a standard spatial coordinate system across subjects is needed. The usual approach consists in using a template to map each subject's fMRI data to a standard coordinate space such as that proposed by the Montreal Neurological Institute (MNI) or Talairach [Talairach and Tournoux, 1988, Mazziotta et al., 1995]. After pre-processing the data are ready to be compared among subjects or conditions.

2.4 Weighted networks as models of the human brain

The human brain can be described as a complex system of highly interconnected elements. A complex networks approach is an effective tool for the analysis of both the structure and the functionality of the brain. One of the main advantages of such an approach is that it can characterize the system's properties at a global level and at an individual element level [Guimerà and Amaral, 2005, Bullmore and Sporns, 2009]. Another advantage is that network theory methodologies are data-driven, making no biological assumptions. A complex networks approach will therefore help us to uncover the topology of the human brain [Bullmore and Sporns, 2009].

2.4.1   fMRI network analyses

Network analysis of fMRI data is a powerful and widely used technique to analyze the functional interactions in the human brain [Wang et al., 2010a, Bullmore and Sporns, 2012]. In fMRI network analyses nodes represent anatomical components of the brain, usually voxels, and the edges between them represent their correlated functional activity [Wang et al., 2010b]. Edges are determined by introducing functional connectivity metrics that will estimate the degree to which each pair of nodes is related; the most widely used is the Pearson correlation coefficient r_{ij} [Liang et al., 2012]. If we denote the time series of a node as $x_i(t)$ and its average as $\overline{x_i}$, the Pearson correlation coefficient is defined as [Pearson, 1894, Song et al., 2011]

$$r_{ij} = \frac{\sum\limits_{t=1}^{T} [x_i(t) - \overline{x_i}][x_j(t) - \overline{x_j}]}{\sqrt{\sum\limits_{t=1}^{T} [x_i(t) - \overline{x_i}]^2 \sum\limits_{t=1}^{T} [x_j(t) - \overline{x_j}]^2}}$$

where T is the number of time points in the series.

The connectivity pattern of the network will be completely characterized by a connection strength matrix called the adjacency matrix A. The matrix A is computed with the use of an adjacency function $a_{ij} = f(r_{ij})$. Hard and soft thresholding approaches are the most widely used for choosing the adjacency function [Zhang and Horvath, 2005]. For hard-thresholding the adjacency function is defined as

$$a_{ij} = f(r_{ij}) = \begin{cases} 1 & |r_{ij}| \geq \tau \\ 0 & |r_{ij}| < \tau \end{cases}$$

where τ denotes a connectivity threshold. Hard-thresholding approaches are often used in the literature [Eguíluz et al., 2005, Joyce et al., 2010], yielding an unweighted network with values of 1 indicating a connection and values of 0 indicating no connection. Another approach that has been recently used in fMRI studies is the soft-thresholding approach [Mumford et al., 2010, Schwarz and McGonigle, 2011]. For

soft-thresholding the power adjacency function is defined as the absolute value of the correlation between nodes i and j raised to a power β

$$a_{ij} = |r_{ij}|^{\beta}$$

[Zhang and Horvath, 2005], therefore each connection is given a weight (a continuous measure that ranges from 0 to 1) resulting in a weighted network. Brain connectivity is believed to be more accurately represented by a weighted network analysis [Mumford et al., 2010, Schwarz and McGonigle, 2011].

There is an important computational limitation when constructing the network, since the large data sets obtained from fMRI studies are very computationally expensive to analyze. The seed voxel is the most commonly used method to overcome such limitations. Seed voxel analysis is based on the choice of the time series of an initial voxel, called a "seed" voxel. Connectivity is then calculated by computing the correlations between this voxel and all the other voxels in the brain. An iterative process follows, in which significant correlations with the seed voxel will serve as an indicator for choosing new seed voxels [Vincent et al., 2006, Slobounov et al., 2011]. Seed voxel approaches can also be applied to regions of interest (ROIs) by restricting the analysis to specific regions in the brain [Achard et al., 2006, He et al., 2007, Iturria-Medina et al., 2008]. In this approach voxels are grouped into ROIs based on standard atlases, and the time series of the voxels are averaged in order to compute correlations between ROIs [Castellanos et al., 2011]. The main disadvantage of the seed voxel method is that the resulting network is completely dependent on the choice of the seed voxel. Inaccurate results might arise from the omission of important connections and isolated regions.

2.4.2 Degree distribution of brain networks

The degree distribution of real life networks has been the focus of much recent research. Studies of brain networks have provided evidence of a scale-free topology (i.e. the degree distribution $P(k)$ is proportional to $k^{-\gamma}$ for some constant γ) in the derived

functional networks at a voxel level [Eguíluz et al., 2005]. However, recent studies increasingly suggest that the topology of such networks follows a variation of the scale-free power law: an exponentially truncated power law in which the probability $P(k)$ is proportional to $k^{-\gamma} \exp(-\alpha k)$ for constants α and γ [Achard et al., 2006, He et al., 2007, Iturria-Medina et al., 2008, Hayasaka and Laurienti, 2010, Ferrarini et al., 2011].

The majority of studies supporting this idea have been based on the analysis of regions of interest (ROIs), i.e., by characterizing functional connectivity only between a specific number of cortical and subcortical regions. [Achard et al., 2006, Iturria-Medina et al., 2008]. The most commonly used technique in these studies is to compute thresholded correlation matrices characterizing functional connectivity between regions; Achard et al. used 90 cortical and subcortical regions while He et al. used 54 cortical grey matter areas [Achard et al., 2006, He et al., 2007]. Diffusion-weighted Magnetic Resonance Imaging (DW-MRI) techniques have also been used to compute the anatomical connection probabilities. Iturria-Medina *et al.* used this technique to analyze the network among 90 cortical and subcortical grey matter areas [Iturria-Medina et al., 2008]. All of these studies reported an exponentially truncated power law degree distribution for the constructed networks.

Few studies have been published at the voxel level. Ferrarini *et al.* recently studied thresholded correlation matrices in which only the strongest connections were retained, and confirmed the superiority of a truncated power-law over the scale-free model [Ferrarini et al., 2011].

It has been found that for brain networks, high-degree nodes tend to be connected to other high-degree nodes [Eguíluz et al., 2005, Joyce et al., 2010]; this property is known as assortative mixing. The degree-dependent average nearest-neighbours degree for weighted networks, k_{nn}^{w}, was introduced by Barrat *et al.* in

2004 as a tool to identify assortative networks:

$$k_{nn,i}^w = \frac{1}{s_i} \sum_{j=1}^{N} w_{ij} k_j$$

where w_{ij} is the weight of the link between nodes i and j, k_j is the number of neighbours of node j, i.e., the unweighted degree of node k, and s_i is the strength, or weighted degree, of node i. The behaviour of k_{nn}^w identifies assortative and disassortative networks in the following way: If k_{nn}^w increases with k, then the network shows an assortative behaviour, whereas a decrease implies a disassortative behaviour [Barrat et al., 2004].

The brain has also been found to have other features of complex networks, such as a small-world topology [Watts and Strogatz, 1998, Sporns and Zwi, 2004, Achard et al., 2006]. Small world networks are characterized by a combination of short path lengths and high clustering, properties thought to be involved both in specialized brain regions and in integrated processing over the whole network [Sporns and Zwi, 2004].

2.4.3 Module identification methods

Complex systems are thought to have a hierarchical modular organization, meaning modules have in themselves a modular structure and can therefore be decomposed or partitioned in subsequent sub-modules. In particular, studies have revealed that brain functional networks have a hierarchical modular organization [Felleman and Van Essen, 1991, Meunier et al., 2009, Modha and Singh, 2010, Ferrarini et al., 2011]. This finding is based on the idea that cortical connectivity has two main roles in neural processing: there are strong intracortical connections between neurones with small physical separation, on the order of a few hundred micrometers, and there is another set of connections with larger physical separation linking different cortical areas [Nicoll and Blakemore, 1993, Varela et al., 2001, Sporns and Zwi, 2004]. Such

modular structure of segregated interconnected groups of nodes has been observed in networks of functional connectivity both for non-human [Hilgetag et al., 2000, Modha and Singh, 2010] and human data [Meunier et al., 2009, He et al., 2009, Ferrarini et al., 2011]. Hierarchical structure can give information on the developmental stage of the brain, for example, in their 2009 fMRI paper Supekar et al. found that children have significantly less hierarchical structure than young adults [Supekar et al., 2009]. Brain networks of patients with schizophrenia are also believed to show a loss in hierarchical organization [Bullmore and Sporns, 2009].

Each algorithm to identify the modular structure of the network will produce a particular partition of the network. A quantitative measure Q called modularity was first introduced by Newman and Girvan to asses the strength of the community structure in a given network [Girvan and Newman, 2001]. Modularity is defined originally for an unweighted, undirected network as

$$Q = \frac{1}{2m} \sum_{B \in D} \sum_{i,j \in B} \left(a_{ij} - \frac{k_i k_j}{2m} \right)$$

where a_{ij} are the entries of the adjacency matrix, k_i is the degree of node i, m is the total number of edges, and B is an index that runs over all the modules found by a given partition D [Girvan and Newman, 2001, Meunier et al., 2009]. There are many methods to find the modular structure of networks, several of which are based on optimizing Q. We present the most relevant for our research along with their advantages and limitations.

The Louvain method is a two phase method that leads to a hierarchical decomposition of the network [Blondel et al., 2008]. The first phase consists of a greedy optimization in which communities of nodes are found by locally optimizing modularity. The second phase consists of building a new network whose nodes are the previously found communities. The output of the algorithm is a series of partitions, a partition for each step. The Louvain method has been proven to be exceptionally efficient in terms of computation time, outperforming other partition methods.

Such low computation times allow the method to analyze networks of considerable size [Blondel et al., 2008]. However, since the method is based on greedy optimization it cannot ensure that a global maximum of modularity has been obtained. It has also been shown that although it identifies the highest levels of modularity with great precision, the resolution of the method needs to be changed in order to expose further partitions [Meunier et al., 2009].

The *Qcut* graph partitioning algorithm was developed by Ruan and Zhang to find communities of highly interconnected nodes [Ruan and Zhang, 2008]. This is another method based on optimizing the network's modularity. It applies a standard spectral clustering algorithm recursively until a maximum value of Q is found. It has been demonstrated that the overall network clustering accuracy of the algorithm *Qcut* is better than that of other methods based on hierarchical clustering [Ruan and Zhang, 2008], however it can neglect possible sub-modular structures. Its accuracy on functional node roles results has not been proven and cannot be ensured so far [Joyce et al., 2010].

A third method is based on the weighted gene coexpression network analysis (WGCNA) approach developed by Zhang and Horvath [Zhang and Horvath, 2005], and it is called weighted voxel coactivation network analysis (WVCNA) [Mumford et al., 2010]. This method relies on the measure of topological overlap [Ravasz et al., 2002] which considers not only the adjacency between two voxels, but also the overlap in the sets of neighbours of the two voxels. The topological overlap is defined by Ravasz *et al.* as

$$W_{ij} = \frac{l_{ij} + a_{ij}}{min\{k_i, k_j\} + 1 - a_{ij}}$$

where $a_{ij} \in [0, 1]$ are the entries of the adjacency matrix A, $l_{ij} = \sum_u a_{iu} a_{uj}$, and $k_i = \sum_u a_{iu}$ is the node's degree. If i and j are connected to each other and all of the neighbours of i are also neighbours of j, then $W_{ij} = 1$. If on the contrary, i and j are not connected and do not have any neighbours in common then $W_{ij} = 0$. We note that each term of l_{ij} represents the strength of the connection between nodes i

and j through another node, u. The total value of l_{ij} reflects the degree to which the neighbourhoods of i and j overlap.

Average linkage hierarchical clustering with the topological overlap dissimilarity measure is used to cluster similar nodes in a dendogram whose branches determine the clusters or modules. The clusters in the resulting dendrogram are then identified using the dynamic branch cutting algorithm of Langfelder *et al.* which identifies modules based not only by absolute height in the dendogram, but also on their shape [Langfelder et al., 2008]. One of the strengths of WGCNA is that it less susceptible to noise than methods based on pairwise correlations since the topological overlap considers a much larger array of correlations. Several advantages of this method were analyzed by Mumford *et al.*, the most important being that modularity-based algorithms favour larger modules whereas WVCNA is capable of finding both large and small modules. It was also shown that WGCNA module identification is more reliable than ICA based methods [Mumford et al., 2010].

2.4.4 Hub roles

Once a modular partition has been found, it is possible to further characterize the topological roles of nodes [Guimerà and Amaral, 2005]. The role a node has in the network affects its connectivity patterns [Guimerà and Amaral, 2005]. Studies have shown that in many networks specialized hub nodes serve as a connection between different modules, while other nodes are involved in maintaining strong intra-modular connections within their own module [Bullmore and Sporns, 2009]; therefore efficient communication is dependant on the role of these specialized nodes. A "map" of nodes' interactions and roles for complex system networks may provide important insight regarding their functionality [Guimerà and Amaral, 2005]. Nodes are initially divided into hubs and non-hubs, where hubs are defined as nodes with a high degree or number of connections. The within-module degree z-score measures how well-connected a node is to its own module, and determines the initial classification; it is

defined as

$$z_i = \frac{k_{iS_i} - \overline{k}_{S_i}}{\sigma_{k_{S_i}}}$$

where S_i denotes the module to which node i belongs. The parameter k_{iS_i} is the degree of node i within the module S_i, in other words, it is number of connections from node i to module S_i, $\overline{k}_{S_i}$ is the average of k over all the nodes in S_i, and $\sigma_{k_{S_i}}$ is the standard deviation of k in module S_i . This measure can be generalized to weighted networks by considering the weighted degree or strength s_i instead of k_i. Nodes with $z \geq 2.5$ are classified as module hubs and nodes with $z < 2.5$ are classified as non-hubs [Guimerà and Amaral, 2005].

The nodes can be further classified in term of their roles with respect to their participation in the network's connectivity. A node can be mainly connected to nodes within its own module; if so it is called a provincial node. If the node tends to link to other modules then it is called a connector node [Guimerà and Amaral, 2005]. The participation coefficient of a node is defined as

$$P_i = 1 - \sum_{s}^{N} \left(\frac{k_{iS}}{k_i} \right)^2$$

where N is the total number of modules, k_i is the degree of node i, and k_{iS} is the number of connections between node i and nodes in module S. The participation coefficient provides a measure of how well-distributed the connections of node i are among modules, it will therefore classify nodes into provincial or connector nodes [Guimerà and Amaral, 2005].

Guimerà *et al.* suggested the following thresholds to further classify low-degree nodes (non-hubs):

- $P \approx 0$: Ultra-peripheral nodes.
- $P < 0.625$: Peripheral nodes.
- $0.62 < P < 0.8$: Non-hub connectors.
- $P > 0.8$: Non-hub kinless nodes.

Whereas hubs are classified into three different roles:

- $P \leq 0.30$: Provincial hubs.
- $0.30 < P \leq 0.75$: Connector hubs.
- $P > 0.75$: Kinless hubs.

Note that high values of z do not mean high participation coefficients. A hub may have a high z-value, therefore it will be well-connected to other nodes within its module; however, its extra-modular connections can be poorly distributed resulting in low participation values. On the other hand, a node may have a number of extra-modular connections uniformly distributed among modules, but not be strongly connected to its own module. This will result in low $z-$values and high participation coefficient values.

Provincial hubs maintain local structure and optimize information processing within their modules, while connector hubs mediate between different modules and are key for transferring information to the rest of the network [Meunier et al., 2009, Joyce et al., 2010, Stam, 2010].

The classification of node roles in this way is referred to as a "cartographic" study; cartographic studies have been made for some real life systems such as the air transportation, brain and metabolic networks [Guimerà and Amaral, 2005, Hagmann et al., 2008, van den Heuvel and Sporns, 2011]. A study made by Guimera *et al.* of air transportation networks found that only 4.1% of the cities are hubs, with equal fractions of provincial and connector. Provincial hubs include Denver, Barcelona and Copenhagen among others, while connector hubs include Chicago, Mexico City and Sydney [Guimerà et al., 2005]. For brain networks, a study by Hagmann *et al.* found that the majority of connector hubs were located in posterior medial and parietal cortex, whereas provincial hubs are found in the frontal, temporoparietal or occipital modules [Hagmann et al., 2008]. Another study found that connector hubs were located in superior frontal and superior parietal cortex, while subcortical regions such as the thalamus and putamen were provincial hubs [van den Heuvel and Sporns, 2011]; the precuneus was found to be a hub in all studies. Similar cartographic studies

have been performed for metabolic networks, for example, for the metabolic network of *E. coli* the non-hub connectors were found to be significantly more conserved than provincial hub metabolites [Guimerà and Amaral, 2005].

2.5 Brain injuries analyzed through network theory

A traumatic brain injury (TBI) refers to a neurological injury caused by a mechanical trauma to the brain. TBI is a major health issue since it can result in a variety of cognitive, somatic and affective symptoms such as memory loss, attention deficit, headaches, insomnia, hypersensitivity to sensory input, anxiety and depression [Alexander, 1995]. Furthermore, in some cases, the effects of a TBI can result in subsequent neurocognitive dysfunction and even permanent damage. For example, individuals with a TBI have been shown to be $1.5 - 1.7$ times more likely to develop epileptic seizures than the general population [Annegers et al., 1998]. A history of head injury has been found to more than double the risk of developing Alzheimer's [Plassman et al., 2000].

A clear link between the neuropsychological symptoms associated with TBI and the underlying structural and functional effects of the TBI is still not completely understood [Slobounov et al., 2011]. Cortical lesions caused by the brain striking adjacent skull areas and diffuse axonal shearing are thought to be key agents of many of the features associated with concussions [Maruta et al., 2010].

Functional magnetic resonance imaging (fMRI) is a well-established and powerful technique for the elucidation of the complex network of functional interactions in the human brain in the event of a brain injury [Slobounov et al., 2011, Bullmore and Sporns, 2012]. In particular, some brain injury and brain disorder associated networks have been shown to manifest abnormalities in their topological properties [Honey and Sporns, 2008, Stam et al., 2009, Cho and Choi, 2010, Bullmore and Sporns, 2012].

The effect of brain disorders on network properties

A loss in the capacity to integrate information is perhaps the most common topological abnormality found in disorders of the brain. For example, an EEG study revealed that after a stroke there is a significant reduction in the brain's ability to integrate information between distant regions when compared with healthy controls [De Vico Fallani et al., 2009, Crofts and Higham, 2009]. Long-distance connections are often the most vulnerable to disruptions, for example, there is a prominent loss in long-range connections in patients with Alzheimer's disease, as shown in recent fMRI studies [Rosenbaum et al., 2008]. Another example comes from multiple sclerosis: since this disorder causes demyelination of axonal tracts, long-range connections are more susceptible to damage [Bullmore and Sporns, 2012].

Intramodular connectivity has also been found to decrease for certain disorders, directly affecting the communication between brain areas and sometimes even disrupting it completely. Such an alteration has direct effects on the modular structure of the network. Schizophrenia has been consistently found to reduce the density of intramodular connections, obstructing the communication between modules [Bassett et al., 2008, Alexander-Bloch et al., 2010, Jalili and Knyazeva, 2011]. Patients with Alzheimer's also showed a weakening in intramodular connections, strongly related to the cognitive decline particular to Alzheimer's disease [de Haan et al., 2012].

The degree to which the brain network exhibits small-world network qualities has been used as a marker for some brain disorders [Cho and Choi, 2010]. Brain networks of patients with Alzheimer's disease, brain tumours, and schizophrenia have shown decreased small-world attributes [Bartolomei et al., 2006, Bassett et al., 2008, Stam et al., 2009], whereas in the process of a seizure there is an increase in small-world properties [Wu et al., 2006].

The degree distribution is the topological property that has exhibited the least alteration in disorders of the brain. Studies in ADHD and schizophrenia showed

that an exponentially truncated degree distribution is consistent across groups [Wang et al., 2009, Lynall et al., 2010], with slight differences in the parameters for the schizophrenia study [Lynall et al., 2010].

Network effects of Traumatic Brain Injuries

Localized injuries to the brain have been modelled through the perturbation of network nodes and connections (for review, see Jirsa, 2010). Studies have revealed that brain networks tend to be resilient to random node removal, as opposed to highly central node removal [Honey and Sporns, 2008, Alstott et al., 2009]. A deterioration of connector hubs is expected to impact the network's processing efficiency, resulting in cognitive and behavioural symptoms [Bullmore and Sporns, 2012].

In their 2008 study, Honey and Sporns analyzed the macaque and cat's cerebral cortices. They used a series of oscillator models to establish the connectivity patterns of 47 regional nodes and to examine the theoretical effects of lesions on the synchronization of brain regions. Focalized lesion effects in connector and provincial hubs were further analyzed. Lesions in provincial hubs were found to have more strongly clustered localized effects, whereas lesions of connector hubs will produce more widely distributed effects [Honey and Sporns, 2008]. It was also demonstrated that brain networks show changes in the small-world index following injury: lesions in provincial hubs resulted in cortical networks with the largest decrease in their small-world topology, as opposed to lesions of connector hubs that resulted in the largest increase [Sporns et al., 2007, Honey and Sporns, 2008]

A noninvasive diffusion imaging study by Alstott *et al.* extended previous theoretical work [Sporns et al., 2007] to the human brain [Alstott et al., 2009]. Average structural connectivity (SC) matrices were created for 998 predefined ROIs. The structural connectivity matrix was then "lesioned" computationally by sequentially deleting single nodes, and by removal of focalized areas. Single nodes were sequentially removed in two ways: either randomly, or by the removal of nodes with the

highest degree and centrality. The size of the largest connected component and the global efficiency (defined as the average of the inverse distance between all nodes) were then compared between lesioned and intact brain. The brain network was found to be resilient to random node removal, as opposed to highly central node removal. Localized lesions were also computed by choosing a central region defined by standardized Talairach coordinates, and removing a fixed number of nodes and their connections from the connectivity matrix. The resultant network's topological properties were then compared to those of the intact brain. Focalized lesion effects were dependent on the lesion location and on the centrality of the removed nodes. For example, lesions in the frontal, parietal and temporal lobes were found to have an extensive impact. Due to computational limitations only a number of focal regions were considered and the lesion sizes did not vary. The effects of axonal disruptions were not considered in this study.

The lack of longitudinal data, small TBI patient sample sizes, and the heterogeneity of injury severity are a few of the limitations encountered by TBI research [Mayer et al., 2009]. The studies of Alstott *et al.* and Honey *et al.* were designed to analyze immediate effects, with no focus on functional recovery [Honey and Sporns, 2008, Alstott et al., 2009]. Nonetheless, the topological properties of the brain under recovery have been the subject of a handful of studies. Slobounov *et al.* analyzed fMRI data from 15 athletes who had suffered mild TBI. Larger cluster sizes were found in concussed athletes when compared to controls; this topological modification could represent an initial effort of the brain towards cortical reorganization [Slobounov et al., 2010]. In a 2011 study, TBI patients underwent MEG recording before and after a neuropsychological rehabilitation program. Path length and clustering were among the topological properties that were found to be restored after the neurorehabilitation [Castellanos et al., 2011].

2.6 Conclusion

Much work has been done in the study of complex systems with the use of network theory; however, many features remain to be understood. Topological properties that shed light on the functionality of the systems they represent need to be analyzed and revisited. In particular, the study of brain networks poses many computational and modelling challenges. Further research can uncover the underlying processes of one of the least understood, as well as one of the most interesting systems in nature.

Bibliography

Achard, S., Salvador, R., Whitcher, B., Suckling, J., and Bullmore, E. (2006). A resilient, low-frequency, small-world human brain functional network with highly connected association cortical hubs. *J Neurosci*, 26(1):63–72.

Albert, R.and Jeong, H. and Barabási, A.-L. (1999). The diameter of the world wide web. *CoRR*, cond-mat/9907038.

Alexander, M. P. (1995). Mild traumatic brain injury: pathophysiology, natural history, and clinical management. *Neurology*, 45(7):1253–1260.

Alexander-Bloch, A., Gogtay, N., Meunier, D., Birn, R., Clasen, L., Lalonde, F., Lenroot, R., Giedd, J., and Bullmore, E. (2010). Disrupted modularity and local connectivity of brain functional networks in childhood-onset schizophrenia. *Front Syst Neurosci*, 4(October):16.

Alonso, R., Brocas, I., and Carrillo, J. D. (2011). Resource allocation in the brain. CEPR Discussion Papers 8408, C.E.P.R. Discussion Papers.

Alstott, J., Breakspear, M., Hagmann, P., Cammoun, L., and Sporns, O. (2009). Modeling the impact of lesions in the human brain. *PLoS Comput Biol*, 5(6).

Annegers, J. F., Hauser, W. A., Coan, S. P., and Rocca, W. A. (1998). A population-based study of seizures after traumatic brain injuries. *New Engl J Med*, 338(1):20–24.

Bagrow, J. P., Lehmann, S., and Ahn, Y.-Y. (2011). Robustness and modular structure in networks. *CoRR*, abs/1102.5085.

Barabási, A.-L. and Albert, R. (1999). Emergence of scaling in random networks. *Science*, 286(5439):509–512.

Barabási, A.-L., Albert, R., and Jeong, H. (2000). Scale-free characteristics of random networks: the topology of the world-wide web. *Phys A*, 281(1-4):69–77.

Barabási, A.-L., Jeong, H., and Albert, R. (2000). Error and attack tolerance of complex networks. *Nature*, 406(6794):378–382.

Barrat, A., Barthélemy, M., Pastor-Satorras, R., and Vespignani, A. (2004). The architecture of complex weighted networks. *Proc Natl Acad Sci U S A*, 101(11):3747–3752.

Bartolomei, F., Bosma, I., Klein, M., Baayen, J., Reijneveld, J., Postma, T., Heimans, J., van Dijk, B., de Munck, J., de Jongh, A., Cover, K., and Stam, C. (2006). How do brain tumors alter functional connectivity? a magnetoencephalography study. *Ann Neurol*, 59(1):128–38.

Bassett, D., Bullmore, E., Verchinski, B., Mattay, V., Weinberger, D., and Meyer-Lindenberg, A. (2008). Hierarchical organization of human cortical networks in health and schizophrenia. *J Neurosci*, 28(37):9239–48.

Bianciardi, M., Fukunaga, M., van Gelderen, P., Horovitz, S., de Zwart, J., and Duyn, J. (2009). Modulation of spontaneous fMRI activity in human visual cortex by behavioral state. *NeuroImage*, 45(1):160 – 168.

Blondel, V. D., Guillaume, J.-L., Lambiotte, R., and Lefebvre, E. (2008). Fast unfolding of communities in large networks. *J Stat Mech Theory Exp*, 2008(10):P10008 (12pp).

Bollobás, B. (1980). The distribution of the maximum degree of a random graph. *Discrete Math*, 32(2):201–203.

Bollobás, B. (2001). *Random graphs.* Cambridge University Press.

Bullmore, E. and Sporns, O. (2009). Complex brain networks: graph theoretical analysis of structural and functional systems. *Nat Rev Neurosci*, 10(3):186–98.

Bullmore, E. and Sporns, O. (2012). The economy of brain network organization. *Nat Rev Neurosci*, 13(5):336–349.

Castellanos, N., Leyva, I., Buldú, J., Bajo, R., Paul, N., Cuesta, P., Ordóñez, V., Pascua, C., Boccaletti, S., Maestú, F., and del Pozo, F. (2011). Principles of recovery from traumatic brain injury: Reorganization of functional networks. *NeuroImage*, 55(3):1189–1199.

Cho, M. W. and Choi, M. Y. (2010). Brain networks: Graph theoretical analysis and development models. *Int J Imaging Syst Technol*, 20(2):108–116.

Crofts, J. and Higham, D. (2009). A weighted communicability measure applied to complex brain networks. *J R Soc Interface*, 6(33):411–4.

Damoiseaux, J., Beckmann, C., Arigita, E. S., Barkhof, F., Scheltens, P., Stam, C., Smith, S., and Rombouts, S. (2008). Reduced resting-state brain activity in the "default network" in normal aging. *Cereb Cortex*, 18(8):1856–1864.

de Haan, W., van der Flier, W., Koene, T., Smits, L., Scheltens, P., and Stam, C. (2012). Disrupted modular brain dynamics reflect cognitive dysfunction in Alzheimer's disease. *NeuroImage*, 59(4):3085–93.

De Vico Fallani, F., Astolfi, L., Cincotti, F., Mattia, D., la Rocca, D., Maksuti, E., Salinari, S., Babiloni, F., Vegso, B., Kozmann, G., and Nagy, Z. (2009). Evaluation of the brain network organization from EEG signals: A preliminary evidence in stroke patient. *Anat Rec*, 292(12):2023–2031.

Du, W., Calhoun, V., Li, H., Ma, S., Object, Kiehl, K., Pearlson, G., and Adali, T. (2012). High classification accuracy for schizophrenia with rest and task fMRI data. *Frontiers in Human Neuroscience*, 6(145):1–12.

Eguíluz, V. M., Chialvo, D. R., Cecchi, G. A., Baliki, M., and Apkarian, A. V. (2005). Scale-free brain functional networks. *Phys Rev Lett*, 94(1):018102.

Erdös, P. and Rényi, A. (1959). On random graphs i. *Publ Math Debrecen*, 6:290.

Faloutsos, M., Faloutsos, P., and Faloutsos, C. (1999). On power-law relationships of the internet topology. In *Proceedings of the conference on Applications, tech-*

nologies, architectures, and protocols for computer communication, SIGCOMM '99, pages 251–262, New York, NY, USA. ACM.

Felleman, D. and Van Essen, D. (1991). Distributed hierarchical processing in the primate cerebral cortex. *Cereb Cortex*, pages 1–47.

Ferrarini, L., Veer, I. M., van Lew, B., Oei, N. Y. L., van Buchem, M. A., Reiber, J. H. C., Rombouts, S. A. R. B., and Milles, J. (2011). Non-parametric model selection for subject-specific topological organization of resting-state functional connectivity. *NeuroImage*, 56(3):1453–1462.

Frackowiak, R., Friston, K., Frith, C., Dolan, R., Price, C., Zeki, S., Ashburner, J., and Penny, W. (2003). *Human brain function.* Academic Press, 2nd edition.

Girvan, M. and Newman, M. E. J. (2001). Community structure in social and biological networks. *Proc Natl Acad Sci U S A*.

Greicius, M. D., Krasnow, B., Reiss, A. L., and Menon, V. (2003). Functional connectivity in the resting brain: a network analysis of the default mode hypothesis. *Proc Natl Acad Sci U S A*, 100:253–258.

Griffeth, L. (2005). Use of PET/CT scanning in cancer patients: technical and practical considerations. *Proc Bayl Univ Med Cent*, 18(4):321–30.

Guimerà, R. and Amaral, L. (2005). Functional cartography of complex metabolic networks. *Nature*, 433:895–900.

Guimerà, R. and Amaral, L. N. A. (2005). Cartography of complex networks: modules and universal roles. *J Stat Mech*, 2005(P02001):P02001+.

Guimerà, R., Mossa, S., Turtschi, A., and Amaral, L. (2005). The worldwide air transportation network: Anomalous centrality, community structure, and cities' global roles. *Proc Natl Acad Sci U S A*, 102(22):7794.

Guimerà, R., Sales-Pardo, M., and Amaral, L. A. N. (2007). Module identification in bipartite and directed networks. cite arxiv:physics/0701151.

Hagmann, P., Cammoun, L., Gigandet, X., Meuli, R., Honey, C. J., Wedeen, V. J., and Sporns, O. (2008). Mapping the structural core of human cerebral cortex. *PLoS Biol*, 6(7):e159+.

Hayasaka, S. and Laurienti, P. J. (2010). Comparison of characteristics between region-and voxel-based network analyses in resting-state fMRI data. *NeuroImage*, 50(2):499–508.

He, Y., Chen, Z. J., and Evans, A. C. (2007). Small-world anatomical networks in the human brain revealed by cortical thickness from MRI. *Cereb Cortex*, 17(10):2407–2419.

He, Y., Wang, J., Wang, L., Chen, Z. J., Yan, C., Yang, H., Tang, H., Zhu, C., Gong, Q., Zang, Y., and Evans, A. C. (2009). Uncovering intrinsic modular organization of spontaneous brain activity in humans. *PLoS ONE*, 4(4):e5226+.

Hilgetag, C. C., Burns, G. A., O'Neill, M. A., Scannell, J. W., and Young, M. P. (2000). Anatomical connectivity defines the organization of clusters of cortical areas in the macaque monkey and the cat. *Philos Trans R Soc Lond B*, 355(1393):91–110.

Honey, C. J. and Sporns, O. (2008). Dynamical consequences of lesions in cortical networks. *Hum Brain Mapp*, 29(7):802–809.

Horowitz, B., Tagamet, M.-A., and McIntosh, A. R. (1999). Neural modeling, functional brain imaging, and cognition. *Trends Cogn Sci*, 3:91–98.

Iturria-Medina, Y., Sotero, R. C., Canales-Rodríguez, E. J., Alemán-Gómez, Y., and Melie-García, L. (2008). Studying the human brain anatomical network via diffusion-weighted MRI and graph theory. *NeuroImage*, 40(3):1064–1076.

Jalili, M. and Knyazeva, M. (2011). EEG-based functional networks in schizophrenia. *Comput Biol Med*, 41(12):1178–86.

Jeong, H., Tombor, B., Albert, R., Oltvai, Z. N., and Barabási, A. L. (2000). The large-scale organization of metabolic networks. *Nature*, 407(6804):651–654.

Jirsa, V. K., Sporns, O., Breakspear, M., Deco, G., and McIntosh, A. R. (2010). Towards the virtual brain: network modeling of the intact and the damaged brain. *Arch Ital Biol*, 148(3):189–205.

Joyce, K., Laurienti, P., Burdette, J., and Hayasaka, S. (2010). A new measure of centrality for brain networks. *PLoS One*, 5(8):e12200.

Langfelder, P., Bin, Z., and Horvath, S. (2008). Defining clusters from a hierarchical cluster tree: The dynamic tree cut package for R. *Bioinformatics*, 24(5):719–720.

Liang, X., Wang, J., Yan, C., Shu, N., Xu, K., Gong, G., and He, Y. (2012). Effects of different correlation metrics and preprocessing factors on small-world brain functional networks: a resting-state functional MRI study. *PLoS One*, 7(3):e32766.

Lynall, M., Bassett, D., Kerwin, R., McKenna, P., Kitzbichler, M., Muller, U., and Bullmore, E. (2010). Functional connectivity and brain networks in schizophrenia. *J Neurosci*, 30(28):9477–9487.

Maruta, J., Lee, S., Jacobs, E., and Ghajar, J. (2010). A unified science of concussion. *Ann N Y Acad Sci*, 1208.

Marx, E.and Deutschlander, A., Stephan, T., Dieterich, M., Wiesmann, M., and Brandt, T. (2004). Eyes open and eyes closed as rest conditions: impact on brain activation patterns. *NeuroImage*, 21(4):1818 – 1824.

Mason, M. F., Norton, M. I., Van Horn, J. D., Wegner, D. M., Grafton, S. T., and Macrae, C. (2007). Wandering minds: the default network and stimulus-independent thought. *Science*, 315(5810):393–395.

Mayer, A., Mannell, M., Ling, J., Elgie, R., Gasparovic, C., Phillips, J., Doezema, D., and Yeo, R. (2009). Auditory orienting and inhibition of return in mild traumatic brain injury: a fMRI study. *Hum Brain Mapp*, 30(12):4152–66.

Mazziotta, J. C., Toga, A. W., Evans, A., Fox, P., and Lancaster, J. (1995). A probabilistic atlas of the human brain: theory and rationale for its development :

the international consortium for brain mapping (ICBM). *NeuroImage*, 2(2, Part 1):89–101+.

Meunier, D., Lambiotte, R., Fornito, A., Ersche, K. D., and Bullmore, E. T. (2009). Hierarchical modularity in human brain functional networks. *Frontiers in neuroinformatics*, 3.

Milgram, S. (1967). The small world problem. *Psychol Today*, 1(1):61–67.

Miller, J. C. (2009). Percolation and epidemics in random clustered networks. *Phys Rev E*, 80(2 Pt 1):020901.

Modha, D. S. and Singh, R. (2010). Network architecture of the long-distance pathways in the macaque brain. *Proc Natl Acad Sci U S A*, 107(30):13485–13490.

Mumford, J., Horvath, S., Oldham, M., Langfelder, P., Geschwind, D., and Poldrack, R. (2010). Detecting network modules in fMRI time series: A weighted network analysis approach. *NeuroImage*, 52(4):1465–1476.

Newman, M. (2001). Scientific collaboration networks. i. network construction and fundamental results. *Phys Rev E*, 64:2001.

Newman, M. E. J. (2002). Assortative mixing in networks. *Phys Rev Lett*, 89(20):208701.

Newman, M. E. J. (2004). Detecting community structure in networks. *Eur Phys J B*, 38:321–330.

Newman, M. E. J. and Girvan, M. (2004). Finding and evaluating community structure in networks. *Phys Rev E*, 69(2):026113.

Nicoll, A. and Blakemore, C. (1993). Patterns of local connectivity in the neocortex. *Neural Comput*, 5(5):665–680.

Pastor-Satorras, R. and Vespignani, A. (2001). Epidemic spreading in scale-free networks. *Phys Rev Lett*, 86(14):3200–3203.

Pearson, K. (1894). Contributions to the mathematical theory of evolution. *Philos Trans R Soc Lond A*, 185:71–110.

Plassman, B. L., Havlik, R. J., Steffens, D. C., Helms, M. J., Newman, T. N., Drosdick, D., Phillips, C., Gau, B. A., Welsh-Bohmer, K. A., Burke, J. R., Guralnik, J. M., and Breitner, J. C. (2000). Documented head injury in early adulthood and risk of alzheimer's disease and other dementias. *Neurology*, 55(8):1158–66.

Ravasz, E., Somera, A., Mongru, D., Oltvai, Z., and Barabási, A. (2002). Hierarchical organization of modularity in metabolic networks. *Science*, 297(5586):1551.

Rosenbaum, R., Furey, M., Horwitz, B., and Grady, C. (2008). Altered connectivity among emotion-related brain regions during short-term memory in alzheimer's disease. *Neurobiol Aging*, pages 1–7.

Ruan, J. and Zhang, W. (2008). Identifying network communities with a high resolution. *Phys Rev E*, 77(016104):1–12.

Schwarz, A. J. and McGonigle, J. (2011). Negative edges and soft thresholding in complex network analysis of resting state functional connectivity data. *NeuroImage*, 55(3):1132–1146.

Slobounov, S., Gay, M., Zhang, K., J., B., Pennell, D., Sebastianelli, W., Horovitz, S. G., and Hallett, M. (2011). Alteration of brain functional network at rest and in response to YMCA physical stress test in concussed athletes: RsfMRI study. *NeuroImage*, 55(4):1716–1727.

Slobounov, S. M., Zhang, K., Pennell, D., Ray, W., Johnson, B., and Sebastianelli, W. (2010). Functional abnormalities in normally appearing athletes following mild traumatic brain injury: a functional MRI study. *Exp Brain Res*, 202(2):341–354.

Smith, S. M. (2004). Overview of fMRI analysis. *Brit J Radiol*, 77(suppl 2):S167–S175.

Song, X.-W., Dong, Z.-Y., Long, X.-Y., Li, S.-F., Zuo, X.-N., Zhu, C.-Z., He, Y., Yan, C.-G., and Zang, Y.-F. (2011). REST: a toolkit for resting-state functional magnetic resonance imaging data processing. *PLoS ONE*, 6(9).

Sporns, O., Honey, C. J., and Kötter, R. (2007). Identification and classification of hubs in brain networks. *PLoS ONE*, 2(10).

Sporns, O. and Zwi, J. D. (2004). The small world of the cerebral cortex. *Neuroinformatics*, 2(2):145–162.

Stam, C., de Haan, W., Daffertshofer, A., Jones, B., Manshanden, I., van Cappellen van Walsum, A., Montez, T., Verbunt, J., de Munck, J., van Dijk, B., Berendse, H., and Scheltens, P. (2009). Graph theoretical analysis of magnetoencephalographic functional connectivity in alzheimer's disease. *Brain*, 132(Pt 1):213–24.

Stam, C. J. (2010). Characterization of anatomical and functional connectivity in the brain: A complex networks perspective. *Int J Psychophysiol*, 77(3):186–194.

Stam, C. J., Nolte, G., and Daffertshofer, A. (2007). Phase lag index: Assessment of functional connectivity from multi channel EEG and MEG with diminished bias from common sources. *Hum Brain Mapp*, 28(11):1178–1193.

Supekar, K., Musen, M., and Menon, V. (2009). Development of large-scale functional brain networks in children. *PLoS Biol*, 7(7).

Talairach, J. and Tournoux, P. (1988). *Co-Planar stereotaxic atlas of the human brain: 3-D proportional system: An approach to cerebral imaging*. Thieme.

van den Heuvel, M. P. and Sporns, O. (2011). Rich-club organization of the human connectome. *J Neurosci*, 31(44):15775–15786.

Vanhaudenhuyse, A., Noirhomme, Q., Tshibanda, L. J.-F., Bruno, M.-A., Boveroux, P., Schnakers, C., Soddu, A., Perlbarg, V., Ledoux, D., and Brichant, J.-F. (2010). Default network connectivity reflects the level of consciousness in non-communicative brain-damaged patients. *Brain*, 133(1):161–171.

Varela, F., Lachaux, J.-P., Rodriguez, E., and Martinerie, J. (2001). The brainweb : phase large-scale integration. *Neuroscience*, 2(April):229–239.

Vincent, J., Snyder, A., Fox, M., Shannon, B., Andrews, J., Raichle, M., and Buckner, R. (2006). Coherent spontaneous activity identifies a hippocampal-parietal memory network. *J Neurophysiol*, 96(6):3517–3531.

Wang, J., Zuo, X., and He, Y. (2010a). Graph-based network analysis of resting-state functional MRI. *Front Syst Neurosci*, 4.

Wang, J., Zuo, X., and He, Y. (2010b). Graph-based network analysis of resting-state functional MRI. *Front Syst Neurosci*, 4.

Wang, L., Li, Y., Metzak, P., He, Y., and Woodward, T. (2010c). Age-related changes in topological patterns of large-scale brain functional networks during memory encoding and recognition. *NeuroImage*, 50(3):862–872.

Wang, L., Zhu, C., He, Y., Zang, Y., Cao, Q., Zhang, H., Zhong, Q., and Wang, Y. (2009). Altered small-world brain functional networks in children with attention-deficit/hyperactivity disorder. *Hum Brain Mapp*, 30(2):638–649.

Watts, D. J. and Strogatz, S. H. (1998). Collective dynamics of 'small-world' networks. *Nature*, 393(6684):440–442.

Wu, H., Li, X., and Guan, X. (2006). Networking property during epileptic seizure with multi-channel EEG recordings. In Wang, J., Yi, Z., Zurada, J., Lu, B.-L., and Yin, H., editors, *ISNN (2)*, volume 3973 of *Lecture Notes in Computer Science*, pages 573–578. Springer.

Zhang, B. and Horvath, S. (2005). A general framework for weighted gene co-expression network analysis. *Stat Appl Genet Mol Biol*, 4(1):Article17.

Zhou, C., Zemanová, L., Zamora, G., Hilgetag, C. C., and Kurths, J. (2006). Hierarchical organization unveiled by functional connectivity in complex brain networks. *Phys Rev Lett*, 97:238103.

Chapter 3

Topology of whole-brain functional MRI networks: improving the truncated scale-free model

3.1 Introduction

Many biological, social, and communication systems can be described as complex networks. In these networks, the system elements are represented by vertices and the interactions between them are modelled by edges; the distribution of edges across vertices is described by a model of the network topology. Real life networks show complex interactions between their elements, and have often been modelled using Erdös-Rényi random graph topology [Erdös and Rényi, 1959]. This model consists of a graph of n vertices in which an edge is included between each pair with probability p. For many real life systems, the underlying topology remains unknown due to lack of data [Barabási and Albert, 1999]; in these cases the Erdös-Rényi random graph topology had been widely assumed [Barabási and Bonabeau, 2003]. In other systems, however, the recent advent of high quality data has offered evidence of more complex network topologies; examples include metabolic networks [Sales-Pardo et al., 2007], transportation systems [Guimerà et al., 2005, Sales-Pardo et al., 2007], the spread of disease [Eubank et al., 2004] and social networks [Newman, 2001].

The degree distribution, $p(k)$, describes the probability that any node is connected to k other nodes. In an Erdös-Rényi random graph, the degree distribution is a binomial distribution [Erdös and Rényi, 1959]. In contrast, scale-free networks are

characterized by a power law degree distribution. i.e. the probability $p(k)$ is proportional to $k^{-\gamma}$ for some constant γ [Barabási and Albert, 1999]. A variation of this topology is the exponentially truncated scale-free topology, in which the probability $p(k)$ is proportional to $k^{-\gamma} \exp(-\alpha k)$ for constants α and γ [Bullmore and Sporns, 2009]. Scale-free networks have been the focus of much recent attention [Barabási and Albert, 1999, Strogatz, 2001, Barabási and Bonabeau, 2003]; air transportation systems and World Wide Web links are examples of networks that are believed to be scale-free [Barabási et al., 2000, Guimerà et al., 2005].

The brain can also be seen as a complex network with highly interconnected elements, on scales ranging from individual neurones to large cortical structures. Functional magnetic resonance imaging (fMRI) measures hemodynamic responses (changes in blood oxygenation levels), identifying areas in the brain that show activation in response to certain stimuli. fMRI has been widely used to study the functionality of the human brain [Salvador et al., 2005, Eguíluz et al., 2005].

In fMRI network analyses, voxels are treated as nodes in a network, and the connections between them are defined by correlated functional activity. However, a standard method to define the existence of these connections has not yet been established. First, the degree to which the functional activities of each pair of voxels are statistically related is assessed. The Pearson correlation coefficient, r_{ij}, is the most commonly used measure of dependence [Liang et al., 2012]. It is defined as the covariance of the time series of fMRI signals between the two voxels i and j, divided by the product of their standard deviations. This measure ranges from 1 to -1.

To build the network given the r_{ij} values, the usual approach is a binary information or hard thresholding approach [Eguíluz et al., 2005]. In hard thresholding, a connection between the nodes only exists if the correlation is above a certain threshold, yielding an unweighted network. However, a discrete measure for connectivity may not be the most accurate description of the structure and organization of the brain, since such an approach might lead to important losses of information. Weighted

network analysis has also been suggested as a more accurate representation of brain connectivity [Schwarz and McGonigle, 2011]. In the soft threshold approach each connection is given a weight (a continuous measure that ranges from 0 to 1) resulting in a weighted network.

One important limitation when working with fMRI networks is the huge amount of data potentially involved. Constructing networks and analyzing their behaviour becomes computationally expensive, and to date very few studies have been published which treat full brain networks. Instead, one voxel (a "seed" voxel) is typically chosen and all correlations with that voxel are computed. New seed voxels, chosen by finding significant correlations with the original seed voxel, are then included in an iterative process [Vincent et al., 2006, Slobounov et al., 2011]. A drawback of this method is that the choice of the initial voxel may bias the results. Another approach is to restrict attention, *a priori*, to only certain areas or regions of interest in the brain [Achard et al., 2006, He et al., 2007, Iturria-Medina et al., 2008]. This method may not completely characterize the full set of interactions among different brain regions.

Previous studies of fMRI human brain imaging have given evidence of a scale-free topology in the derived functional unweighted networks at a voxel level [Eguíluz et al., 2005]. However, increasing evidence suggests that the topology of such networks follows an exponentially truncated power law rather than a true power law [Achard et al., 2006, He et al., 2007, Iturria-Medina et al., 2008, Bullmore and Sporns, 2009, Hayasaka and Laurienti, 2010, Ferrarini et al., 2011]. To date, many studies supporting this idea have been based on the analysis of ROIs rather than in networks constructed retaining a high number of voxels. For example, Achard *et al.* computed thresholded correlation matrices characterizing functional connectivity between 90 cortical and subcortical regions [Achard et al., 2006]. Iturria-Medina *et al.* used diffusion-weighted Magnetic Resonance Imaging (DW-MRI) techniques to compute the anatomical connection probabilities, also between 90 cortical and subcortical grey matter areas [Iturria-Medina et al., 2008], while He *et al.* computed correlation matri-

ces of 54 cortical grey matter areas [He et al., 2007]. All of these studies reported an exponentially truncated power law degree distribution for the constructed networks. At the voxel level, Ferrarini *et al.* confirmed the superiority of a truncated power law over the scale-free model [Ferrarini et al., 2011].

In the work described in the following sections, complete fMRI data sets of 10 healthy volunteers were analyzed. Seed voxels or restrictions on specific areas of the brain were not used, such that all correlations between approximately 190000 voxels for each subject were computed. We tested the degree to which the resultant whole brain networks satisfied not only scale-free and exponentially truncated scale-free topologies, but also a number of novel, more complex topologies which could be differentiated in this study due to the rich dataset we analyse. The differences between weighted and unweighted networks, resulting from the use of soft and hard thresholding respectively, were also explored. To our knowledge, this is the first time that the topology of whole brain fMRI datasets has been analyzed.

3.2 Methods

3.2.1 fMRI data acquisition

For a complete description of the cognitive task and data acquisition see [Greening et al., 2011]. Briefly, 10 subjects were scanned on a forced choice response reversal task using a 3T Siemens MRI scanner with a 32 channel head coil. We performed 6 runs of the task while collecting the Blood Oxygenation Level Dependent (BOLD) signal. Thus we used a T2*-gradient echo-planar imaging sequence (repetition time = 3 seconds; echo time = 30ms; 120x120mm matrix; field of view of 240mm). We acquired 45 slices at 2x2mm in-plane resolution in the axial plane and a slice thickness of 2.5mm, yielding whole brain coverage in 2x2x2.5mm voxels. In each run we acquired 106 whole brain volumes in this manner, for a total of 636 total volumes across the six runs.

The time series data obtained during the 6 functional runs was preprocessed using Analysis of Functional Neuroimaging (AFNI) software [Cox, 1996]. During pre-processing we removed the first six volumes of each run so as to ensure magnetization equilibrium was reached, leaving a total of 600 volumes per subject. The voxel time series for each volume was aligned to the same temporal origin, and each volume was registered to the first volume of the first run to correct for motion.

The time series data for each voxel were then normalized at each time point by dividing the signal intensity by the mean signal intensity of that voxel for all volumes within each run, and the six runs were concatenated. This yielded the raw time series data.

A regression analysis using a general linear model was performed to estimate the contribution of all conditions as well as baseline drift in the MRI signal. We were then able to remove the estimated baseline drift from the raw time series data. This allowed for analysis of the raw data while controlling for the possible confound of drift in the magnetic field.

The three-dimensional raw time series data minus drift were then warped into standard space (based on the atlas of Talairach and Tournoux). Finally, a whole-brain mask was applied to the data to remove voxels that were clearly not part of the brain from analysis.

All data were collected as approved by Western University Human Research Ethics Board.

3.2.2 Analysis

The first step in the analysis after pre-processing was to find a measure of similarity s_{ij} between each pair of voxels i and j. The Pearson correlation coefficient r_{ij} between the time series of each pair of voxels was computed, and the absolute value of

the correlation coefficient was used to construct the $N \times N$ similarity matrix $S = |r_{ij}|$ (where N is the number of voxels per subject, approximately 2×10^5).

We then computed a connection strength matrix, the adjacency matrix A. In order to do so, an adjacency function $a_{ij} = f(s_{ij})$ must be defined, where f is a monotonically increasing function [Zhang and Horvath, 2005]. In many standard network approaches the adjacency function is defined as the signum function, in which two voxels i and j are considered to be either connected ($a_{ij} = 1$) or disconnected ($a_{ij} = 0$) if the magnitude of the correlation between them is above or below a certain hard threshold τ.

$$a_{ij} = f(s_{ij}) = \begin{cases} 1 & s_{ij} \geq \tau \\ 0 & s_{ij} < \tau \end{cases}$$

An important drawback when using the signum function is that valuable information might be lost due to this hard thresholding approach. Therefore we also consider the power adjacency function, defined as the absolute value of the correlations r_{ij} raised to a power β [Zhang and Horvath, 2005].

$$a_{ij} = s_{ij}^{\beta} = |r_{ij}|^{\beta} \ .$$

The use of the signum function leads to an unweighted, undirected network; whereas the use of the power adjacency functions leads to a weighted undirected network. An advantage of using the power adjacency function is the robustness of weighted network analyses with respect to the choice of β, when compared to unweighted networks [Zhang and Horvath, 2005].

The node connectivities and overall network connectivity were also computed. The connectivity of a node for an unweighted network is defined as the number of direct neighbours of a node. For weighted networks, the connectivity is defined as the sum of the weights of the links between the node and all of its neighbours, i.e. the row sum of the adjacency matrix.

A topological property that has been observed in brain networks and is closely related to the degree distribution is the assortativity of the network [Eguíluz et al., 2005, Joyce et al., 2010]. We explore this property in Appendix A.

The complete topology of the network is encapsulated in the adjacency matrix $A = a_{ij}$, which indicates which voxels are connected and the strength of each connection. As mentioned in the Introduction, a scale-free topology ($p(k) \propto k^{-\gamma}$) is often assumed for real life systems [Eguíluz et al., 2005]. This topology has been shown to remain unaltered even for tasks engaging different brain regions [Eguíluz et al., 2005]. A variation of this topology, the truncated scale-free topology ($p(k) \propto k^{-\gamma} \exp(-\alpha k)$), has also gained attention as a strong candidate for brain networks [Achard et al., 2006, He et al., 2007, Iturria-Medina et al., 2008, Bullmore and Sporns, 2009, Hayasaka and Laurienti, 2010, Ferrarini et al., 2011].

We analyzed the goodness-of-fit of both scale-free and truncated scale-free models to our dataset, under both hard and soft thresholding. However, since the dataset is extremely rich, we also explored a large number of more complex models. In particular, motivated by the shape of the degree distribution, we tested the addition of quadratic and cubic terms in both k and $\log(k)$, as given by:

$$log(p) = c - \alpha_1 k - \alpha_2 k^2 - \alpha_3 k^3 - \gamma_1 log(k) - \gamma_2 (log(k))^2 - \gamma_3 (log(k))^3 \qquad (3.1)$$

For completeness, we tested this full 7 parameter model, as well as the $2^7 = 128$ nested models which include every possible combination of terms in the full model. In the figures to follow, we mainly illustrate the results for a subset of these models, which we will denote as follows:

$$log(p) = c - \gamma_1 log(k) \qquad\qquad \text{scale-free} \qquad (3.2)$$

$$log(p) = c - \alpha_1 k - \gamma_1 log(k) \qquad\qquad \text{truncated scale-free} \qquad (3.3)$$

$$log(p) = c - \alpha_1 k - \alpha_2 k^2 - \gamma_1 log(k) \qquad\qquad \text{quadratic} \qquad (3.4)$$

$$log(p) = c - \alpha_1 k - \alpha_2 k^2 - \gamma_1 log(k) - \gamma_2 (log(k))^2 \qquad \text{log quadratic} \qquad (3.5)$$

Initially, the six concatenated runs for each subject were used to explore the behaviour of the four models above under hard and soft thresholding. We computed Akaike Information Criterion (AIC) values [Akaike, 1981], along with the mean connectivity of the network, for different values of the soft thresholding parameter β or the hard thresholding parameter τ. We then consider the balance between goodness-of-fit and connectivity to choose an appropriate threshold. To test the robustness of these results with respect to the choice of the threshold, we also computed the standard deviation of the resulting AIC values. Finally we explored models including all possible combinations of terms, to determine which terms are necessary for significant improvements in model fit, measured again by the Akaike Information Criterion.

We analyzed the weighted network for each subject with the use of Weighted Gene Co-Expression Network Analysis (WGCNA) software [Zhang and Horvath, 2005]. This software package was initially developed to find modules of genes in gene networks, but can be used more generally to analyze any weighted network. R (http://www.R-project.org) was used to carry out all the calculations. This work was made possible by the facilities of the Shared Hierarchical Academic Research Computing Network (SHARCNET:www.sharcnet.ca) and Compute/Calcul Canada.

3.3 Results

After pre-processing, an average of $N = 189273$ voxels were retained for each subject. As explained in the Introduction, one of the limitations of analyzing whole brain fMRI data sets is computational expense. In the present work the analysis of the complete data sets for the 10 subjects took 1.3 months of CPU time (Hound system in SHARCNET, with 480 InfiniBand cores, and 128GB of node memory).

3.3.1 Comparisons between hard and soft thresholding

To contrast hard and soft thresholding, the AIC values were computed for the subset of four models proposed in this paper, for both hard and soft thresholding as shown in Figures 3.1a and 3.1b respectively for a representative subject. Soft thresholding yielded substantially better fits to the data, across all parameter values. Best fits were obtained for values β ranging from four to six.

For Figures (3.1a), (3.1b), (3.2) and (3.3):

—— Scale-Free
--- Truncated Scale-Free
······ Quadratic
---- Log quadratic

These results were consistent across the 10 subjects. Figure 3.2 shows the mean and standard deviations for the AIC values for soft thresholding, for β values between 1 and 9. We note that the scale-free model showed the worst model fit, and the most variation among subjects. In contrast, the low AIC and small standard deviations achieved by the log quadratic model, particularly for β values of 4 to 6, demonstrates that good model fits were obtained by this model for all 10 subjects. We conclude that the combination of soft thresholding and the log quadratic model best fit the whole brain fMRI networks for this subset of models. In particular we note from Figure 3.2 that the lowest AIC value for the log quadratic model is achieved when
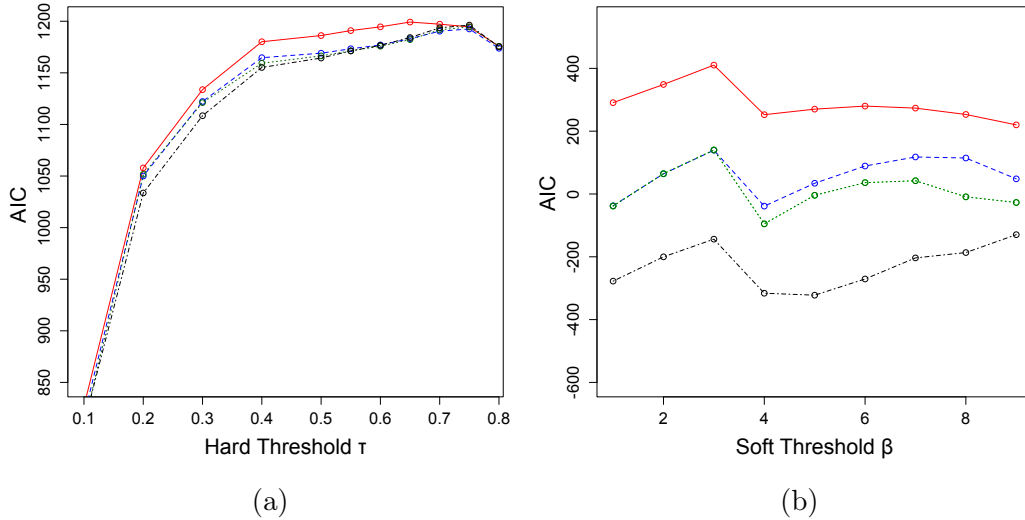
Figure 3.1: Akaike Information Criterion (AIC) values for scale-free (red solid line), truncated scale-free (blue dashed line), quadratic (green dotted line) and log quadratic (black dot-dashed line) models, versus the threshold parameter for either hard or soft thresholding (panels (*a*) and (*b*) respectively).

$\beta = 6$.

As the soft threshold power β is increased, overall network connectivity is concommitently reduced. Figure 3.3 explores this balance, demonstrating that for values of β at which excellent data fits are obtained, network connectivity remains high; for example at $\beta = 6$ the mean connectivity for the quadratic model is approximately 30. We therefore chose to use soft thresholding and a β value of 6 to further compare the full range of models, equations 3.2 to 3.5.
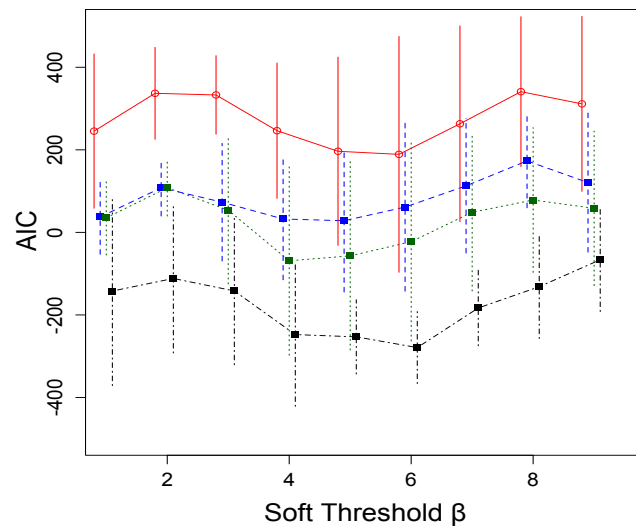
(a)

Figure 3.2: Model fit versus soft threshold power. Data from each subject were fit to the model and AIC values computed, then AIC values were averaged across subjects. The average AIC values are shown for the four model topologies: scale-free (red solid line), truncated scale-free (blue dashed), quadratic (green dotted) and log quadratic (black dot-dashed). Error bars show ±1 standard deviation and are staggered for clarity.
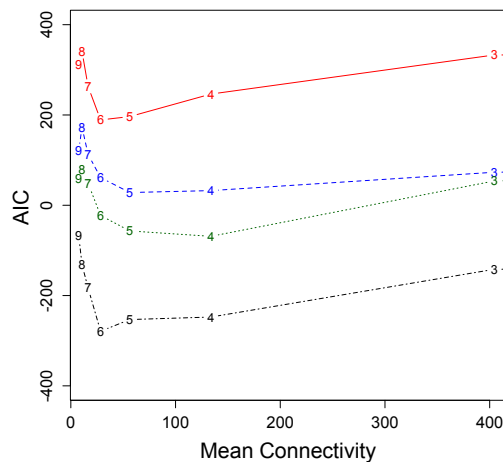
Figure 3.3: Plot of the average AIC values vs connectivity for scale-free (red solid line), truncated scale-free (blue dashed), quadratic (green dotted) and log quadratic (black dot-dashed) topologies for β values from 3 to 9.

3.3.2 Model choice

Since both the scale-free and truncated scale-free models have been used extensively in the literature, we first compared the performance of these models on the whole brain dataset. As expected the truncated scale-free model provides a better fit to the degree distribution than the scale-free model. An F-test applied to these nested models revealed that for 8 of the 10 subjects, a truncated scale-free topology was an improvement over the scale-free model, yielding p-values below 0.0001 for $\beta < 7$.

The large datasets analyzed here, however, gave us substantial power to analyze the degree distribution in greater detail than has been previously possible. Figure 3.4 shows one example of a degree distribution, $p(k)$, obtained using soft thresholding for a representative subject. The overall shape of the degree distribution illustrated here was common to all subjects. Clearly the scale-free (red solid line) and truncated scale-free (blue dashed line) models do not have enough flexibility to capture the network topology, when viewed at this level of detail. The best-fit given by the log

quadratic model (black dot dashed line) is shown for comparison.
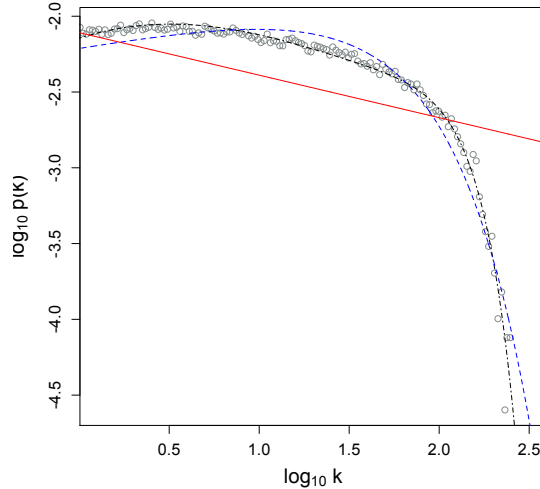
Figure 3.4: Log-log plot of the degree distribution $p(k)$ vs the connectivities k of a representative subject. The red solid line corresponds to a scale-free model fit, the blue dashed line to the truncated scale-free fit, and the black dot-dashed line corresponds to the log quadratic fit, for soft thresholding (with $\beta = 6$).

3.3.3   Further models

Since the inclusion of more parameters typically improves model fit, all possible combinations between the full model terms (including cubic terms) were tested for statistically significant improvement in fit, through the AIC. Using soft thresholding and $\beta = 6$, we computed the AIC for all 128 models, using the whole brain datasets of all subjects. We then compared all the models which have exactly n free parameters, finding the n-parameter model with the lowest mean AIC across subjects. Figure 3.5 shows the AIC values thus obtained for the "best" n-parameter model versus the number of parameters, n. For $\beta = 6$ we find that the log quadratic model ($n=4$) gave the best fit, and the inclusion of additional terms did not improve, or marginally improved the fit. For $\beta = 4$ or 5, the fit showed a minor improvement when the cubic

terms were included.
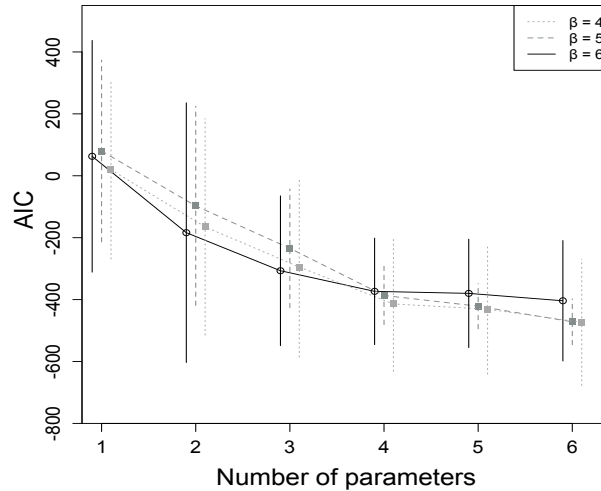
Figure 3.5: AIC versus model complexity for all subjects. The x-axis gives the number of free parameters in the model while the y-axis shows the mean AIC value across subjects for the n-parameter model with the lowest AIC. Error bars show ± 1 standard deviation.

Based on the results given in the previous sections, the soft threshold parameter $\beta = 6$ provided the best balance between low AIC, connectivity, and small variation among subjects; therefore, using this parameter, we conclude that the log quadratic model in which the degree distribution $p(k)$ follows

$$log(p) = c - \alpha_1 k - \alpha_2 k^2 - \gamma_1 log(k) - \gamma_2 (log(k))^2$$

provides the optimal model fit for whole brain fMRI data.

3.4 Discussion

Our analysis represents the first investigation of network connectivity of whole brain fMRI data at the voxel level, retaining all nodes and connections between approxi-

mately 190,000 voxels per subject for 10 subjects. Although it is often possible, and desirable, to focus attention on specific functional areas in fMRI studies, our results are completely unrestricted by anatomical region or by the choice of seed voxels. We thus aim to capture the most general features of functional connections at the voxel level. A task involving behavioural and cognitive flexibility was chosen due to the authors' interest in further research on the modulatory role of the prefrontal cortex on other structures (such as motor and affective). Eguíluz et al. [Eguíluz et al., 2005] demonstrated that the scale-free character of brain networks remained unaltered even for tasks engaging different brain regions, thus corroborating the generality of our findings.

The very large dataset we analyze allows us to finely differentiate between the models of network topology that have been previously suggested for fMRI data, along with new models which are natural extensions of previous work. It is important to mention that the vast majority of white matter nodes have degree < 1, and therefore they have no influence in our data fitting. The results we obtain support recent research suggesting that the network of correlated voxels in human brain fMRI data is better described by an exponentially truncated scale-free topology than a scale-free topology. We further demonstrate that the inclusion of two additional terms, yielding a novel topology we call the "log quadratic" model, gives a statistically significant improvement to model fit; with the inclusion of further terms the fit either does not improve or improves only marginally.

The two terms we add to the truncated scale-free model allow for greater flexibility in capturing the curvature of the degree distribution at a logarithmic scale. The statistically significant improvement in model fit is not surprising, given the observable bend or "kink" in this curvature, as seen near the intersection of the lines plotted in Figure 3.4. While our proposal of these model terms is largely empirical, we suggest that this bend may result from a class of high-degree nodes, the hubs, whose underlying topology scales differently than that of low-degree nodes. While earlier analyses based on seed voxels or regions of interest may have adequately sam-

pled these hubs, the preferential omission of low degree nodes, reducing the right hand side of the degree distribution, might also obscure this phenomenon. Clearly an investigation of the neuroanatomical locations and topological features of these hubs would be an important avenue for future work.

To further investigate the effects of thresholding, we compared the use of hard thresholding (connections have weight 1 if the correlation is above the threshold, 0 otherwise) with soft thresholding (connection weight is given by the correlation raised to some power; higher powers reduce connectivity). It was clear from this analysis that soft thresholding was superior to hard thresholding, and that the log quadratic model better fit the data irrespective of thresholding technique. The best fits were obtained with a combination of the log quadratic model and soft thresholding. This combination also yielded the best overall balance between model fit and connectivity.

With the use of network theory approaches, fMRI data sets can provide deep insights regarding the structural properties of networks of interaction in the brain. These methodologies allow us to understand the topology of such networks, but can also inform our understanding of functionality [Bullmore and Sporns, 2009]. An advantage of using network theory methodologies is that not only can we characterize general properties of the network as a whole, but also the properties of each individual node. For example, we can compute metrics such as the network's clustering coefficient, global connectivity and degree distribution, as well as, at the node level, features such as node centrality or within-module connectivity [Guimerà et al., 2005, Guimerà and Amaral, 2005, Joyce et al., 2010]. Although the analysis of individual node characteristics in whole brain data is still computationally prohibitive, we look forward to future work in this fascinating area.

Bibliography

Achard, S., Salvador, R., Whitcher, B., Suckling, J., and Bullmore, E. (2006). A resilient, low-frequency, small-world human brain functional network with highly connected association cortical hubs. *J Neurosci*, 26(1):63–72.

Akaike, H. (1981). Likelihood of a model and information criteria. *J Econometrics*, 16(1):3–14.

Barabási, A.-L. and Albert, R. (1999). Emergence of scaling in random networks. *Science*, 286(5439):509–512.

Barabási, A.-L., Albert, R., and Jeong, H. (2000). Scale-free characteristics of random networks: the topology of the world-wide web. *Phys A*, 281(1-4):69–77.

Barabási, A.-L. and Bonabeau, E. (2003). Scale-free networks. *Sci Am*, 288(5):50–59.

Bullmore, E. and Sporns, O. (2009). Complex brain networks: graph theoretical analysis of structural and functional systems. *Nat Rev Neurosci*, 10(3):186–98.

Cox, R. W. (1996). AFNI: software for analysis and visualization of functional magnetic resonance neuroimages. *Comput Biomed Res*, 29(3):162–173.

Eguíluz, V. M., Chialvo, D. R., Cecchi, G. A., Baliki, M., and Apkarian, A. V. (2005). Scale-free brain functional networks. *Phys Rev Lett*, 94(1):018102.

Erdös, P. and Rényi, A. (1959). On random graphs i. *Publ Math Debrecen*, 6:290.

Eubank, S., Guclu, H., Kumar, V. A., Marathe, M. V., Srinivasan, A., Toroczkai, Z., and Wang, N. (2004). Modelling disease outbreaks in realistic urban social networks. *Nature*, 429(6988):180–184.

Ferrarini, L., Veer, I. M., van Lew, B., Oei, N. Y. L., van Buchem, M. A., Reiber, J. H. C., Rombouts, S. A. R. B., and Milles, J. (2011). Non-parametric model selection for subject-specific topological organization of resting-state functional connectivity. *NeuroImage*, 56(3):1453–1462.

Greening, S. G., Finger, E. C., and Mitchell, D. G. V. (2011). Parsing decision making processes in prefrontal cortex: Response inhibition, overcoming learned avoidance, and reversal learning. *NeuroImage*, 54(2):1432–1441.

Guimerà, R. and Amaral, L. N. A. (2005). Cartography of complex networks: modules and universal roles. *J Stat Mech*, 2005(P02001):P02001+.

Guimerà, R., Mossa, S., Turtschi, A., and Amaral, L. (2005). The worldwide air transportation network: Anomalous centrality, community structure, and cities' global roles. *Proc Natl Acad Sci U S A*, 102(22):7794.

Hayasaka, S. and Laurienti, P. J. (2010). Comparison of characteristics between region-and voxel-based network analyses in resting-state fMRI data. *NeuroImage*, 50(2):499–508.

He, Y., Chen, Z. J., and Evans, A. C. (2007). Small-world anatomical networks in the human brain revealed by cortical thickness from MRI. *Cereb Cortex*, 17(10):2407–2419.

Iturria-Medina, Y., Sotero, R. C., Canales-Rodríguez, E. J., Alemán-Gómez, Y., and Melie-García, L. (2008). Studying the human brain anatomical network via diffusion-weighted MRI and graph theory. *NeuroImage*, 40(3):1064–1076.

Joyce, K., Laurienti, P., Burdette, J., and Hayasaka, S. (2010). A new measure of centrality for brain networks. *PLoS One*, 5(8):e12200.

Liang, X., Wang, J., Yan, C., Shu, N., Xu, K., Gong, G., and He, Y. (2012). Effects of different correlation metrics and preprocessing factors on small-world brain functional networks: a resting-state functional MRI study. *PLoS One*, 7(3):e32766.

Newman, M. E. J. (2001). Scientific collaboration networks. ii. shortest paths, weighted networks, and centrality. *Phys Rev E*, 64:016132+.

R Development Core Team (2008). *R: A Language and Environment for Statistical Computing*. R Foundation for Statistical Computing, Vienna, Austria. ISBN 3-900051-07-0.

Sales-Pardo, M., Guimerà, R., Moreira, A., and Amaral, L. (2007). Extracting the hierarchical organization of complex systems. *Proc Natl Acad Sci U S A*, 104:15224–15229.

Salvador, R., Suckling, J., Coleman, M., Pickard, J., Menon, D., and Bullmore, E. (2005). Neurophysiological architecture of functional magnetic resonance images of human brain. *Cereb Cortex*, 15(9):1332–42.

Schwarz, A. J. and McGonigle, J. (2011). Negative edges and soft thresholding in complex network analysis of resting state functional connectivity data. *NeuroImage*, 55(3):1132–1146.

Slobounov, S., Gay, M., Zhang, K., J., B., Pennell, D., Sebastianelli, W., Horovitz, S. G., and Hallett, M. (2011). Alteration of brain functional network at rest and in response to YMCA physical stress test in concussed athletes: RsfMRI study. *NeuroImage*, 55(4):1716–1727.

Strogatz, S. H. (2001). Exploring complex networks. *Nature*, 410(6825):268–276.

Vincent, J., Snyder, A., Fox, M., Shannon, B., Andrews, J., Raichle, M., and Buckner, R. (2006). Coherent spontaneous activity identifies a hippocampal-parietal memory network. *J Neurophysiol*, 96(6):3517–3531.

Zhang, B. and Horvath, S. (2005). A general framework for weighted gene co-expression network analysis. *Stat Appl Genet Mol Biol*, 4(1):Article17.

Chapter 4

Network analysis of human fMRI data suggests modular restructuring after simulated acquired brain injury

4.1 Introduction

Mild traumatic brain injury (TBI), or concussion, refers to a neurological injury caused by a mechanical trauma to the brain. TBI can result in a variety of symptoms such as confusion, amnesia, irritability, emotional lability, severe headaches, and hypersensitivity to sensory input. Although the concerns over the apparent growing rates of concussion in professional sports are now widely publicized, TBI is a major health concern in the general population. For example, it is estimated that between 1.4 and 3.8 million TBIs occur each year in the United States [Langlois and Rutland-Brown, 2006, Maruta et al., 2010, Faul et al., 2010]. TBI is associated with a complex series of neurochemical, neurometabolic, and anatomical effects that are poorly understood. In some cases, these effects are thought to result in subsequent neurocognitive dysfunction and even permanent damage [Johnson et al., 2012].

Although the precise pathophysiology behind the neurocognitive and emotional dysfunction associated with TBI remains unclear, there are several proposed models. First, closed head injuries are associated with considerable acceleration and deceleration forces which can result in cortical contusions as neural regions strike adjacent areas of the skull. Because of their location and close proximity to the skull, the frontal lobes are susceptible to damage in closed head injuries [Levin et al., 1987].

Another pathology thought to play an important role in the neurocognitive seque-
lae of TBI is diffuse axonal injury [Johnson et al., 2012]. TBI can lead to axonal
degeneration, microscopic lesions, myelin loss, and axonal swelling [Maruta et al.,
2010, Johnson et al., 2012]. Together, cortical lesions and DAI are thought to under-
lie many of the features associated with concussion.

At present, the precise nature of the events that lead to cognitive and emo-
tional dysfunction following TBI are poorly understood [Maruta et al., 2010]. A
better understanding of the nature of the neurological effects of concussion is essen-
tial to determine the best intervention and the length of time required before high-risk
activities can be safely resumed. Functional magnetic resonance imaging (fMRI) is
a well-established and powerful technique for the elucidation of the complex net-
work of functional interactions in the human brain. The hemodynamic signals of
fMRI typically reveal task-specific correlations between anatomically distinct regions
of the brain; a high degree of temporal correlation is assumed to represent a func-
tional connection between brain areas. Recent advances in network analysis further
allow correlated fMRI signals to be clustered into distinct groups of highly intercon-
nected voxels, known as modules [Bullmore and Sporns, 2009, Wang et al., 2010a].
The modular composition of the human brain has been previously studied for both
resting-state [Meunier et al., 2009, He et al., 2009, Wang et al., 2010b, Moussa et al.,
2012], and task-related functional networks [Kitzbichler et al., 2011, Gallos et al.,
2012]. Changes in modular composition have been described in diverse disorders in-
cluding Alzheimer's disease [de Haan et al., 2012] and schizophrenia [Alexander-Bloch
et al., 2010].

In order to shed light on the effects of TBI at the functional network or mod-
ular level, our research groups are engaged in the acquisition and modular analysis
of fMRI data from subjects post-TBI. Complementary to this effort, however, we
need to gain an understanding of how modular structure might be altered by specific
mechanisms of brain injury, such as cortical contusions or axonal injury. In order to
do so, we explored a model of TBI in which we could precisely control the extent and

type of brain injury, examining in detail the effects of distinct mathematical models of TBI at the network level. One of the main advantages of mathematical analysis over testing patients who have suffered a TBI is that mathematical models allow us to vary the extent and location of the injury precisely in a non-invasive manner.

In the present study, we first generated undirected functional modular networks for a sample of control subjects, during the performance of a task designed to probe decision making and inhibitory functions within the human prefrontal cortex [Clark et al., 2007, Greening et al., 2011], functions known to be disruptive following frontal lobe pathology [Aron et al., 2004, Roberts, 2006], and concussion [Mattson and Levin, 1990]. Given the susceptibility of the frontal lobes to damage during TBIs, and the sensitivity of this task to prefrontal dysfunction, we reasoned that this task would be appropriate for modelling the effects of concussion on brain function.

The effects of three potential mechanisms of simulated TBI on the integrity of these functional networks were examined: diffuse axonal degeneration, focal TBIs and diffuse microlesions. Diffuse axonal degeneration represents non-specific axonal injuries and was modelled by the weakening of connections throughout the brain. In contrast, focal TBIs were simulated through the destruction of specific voxels at points of impact which might approximate contusions sustained from coup or contre coup injuries. Diffuse microlesions involved the destruction of randomly chosen network nodes distributed throughout the brain.

In order to test the TBI models proposed in this paper, we compared the original, unperturbed networks to the networks computed after the simulated TBI was imposed. Complete fMRI data sets were analyzed without the use of seed voxels or restrictions on specific brain areas in order to retain as much information as possible. In particular, we were interested in which modules are preserved or degenerated during injury, and to what extent. To quantify this, we compared the coordinates of the injured modules with the coordinates of the pre-injured modules to determine how much of the pre-injury structure was preserved after the injury. We refer to this

concept as "percentage identity" and introduce it in this paper as an outcome measure. The "percentage identity" will therefore quantify the percentage of a post-injury module's voxels that belong to a given pre-injury module. Injuries that disintegrate the original modular structure resulting in low percentage identity values will be regarded as highly disruptive. A second outcome measure was also considered; we refer to any post-injury modules that retained a high percentage of the pre-injury modular structure as "main post-injury subdivisions". The percentage threshold above which a post-injury module was considered a main post-injury subdivision was defined heuristically as 10%. These two measures combined describe the extent to which the modular structure of the network has degenerated. For example, if a given module has only one main post-injury subdivision with a high percentage identity, this implies that the modular structure was largely preserved. In contrast, if such a module had many main post-injury subdivisions with low percentage identity values, this module was highly disrupted by the injury.

4.2 Materials and methods

4.2.1 MRI data acquisition and preprocessing

For a complete description of the cognitive task and data acquisition see Greening *et al.*, 2011. One of the limitations of analyzing whole brain fMRI data sets is computational expense. To overcome this limitation some studies consider small sample sizes [Eguíluz et al., 2005, Achard et al., 2006, Hagmann et al., 2008], and choose representative subjects to present their results [Meunier et al., 2009, Joyce et al., 2010]. For this study a subset of the original sample was used. However, the large datasets of each subject give us substantial power to analyze the TBI models in great detail. Briefly, 3 subjects were scanned on a forced choice response reversal task using a 3T Siemens MRI scanner with a 32 channel head coil. We performed 6 runs of the task while collecting the Blood Oxygenation Level Dependent (BOLD) signal. We used a T2-gradient echo-planar imaging sequence (repetition time = 3 seconds; echo time = 30ms; 120x120mm matrix; field of view of 240mm). We acquired 45 slices at

2x2mm in-plane resolution in the axial plane and a slice thickness of 2.5mm, yielding whole brain coverage in 2x2x2.5mm voxels. In each run we acquired 106 whole brain volumes in this manner, for a total of 636 total volumes across the six runs. The time series data obtained during the 6 functional runs was preprocessed using Analysis of Functional Neuroimaging (AFNI) software [Cox, 1996]. During pre-processing we removed the first six volumes of each run so as to ensure magnetization equilibrium was reached, leaving a total of 600 volumes per subject. The voxel time series for each volume was aligned to the same temporal origin, and each volume was registered to the first volume of the first run to correct for motion.

The time series data for each voxel were then normalized at each time point by dividing the signal intensity by the mean signal intensity of that voxel for all volumes within each run. A regression analysis using a general linear model was performed to remove the estimated baseline drift from the raw time series data. The three-dimensional raw time series data minus drift were then warped into standard space, based on the atlas of Talairach and Tournoux [Talairach and Tournoux, 1988]. Finally, a whole brain mask was applied to the data to remove voxels that were clearly not part of the brain from analysis. Thus, our final dataset consisted of 600 volumes for 3 subjects, with full brain coverage resulting in an average of 190000 voxels per subject. All data were collected as approved by Western University Human Research Ethics Board.

4.2.2   Correlation analysis

After pre-processing the Pearson correlation coefficient r_{ij} between the time series of each pair of voxels was computed, such that $|r_{ij}|$ gives a measure of the similarity or temporal correlation between voxels i and j. We then computed a connection strength matrix or adjacency matrix A. Based on previous analyses [Ruiz-Vargas et al., tics], we used the power adjacency function, defined as the absolute value of the correlations, r_{ij}, raised to the power $\beta = 6$:

$$a_{ij} = |r_{ij}|^{\beta} \ .$$

In previous work we have demonstrated that a value of 6 for the parameter β yields a good compromise between reducing noise and retaining high network connectivity in whole-brain fMRI data [Ruiz-Vargas et al., tics]. The connectivity of a node is defined as the sum of the weights of the links between the node and all of its neighbours, i.e. the row sum of the adjacency matrix.

4.2.3 Modular analysis

For the analysis, three subjects with very similar modular structure were chosen. In the figures to follow, we illustrate results obtained in one representative subject. This subject was chosen based on previous results drawn from the same data set, in which the whole brain network topology was analyzed in detail, for 10 subjects. The representative subject chosen for this paper showed low Akakike Information Criterion (AIC) values in excellent accordance with whole brain network topology found in previous studies [Ruiz-Vargas et al., tics].

To identify the modules of the network, average linkage hierarchical clustering was used to cluster similar nodes in a dendogram, whose branches determine the modules [Langfelder et al., 2008]. Instead of the commonly-used pairwise correlation r_{ij}, we used topological overlap as a measure of similarity at this stage of the analysis [Ravasz et al., 2002, Zhang and Horvath, 2005]. Using the topological overlap is advantageous over pairwise correlation since it considers not only the adjacency between two voxels, but also the overlap in the sets of neighbours of the two voxels. In particular, modules are defined as groups of nodes with high topological overlap, defined as:

$$W_{ij} = \frac{l_{ij} + a_{ij}}{min\{k_i, k_j\} + 1 - a_{ij}}$$

where $l_{ij} = \sum_u a_{iu} a_{uj}$, $k_i = \sum_u a_{iu}$ is the node connectivity, and $a_{ij} \in [0, 1]$ are the entries of the adjacency matrix [Ravasz et al., 2002].

Finally the modules were automatically detected using the tree cut method [Langfelder et al., 2008] which identifies modules based not only on absolute height in the dendogram, but also on their shape.

Pre- and post-injury modules were then compared. This was done by comparing the coordinates of the injured modules with the coordinates of the pre-injured modules, and computing the percentage of each post-injury module's voxels which belonged to a specific pre-injury module. The numbers of voxels in each module that belong to the main brain areas, based on the atlas of Talairach and Tournoux, were also calculated and used as another measure to compare modules.

The weighted network for each subject was analyzed with the use of Weighted Gene Co-Expression Network Analysis (WGCNA) software [Zhang and Horvath, 2005] and R (http://www.R-project.org) [R Development Core Team, 2008]. This work was made possible by the facilities of the Shared Hierarchical Academic Research Computing Network (SHARCNET:www.sharcnet.ca) and Compute/Calcul Canada.

4.2.4 Injury models

We simulated three mathematical models of TBIs, in order to examine their effects on the modular structure of the original intact network.

The first model was full brain axonal degeneration, in which the strength of every connection in the brain was reduced. We used a simple model in which the strength of each connection was reduced by a factor which depends linearly on the physical distance d_{ij} between voxels i and j in the subject's brain.

The full brain degeneration model was constructed as follows: An edge $i - j$ was selected from the network. The edge's strength was then weakened based on its physical length d_{ij} (distance between the chosen voxels i and j). In order to do so, the entries of the adjacency matrix were raised to a power α. Recalling that the entries

had previously been raised to a power of $\beta = 6$ to reduce the noise as explained in the analysis section this yields:

$$\tilde{a}_{ij} = a_{ij}^\alpha = |r_{ij}|^{6\alpha}$$

where $\tilde{a}_{ij}$ are the new entries of the adjacency matrix for the damaged edges. The parameter α was reduced linearly with physical distance, such that

$$\alpha = \alpha_{max} - \frac{d_{max} - d_{ij}}{d_{max} - d_{min}}(\alpha_{max} - 1)$$

where $d_{max} = max\{d_{ij}\}$, $d_{min} = min\{d_{ij}\}$, and α_{max} is the maximum value of α to be considered. This procedure was repeated for all the edges in the network.

Axonal degeneration or "shearing" was performed for all three subjects and three different values of α_{max} were considered such that the overall exponent $6\alpha_{max} = 12, 9$ or 7.

The focal TBI and diffuse microlesion injuries were modelled by removing nodes from the network. In focal TBIs, the subject's brain is injured only in a specific area, as opposed to axonal degeneration which may affect the whole brain. To simulate focal TBI, the voxels chosen as the focal points of the injury were identified manually with the use of AFNI. The area affected by the injury was modelled as a sphere centred at the focal point. We assume that every voxel inside the sphere was removed from the network, whereas the voxels outside of the sphere remained unharmed. This was achieved by removing the rows and columns of the adjacency matrix that correspond to the chosen nodes. For the simulations the focal points considered were the most frontal voxels of each hemisphere with spatial (x,y,z) coordinates of (-17,-65,12) and (15,-65,2); the coordinates are based on the Talairach Tournoux atlas. Let L be the largest physical distance within the network; physically this is the distance from the most anterior part of the frontal lobe to the most posterior aspect of the occipital lobe. We report findings for a sphere radius of $L/10$ and $L/20$, which roughly correspond to injuries with radii of 17 and 8 mm respectively.

The diffuse microlesion injury involved randomly selecting nodes and removing them from the network. This was achieved by removing the rows and columns of the adjacency matrix that correspond to each node. This procedure was repeated for a fraction of the nodes in the network. We report findings for the removal of 1/20th of the total of nodes in the network. The severity of the latter two injuries was chosen in such a way that the overall connectivity of the network was reduced by a similar amount after each injury.

Two other models were also considered: random weakening of nodes and targeted attacks. Results for these models are shown in Appendix B.

4.3   Results

4.3.1   Pre-injury modular decomposition

The modular analysis of the original, unperturbed networks revealed five main modules. The modules were numbered based on their size (for example, module 1 corresponds to the largest module). The percentage identity between modules was measured between all subjects; high percentage identity values revealed that these modules were consistent across subjects. Figure 4.1 shows the five modules for a representative subject. The brain regions included in each module are:

- Module one : right and left middle frontal gyrus, right superior frontal gyrus, right precuneus, left and right inferior frontal gyrus

- Module two: left middle frontal gyrus, left and right precuneus, left superior temporal gyrus, right precentral gyrus, right inferior frontal gyrus, left cingulate gyrus, left superior parietal lobule.

- Module three: left middle frontal gyrus, left middle temporal gyrus, left inferior frontal gyrus, left precentral gyrus, left superior frontal gyrus, left medial

frontal gyrus, left precuneus.

- Module four: right cingulate gyrus, left superior temporal gyrus, left cingulate gyrus, right inferior parietal lobule, left and right precentral gyrus, right medial frontal gyrus, left and right insula.

- Module five: left middle occipital gyrus, left declive, right middle occipital gyrus, right lingual gyrus, left cuneus, right and left inferior occipital gyrus
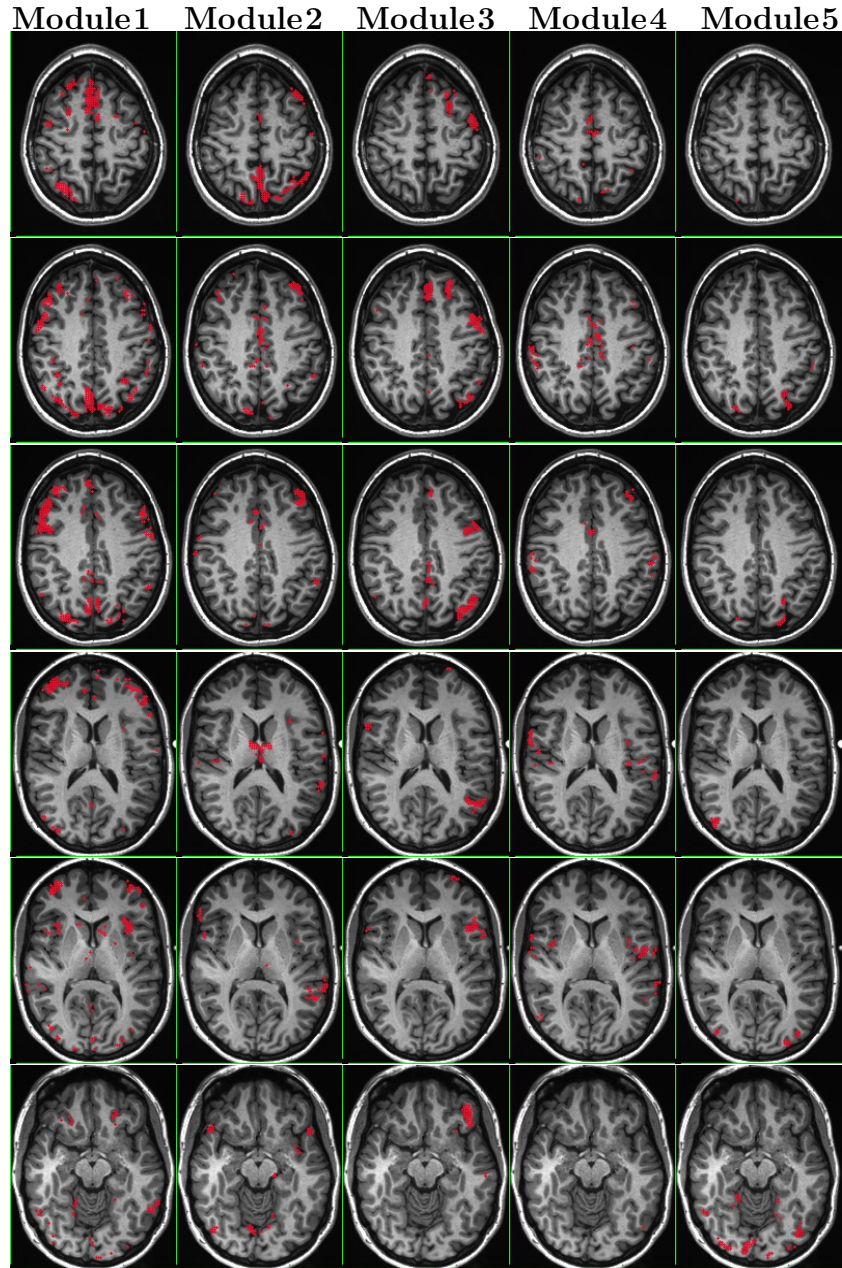
Figure 4.1: Modular structure for one representative subject. Six horizontal slices are shown for the five largest modules identified by modular analysis.

4.3.2 Diffuse axonal injury across the whole brain

After performing the clustering analysis for both the pre-injury and post-diffuse axonal injury (DAI) network, it was found that the largest module had 3 main post-

injury subdivisions irrespective of the value of α. For the representative subject with an α value of 2, the first of the main post-injury subdivisions retained 64% identity with the corresponding pre-injury module, that is, 64% of its voxels were part of the largest pre-injury module. The second main post-injury subdivision retained 47% identity with the pre-injury module, whereas the last only retained 11%. This is illustrated in Figure 4.2, which shows a colour plot for percentage identity pre- and post-injury. Figure 4.2 illustrates that pre-injury module 1 subdivides into three post-injury modules, while pre-injury module 3 is absent from the post-injury modules. In contrast, pre-injury modules 5 and 6 are relatively unaffected by the injury.
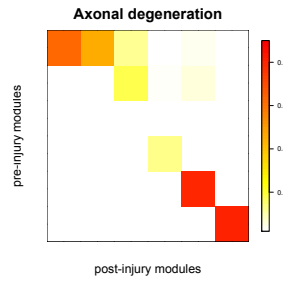
Figure 4.2: Percentage identity colour plot for axonal degeneration ($\alpha = 2$). On the y axis the pre-injury modules are shown from 1 to 6, top to bottom, and on the x axis the main post-injury subdivisions. Darker colour indicates a higher percentage identity between the two modules. The figure illustrates that the first pre-injury module is partitioned into three modules post-injury, while the 5th and 6th pre-injury modules are relatively unaffected by the injury.

4.3.2.1 Effects of simulated axonal degeneration on prefrontal cortical networks

Figure 4.3a shows a histogram of the fraction of voxels in the largest pre-injury module, pre-injury module 1, that belong to each prefrontal cortical region for $\alpha = 2$; highly represented regions in this module are shown. The compositions of all the main post-injury subdivisions (shown as Post-Injury 1, 2 and 3 in the graph) are shown for comparison.

Figure 4.3b indicates that post-injury modules 1 and 2 include several of the prefrontal cortical areas that are highly represented in pre-injury module 1. However, we note that some of the cortical areas in pre-injury module 1 are not present in any of the three main post-injury subdivisions depicted in the graph. They are present in a fourth post-injury module, with a percentage identity with the pre-injury module that was too low (7%) to define it as a main subdivision.
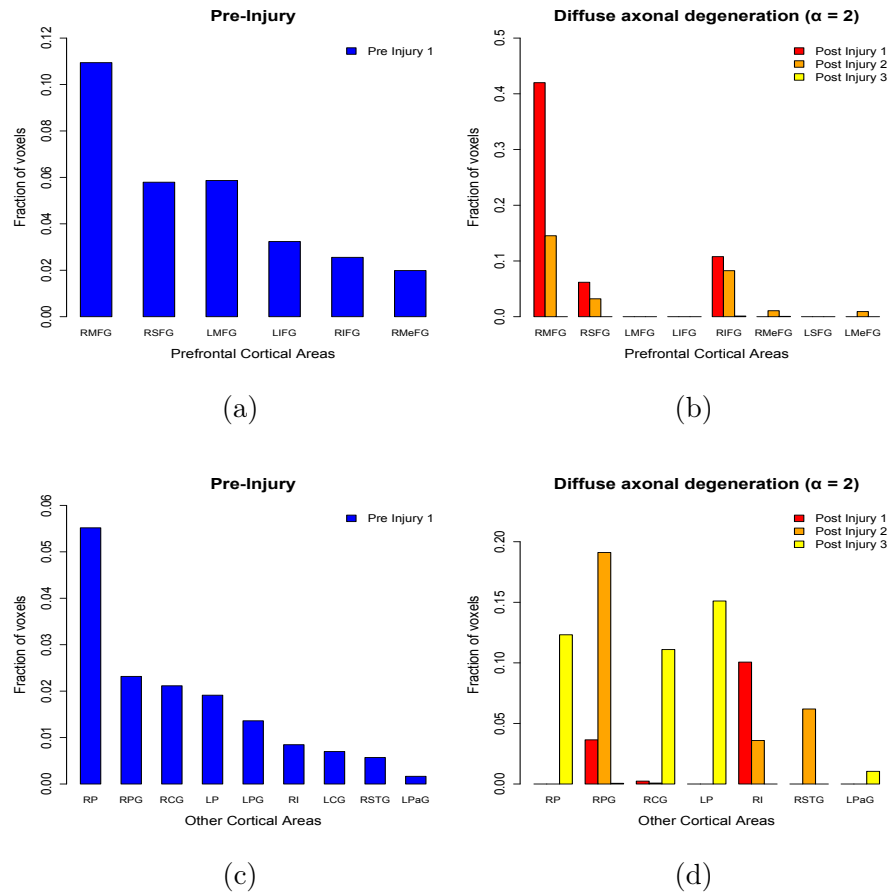
Figure 4.3: Fraction of voxels per cortical brain area. The first column shows the number of voxels per brain area divided by the total number of voxels in the largest pre-injury module (blue bars) for prefrontal and other cortical networks; the second column shows the number of voxels divided by the total for each of the main (largest percentage identity) post axonal degeneration ($\alpha = 2$) subdivisions. Brain areas are right middle frontal gyrus (RMFG), right superior frontal gyrus (RSFG), left middle frontal gyrus (LMFG), left inferior frontal gyrus (LIFG), right inferior frontal gyrus (RIFG), right medial frontal gyrus (RMeFG), left superior frontal gyrus (LSFG), left medial frontal gyrus (LMeFG), right precuneus (RP), right precentral gyrus (RPG), right cingulate gyrus (RCG), left precuneus (LP), left precentral gyrus (LPG), right insula (RI), left cingulate gyrus (LCG), right superior temporal gyrus (RSTG), left parahippocampal gyrus (LPaG).

4.3.2.2   Effects of simulated axonal degeneration on other networks

A histogram of other cortical brain areas is shown in Figure 4.3c. As we can see from Figure 4.3d, after axonal degeneration some important areas that once belonged to the same module were functionally separated: the precuneus and parahippocampal gyrus (RP,LP, LPaG) are mainly included in the third main post-injury subdivision (yellow bars), whereas the right precentral gyrus (RPG) and the right superior temporal gyrus (RSTG) are mainly included in the second main post-injury subdivision (orange bars). The right insula (RI) is mostly included the first main post-injury subdivision (red bars).

The sub-division of the pre-injury module can also be visualized in Figure 4.4. It is clear that the areas that formed a single module before the injury are now part of three distinct modules.
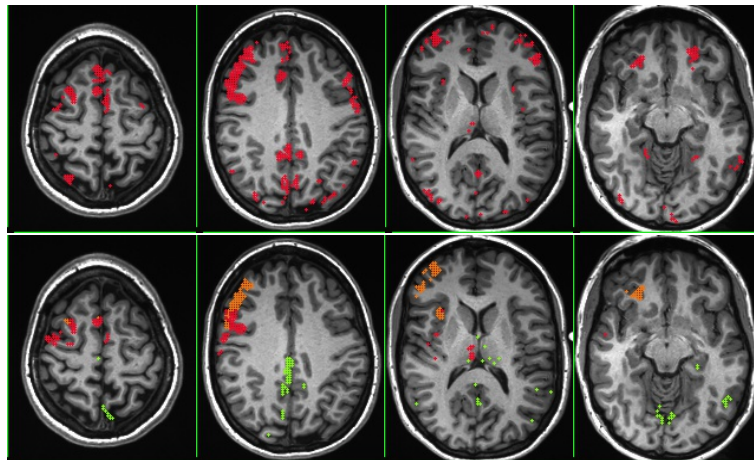

Figure 4.4: Modular subdivision after axonal degeneration ($\alpha = 2$). The top panels show the largest pre-injury module for four different slices. The bottom panels show the same slices for the three modules recovered after the injury, in colours red, orange and green.

4.3.2.3   Connectivities of pre-injury and post axonal degeneration networks

In addition, connectivities were calculated for both networks. Depending on the severity of the injury modelled ($\alpha\beta = 7, 9$ or 12), the overall network connectivity decreases between 20 and 60% after axonal degeneration. However, Table 4.1 shows that there was a significant increase of intra-modular connectivity in the two modules that most preserve the structure of the largest pre-injury module, suggesting that the resultant modules are more tightly connected than the pre-injury module, and therefore, more resilient.

4.3.2.4   Summary of axonal degeneration results

For axonal degeneration, for all subjects and all values of α_{max} considered, in the majority of the simulations, the largest module in each network were divided into three main post-injury subdivisions. The rest of the modules were damaged in accordance to the degree of the injury, but the subdivision of the largest module was common to all types of injury. It is also of interest to note that the third pre-injury module, consisting mostly of voxels from the left middle cortex, was no longer present in any of the main post-injury subdivisions, meaning it was either completely lost after the injury or broke into much smaller modules.

4.3.3   Simulated diffuse microlesions and focal lesions

For the remaining two injury models damage was inflicted through removal of a fraction of the nodes.

For the focal TBI model we found that for a small radius ($r = L/20$ or about 8 mm) the modules were not significantly affected by the injury. The modules were very resilient, preserving a high percentage of the pre-injury structure. This is due to the fact that only a negligible percentage of the modules' voxels were within the injured spheres, therefore the removal of the sphere had little to no effect in the overall modular structure for a small radius. However, for a larger radius ($r = L/10$ or about

17 mm) the injury caused a division of the largest module. The first main post-injury subdivision retained 90% identity with the pre-injury structure; whereas the second main post-injury subdivision shared 12% identity with the pre-injury structure.

The model of diffuse microlesions yielded the following results: when 1/20th of the nodes were removed, it likewise resulted in a division of the first module. The first main post-injury subdivision preserved 85% of the pre-injury structure, whereas the second main post-injury subdivision preserved 15% of the pre-injury structure.

4.3.3.1 Effects of node removal on prefrontal cortical networks

Figure 4.5a shows a histogram of the fraction of voxels in the largest pre-injury module that belong to each prefrontal cortical region; highly represented regions in this module are shown. The composition of all the main post-injury subdivisions with a high percentage identity is shown for comparison for both injuries. This figure also gives a direct comparison between the effect of diffuse microlesions (1/20th of nodes affected) and focal TBI ($r = L/10$) on the prefrontal cortical networks.

For the focal lesion model, Figure 4.5b shows that the middle frontal gyrus (RMFG and LMFG) is mostly included in the first main post-injury subdivision, as well as the left inferior frontal gyrus (LIFG) and right medial frontal gyrus (RMeFG). The rest of the frontal areas share a similar percentage identity between the two main post-injury subdivisions.

In contrast, for diffuse microlesions, Figure 4.5c shows that the first main post-injury subdivision mostly includes the right hemisphere prefrontal cortical areas, among them the right middle frontal gyrus (RMFG), right superior frontal gyrus (RSFG), the right inferior frontal gyrus (RIFG) and the right medial frontal gyrus (RMeFG), whereas the left superior frontal gyrus, and the left medial frontal gyrus clearly belong to the second main post-injury subdivision.

4.3.3.2 Effects of node removal on other cortical areas

Figure 4.6 provides similar histograms corresponding to other cortical areas; Figure 4.6b shows that after focal TBI with $r = L/10$ the right precuneus is mainly included in the first main post-injury subdivision. The right insula and right superior temporal gyrus are mainly included in the second post injury module.

Figure 4.5: Fraction of voxels per prefrontal cortical brain area. The first panel shows the number of voxels per brain area divided by the total number of voxels in the largest pre-injury module (blue bars); whereas the second and third panels show the number of voxels divided by the total for each of the main (largest percentage identity) post-injury subdivisions for focal TBI ($r = L/10$) and diffuse microlesions (1/20th nodes removed). Brain areas are right middle frontal gyrus (RMFG), right superior frontal gyrus (RSFG), left middle frontal gyrus (LMFG), left inferior frontal gyrus (LIFG), right inferior frontal gyrus (RIFG), right medial frontal gyrus (RMeFG), left superior frontal gyrus (LSFG), left medial frontal gyrus (LMeFG).

(a)

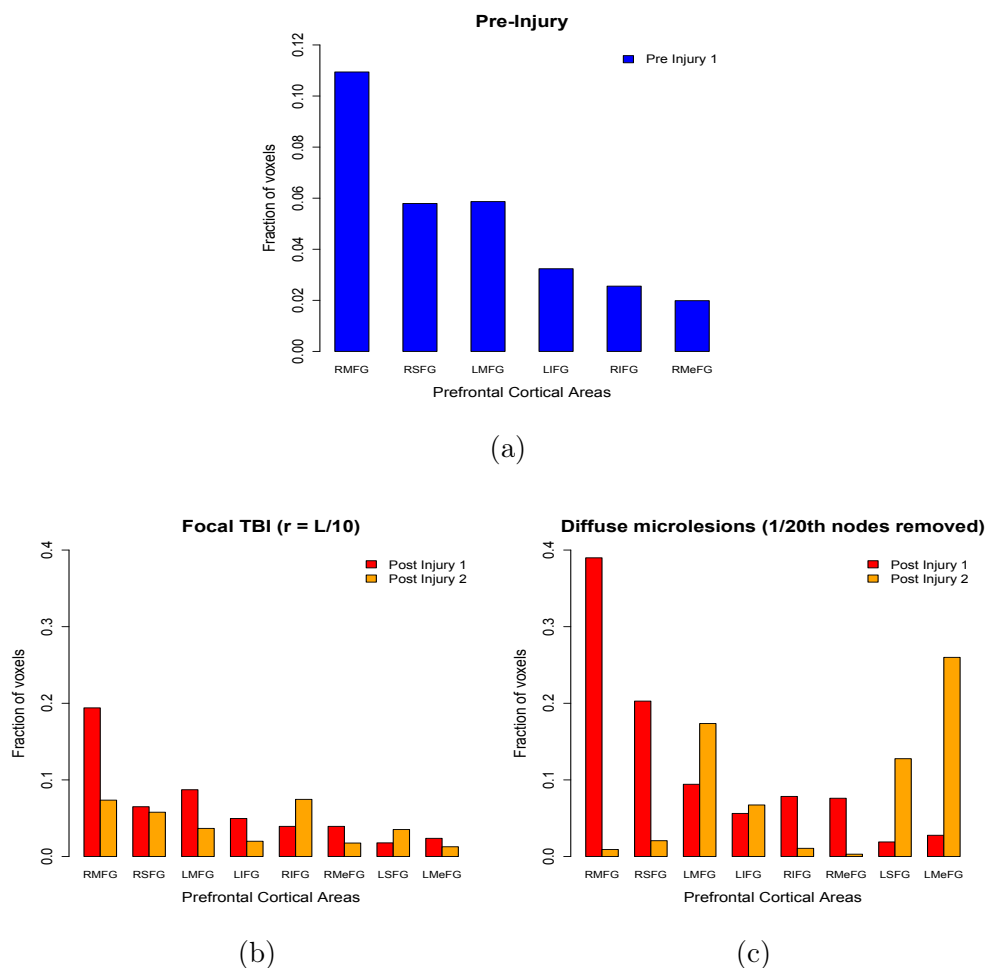(b)   (c)

Figure 4.6: Fraction of voxels per brain area. The first panel shows the number of voxels per brain area divided by the total number of voxels in the largest pre-injury module (blue bars); whereas the second and third panels show the number of voxels divided by the total for each of the main (largest percentage identity) post-injury subdivisions for focal TBI ($r = L/10$) and diffuse microlesions ($1/20th$ nodes removed). Brain areas are right precuneus (RP), right precentral gyrus (RPG), right cingulate gyrus (RCG), left precuneus (LP), right cuneus (RC), left precentral gyrus (LPG), left insula (LI), right insula (RI), left cingulate gyrus (LCG), right superior temporal gyrus (RSTG)

For diffuse microlesions, Figure 4.6c shows that the injury caused a division between the right and left hemisphere. The first main post-injury subdivision includes mainly the areas of the right hemisphere, such as the right precuneus (RP), right precentral gyrus (RPG) and the right cingulate gyrus (RCG); whereas the left

precuneus (LP), left precentral gyrus (LPG) and the left cingulate gyrus (LCG) are mainly included in the second main post-injury subdivision. However, both the right and left insula (RI,LI) are included in the first main post-injury subdivision. The sub-division of the pre-injury module can also be visualized in Figure 4.7. It is clear that the areas that formed a single module before the injury are now part of three distinct modules.

4.3.3.3   Connectivities of pre- and post-injury networks

For the focal TBI, the overall mean connectivity of the injured network, as well as the intra- and extra-modular connectivities remained similar to that of the pre-injury network for small values of r (data not shown). For $r = L/10$ overall connectivity decreased by between 2 and 3%, while the intra- and extra-modular connectivities of the main post-injury subdivision with the highest percentage identity increased as shown in Table 4.1.

For diffuse microlesions, the overall network connectivity decreased by 3% when 1/20th of the nodes were removed. The main post-injury subdivisions also showed an increase in the intra- and extra-modular connectivities as shown in Table 4.1.

4.3.3.4   Summary of focal TBI and diffuse microlesion results

When simulating a focal TBI for two frontal focal points, the first main post-injury subdivision preserved most of the original pre-injury structure, with the exception of the right insula and right superior temporal gyrus, both of which became partially disconnected from the other brain regions in the module. For diffuse microlesions, the largest module consistently divided after the injury. In particular, the left hemisphere was functionally separated from the right, except for the right and left insula which were both present in the right module. The division of the largest module along hemispheric lines, and the the resilience of the remaining modules, as well as the overall connectivity results were typical of all 3 subjects.
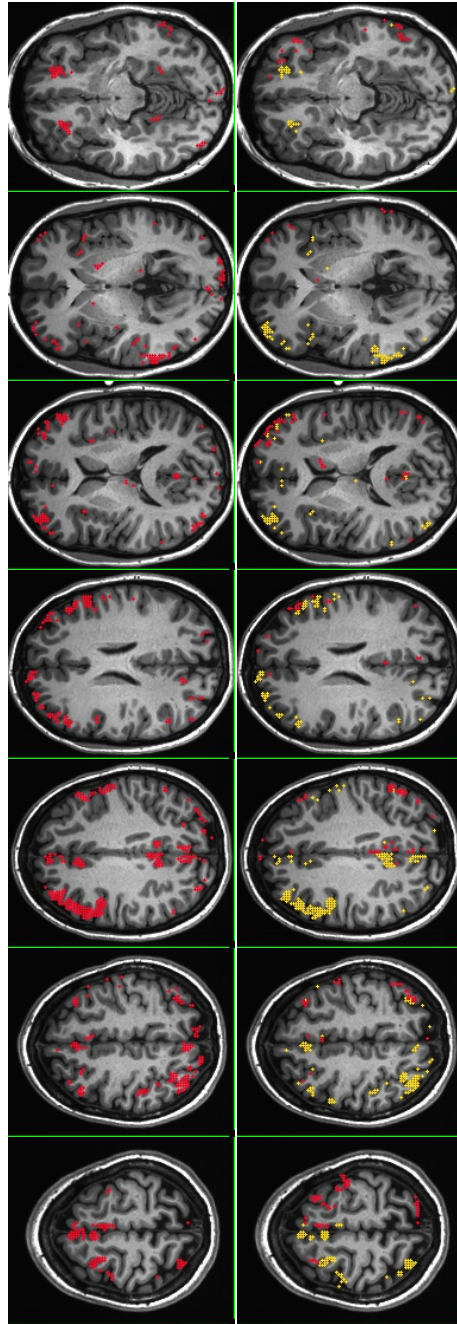
Figure 4.7: Modular subdivision after diffuse microlesion (1/20th nodes removed). The top panels show the largest pre-injury module for seven different slices. The bottom panels show the same slices for the two modules recovered after the injury, in colours red and yellow.

Module	Injury Type	Number of Voxels	Intramodular Connectivity	Extramodular Connectivity	Percentage Identity
Pre-Injury	None	4096	0.0067	0.0217	100%
Post-Injury 1	Axonal degeneration ($\alpha = 2$)	1603	0.0133	0.0275	64%
Post-Injury 2	Axonal degeneration ($\alpha = 2$)	1553	0.0181	0.0482	47%
Post-Injury 3	Axonal degeneration ($\alpha = 2$)	5155	0.0025	0.0109	11%
Post-Injury 1	Focal TBI ($r = L/10$)	3201	0.0093	0.0302	90%
Post-Injury 2	Focal TBI ($r = L/10$)	5965	0.0043	0.0149	12%
Post-Injury 1	Diffuse microlesions (1/20)	2227	0.0155	0.0593	85%
Post-Injury 2	Diffuse microlesions (1/20)	1308	0.0126	0.1096	15%

Table 4.1: Connectivity Table. Shown in this table, the number of voxels, intramodular and extramodular connectivity, and percentage identity for the largest pre-injury module, and subsequent main post-injury subdivisions for each model.

4.4 Discussion

The main purpose of this study was to model the possible effects of a TBI on the modular organization of the human brain. Briefly, three theoretical models for TBI were modelled. Axonal injury was modelled through a diffuse axonal degeneration model, focal lesions were modelled through localized node removal, and diffuse microlesions were modelled through random node removal. Percentage identity and main post-injury subdivision were introduced in this paper as outcome measures, along with extra- and intra-modular connectivity. The modelled injuries were shown to provoke disruptions in the modular structure of the brain network. For all three TBI models, the largest disruption occurred in the largest pre-injury module. Further analyses of the outcome measures revealed key differences among the effects of the modelled TBI's; these differences along with clinical implications of the study are discussed in detail below.

4.4.1 Impacts of TBI on modular structure

The mathematical model for full brain axonal degeneration was found to cause consistent changes in the modular organization of the network. The pre-injury module which consisted largely of the left middle cortex showed the biggest disruption, having no main post-injury subdivisions. The largest pre-injury module's structure also showed significant damage by decomposing into 3 main post-injury subdivisions; however high values of percentage identity were found for two of the subdivisions, indicating that they preserved some of the original modular structure. In addition, axonal degeneration caused some regions to be virtually absent from the main post-injury subdivisions, for example the left middle frontal gyrus and the right medial frontal gyrus.

Diffuse microlesions and focal TBI were modelled in such a way that the post-injury networks in both cases attained similar whole brain connectivity. Since the overall magnitude of these injuries is therefore similar, this allowed us to make a meaningful comparison between the two injuries. In both cases, the largest pre-injury

module's structure showed the most damage by decomposing into 2 main post-injury subdivisions. For both models, high values of percentage identity were found for the first of these subdivisions, indicating that much of the original structure was preserved post-injury. The structure of the post-injury subdivisions, however, differed for the two injury models. When diffuse microlesions were modelled (through random node removal), the left and right hemispheres were functionally separated post-injury. However, for the focal TBI a different pattern emerged, in which most brain areas were equally represented in both of the main post-injury subdivisions.

For each main post-injury subdivision, we also calculated the intramodular connectivity, or mean connectivity among nodes within the same module. After diffuse axonal degeneration, the post-injury subdivisions which had the highest percentage identity showed an increase in intramodular connectivity compared to the pre-injury module. This result suggests that these post-injury models might be less susceptible to further damage, whereas those with lower percentage identity might be more susceptible. Similarly, an increase in intramodular connectivity was observed in the main post-injury subdivision after either diffuse microlesions or focal TBI. In all three models, the extra modular connectivity was also found to increase for the post-injury subdivision that retained the highest percentage identity with the original module. This result suggests that even if the largest subdivision did not preserve the entirety of the original module's structure, it "compensated" by strengthening the connections among its own nodes, and increasing connection strength with other modules.

4.4.2 Clinical implications

Our research predicts that TBI may hinder the exchange of information between brain areas that are initially well-connected. In particular, we observed that the largest network of interconnected brain areas was consistently disrupted, irrespective of the underlying model of TBI. The three TBI mechanisms that we investigated, however, predicted different patterns of disruption in the functional network.

This study suggests that axonal injuries may significantly disrupt the overall modular structure of the network. In particular, there was a disruptive effect in the so-called default mode network (DMN), which is believed to be a baseline mode of brain function that is non-active during goal-directed activity [Raichle et al., 2001]. The DMN includes the posterior cingulate cortex, precuneus, and some areas on the medial temporal and medial prefrontal cortex [Raichle et al., 2001]. The precuneus and the posterior cingulate gyrus maintained high levels of communication between them, but were limited in their connections with the temporal and prefrontal cortical areas. A study by Bonelle *et al.* found that effective inhibitory control was associated with rapid deactivation of the DMN [Bonnelle et al., 2012]. Interestingly, in the same study it was found that abnormality of the DMN was specifically predicted by amount of white matter damage connecting the anterior insula to other prefrontal areas. It is worth noting that our axonal degeneration model also resulted in the anterior insula and inferior frontal gyrus (two areas associated with behavioural control and response inhibition [Aron et al., 2007, Mitchell, 2011] being disconnected from other prefrontal modules (see Figure 4.4). This result adds convergent validity to our mathematical model. Additionally, there was also a disengagement between sensory areas (e.g. precuneus) and the prefrontal cortex which plays a role in exerting executive control over sensory input [Knight et al., 1999]. This result may be closely related to the hypersensitivity to sensory input that is often associated with concussion.

According to our results, injuries that involve small volumes of brain tissue at diffuse locations may have a disruptive effect on the communication between the left and right hemispheres. Whereas pre-injury modules showed evidence of interhemispheric connectivity, these modules were split into separate left and right modules after this type of injury was imposed. Interestingly, the insula did not suffer from the same type of separation; both the left and right insula remained connected to each other, and connected to the right hemisphere module. The separation of brain areas along hemispheric boundaries suggests that aspects of cognition that require efficient communication between the hemispheres may be most affected by this type of injury.

In contrast, after after focal TBI simulation, brain areas in the first pre-injury module split almost symmetrically, such that both post-injury modules were composed of the same brain areas. Even though these two post-injury modules include voxels from similar brain regions, the exchange of information between them is limited. It is difficult to speculate regarding the behavioural or cognitive consequences of this kind of functional pattern. One possible outcome would be a reduction in the efficiency of cognitive processing, since the brain may now maintain two modules performing similar tasks with limited communication between them. Another possibility is that effects are more subtle in this case, since the post-injury module, whilst containing less voxels, retains a relatively high percentage of the pre-injury module.

4.4.3 Further considerations

It is important to note that the models of TBI which we explore are not mutually exclusive, and dysfunction following TBIs can result from a combination of diffuse and focal injuries. While we were able to strictly control the nature and extent of the simulated injuries, one limitation of the random node removal approach is the size of the removed nodes. Our data consists of nodes of $2 \times 2 \times 2.5$ mm, therefore we cannot remove smaller areas than this.

The results we discuss focus primarily on the largest pre-injury module because this module includes important areas of the prefrontal cortex that were of particular interest in the task context. In addition, and in line with evidence suggesting that the prefrontal cortex is particularly susceptible to TBI, this module was most disrupted by the injury models presented. Further analysis of the effects of a TBI on the smaller modules will also be of interest.

As mentioned in the Introduction, to accurately identify the cognitive consequences of the post-injury patterns predicted in this study, the impact of lesions in patient populations must be examined. Since the patterns of disruption differed among the three modes of injury we modelled, our work may shed light on possible

underlying pathologies, given fMRI modular analysis of subjects post-TBI. In addition, it will be useful to correlate neuropsychological and behavioural measures with changes in functional connectivity in this population.

Overall, we provide several mathematical models of TBI and a comprehensive analysis of their effects on modular structure of the functional brain network at the voxel level. This approach provides insight regarding the behavioural and cognitive effects of TBI and may also be used in future work to elucidate the functional mechanisms underlying other kinds of neurological and neuropsychiatric disorders.

Bibliography

Achard, S., Salvador, R., Whitcher, B., Suckling, J., and Bullmore, E. (2006). A resilient, low-frequency, small-world human brain functional network with highly connected association cortical hubs. *J Neurosci*, 26(1):63–72.

Alexander-Bloch, A., Gogtay, N., Meunier, D., Birn, R., Clasen, L., Lalonde, F., Lenroot, R., Giedd, J., and Bullmore, E. (2010). Disrupted modularity and local connectivity of brain functional networks in childhood-onset schizophrenia. *Front Syst Neurosci*, 4(October):16.

Aron, A. R., Durston, S., Eagle, D. M., Logan, G. D., Stinear, C. M., and Stuphorn, V. (2007). Converging evidence for a fronto-basal-ganglia network for inhibitory control of action and cognition. *J Neurosci*, 27(44):11860–11864.

Aron, A. R., Robbins, T. W., and Poldrack, R. A. (2004). Inhibition and the right inferior frontal cortex. *Trends Cogn Sci*, 8:170–177.

Bonnelle, V., Ham, T., Leech, R., Kinnunen, K., Mehta, M., Greenwood, R., and Sharp, D. (2012). Salience network integrity predicts default mode network function after traumatic brain injury. *Proc Natl Acad Sci U S A*, 109(12):4690–5.

Bullmore, E. and Sporns, O. (2009). Complex brain networks: graph theoretical analysis of structural and functional systems. *Nat Rev Neurosci*, 10(3):186–98.

Clark, L., Blackwell, A. D., Aron, A. R., Turner, D. C., Dowson, J., Robbins, T. W., and Sahakian, B. J. (2007). Association between response inhibition and working memory in adult ADHD: a link to right frontal cortex pathology?. *Biol Psychiat*, 61(12):1395–1401.

Cox, R. W. (1996). AFNI: software for analysis and visualization of functional magnetic resonance neuroimages. *Comput Biomed Res*, 29(3):162–173.

de Haan, W., van der Flier, W., Koene, T., Smits, L., Scheltens, P., and Stam, C. (2012). Disrupted modular brain dynamics reflect cognitive dysfunction in Alzheimer's disease. *NeuroImage*, 59(4):3085–93.

Eguíluz, V. M., Chialvo, D. R., Cecchi, G. A., Baliki, M., and Apkarian, A. V. (2005). Scale-free brain functional networks. *Phys Rev Lett*, 94(1):018102.

Faul, M., Xu, L., Wald, M. M., and Coronado, V. G. (2010). Traumatic brain injury in the United States: Emergency department visits, hospitalizations and deaths 2002–2006. *Atlanta, GA: Centers for Disease Control and Prevention, National Center for Injury Prevention and Control.*

Gallos, L. K., Sigman, M., and Makse, H. A. (2012). The conundrum of functional brain networks: small-world efficiency or fractal modularity. *Frontiers in physiology*, 3.

Greening, S. G., Finger, E. C., and Mitchell, D. G. V. (2011). Parsing decision making processes in prefrontal cortex: Response inhibition, overcoming learned avoidance, and reversal learning. *NeuroImage*, 54(2):1432–1441.

Hagmann, P., Cammoun, L., Gigandet, X., Meuli, R., Honey, C. J., Wedeen, V. J., and Sporns, O. (2008). Mapping the structural core of human cerebral cortex. *PLoS Biol*, 6(7):e159+.

He, Y., Wang, J., Wang, L., Chen, Z. J., Yan, C., Yang, H., Tang, H., Zhu, C., Gong, Q., Zang, Y., and Evans, A. C. (2009). Uncovering intrinsic modular organization of spontaneous brain activity in humans. *PLoS ONE*, 4(4):e5226+.

Johnson, V., Stewart, W., and Smith, D. (2012). Axonal pathology in traumatic brain injury. *Exp Neurol.*

Joyce, K., Laurienti, P., Burdette, J., and Hayasaka, S. (2010). A new measure of centrality for brain networks. *PLoS One*, 5(8):e12200.

Kitzbichler, M. G., Henson, R. N. A., Smith, M. L., Nathan, P. J., and Bullmore, E. T. (2011). Cognitive effort drives workspace configuration of human brain functional networks. *J Neurosci*, 31(22):8259–8270.

Knight, R., Staines, W., Swick, D., and Chao, L. (1999). Prefrontal cortex regulates inhibition and excitation in distributed neural networks. *Acta Psychol Amst*, 101(2-3):159–78.

Langfelder, P., Bin, Z., and Horvath, S. (2008). Defining clusters from a hierarchical cluster tree: The dynamic tree cut package for R. *Bioinformatics*, 24(5):719–720.

Langlois, J. and Rutland-Brown, W.and Wald, M. (2006). The epidemiology and impact of traumatic brain injury: A brief overview. *J Head Trauma Rehab*, 21(5):375–378.

Levin, H. S., Mattis, S., Ruff, R. M., Eisenberg, H. M., Marshall, L. F., Tabaddor, K., High Jr, W. M., and Frankowski, R. F. (1987). Neurobehavioral outcome following minor head injury: a three-center study. *J Neurosurg*, 66(2):234–243.

Maruta, J., Lee, S., Jacobs, E., and Ghajar, J. (2010). A unified science of concussion. *Ann N Y Acad Sci*, 1208.

Mattson, A. J. and Levin, H. (1990). Frontal lobe dysfunction following closed head injury. a review of the literature. *J Nerv Ment Dis*, 178(5):282–91.

Meunier, D., Lambiotte, R., Fornito, A., Ersche, K. D., and Bullmore, E. T. (2009). Hierarchical modularity in human brain functional networks. *Frontiers in neuroinformatics*, 3.

Mitchell, D. (2011). The nexus between decision making and emotion regulation: A review of convergent neurocognitive substrates. *Behav Brain Res*, 217(1):215–31.

Moussa, M. N., Steen, M. R., Laurienti, P. J., and Hayasaka, S. (2012). Consistency of network modules in resting-state fMRI connectome data. *PLoS ONE*, 7(8):e44428+.

R Development Core Team (2008). *R: A Language and Environment for Statistical Computing.* R Foundation for Statistical Computing, Vienna, Austria. ISBN 3-900051-07-0.

Raichle, M. E., MacLeod, A. M., Snyder, A. Z., Powers, W. J., Gusnard, D. A., and Shulman, G. L. (2001). A default mode of brain function. *Proc Natl Acad Sci U S A*, 98(2):676–682.

Ravasz, E., Somera, A., Mongru, D., Oltvai, Z., and Barabási, A. (2002). Hierarchical organization of modularity in metabolic networks. *Science*, 297(5586):1551.

Roberts, A. C. (2006). Primate orbitofrontal cortex and adaptive behaviour. *Trends Cogn Sci*, 10(2):83–90.

Ruiz-Vargas, E., Greening, S., Mitchell, D., and Wahl, L. (In review, SIAM J. Applied Mathematics). Topology of whole-brain fMRI networks: improving the truncated scale-free model.

Talairach, J. and Tournoux, P. (1988). *Co-Planar stereotaxic atlas of the human brain: 3-D proportional system: An approach to cerebral imaging.* Thieme.

Wang, J., Zuo, X., and He, Y. (2010a). Graph-based network analysis of resting-state functional MRI. *Front Syst Neurosci*, 4.

Wang, J., Zuo, X., and He, Y. (2010b). Graph-based network analysis of resting-state functional MRI. *Front Syst Neurosci*, 4.

Zhang, B. and Horvath, S. (2005). A general framework for weighted gene co-expression network analysis. *Stat Appl Genet Mol Biol*, 4(1):Article17.

Chapter 5

The gateway coefficient: a novel metric for identifying critical connections in modular networks

5.1 Introduction

Graph theoretical approaches have gained interest as tools to study a wide range of complex systems. Networks such as the internet, air traffic and land transportation infrastructure can be modelled through graph theory [Strogatz, 2001], which provides powerful metrics for quantifying a system's structural properties. Several topological properties of real life networks have been studied in depth, such as small-world topologies [Watts and Strogatz, 1998], clustering coefficients [Watts and Strogatz, 1998, Newman, 2001, Bullmore and Sporns, 2009] and modularity [Girvan and Newman, 2001, Newman and Girvan, 2004, Guimerà et al., 2007]. These properties not only provide insight into the systems' structure, but have also proven to be key markers of system behaviour. For example, a reduction in the small world topology of brain networks is associated with certain brain disorders [Bartolomei et al., 2006, Bassett et al., 2008, Stam et al., 2009, Cho and Choi, 2010]; another example arises in air transportation networks, in which the degree distribution can provide predictive measures of the system's resilience to failures and targeted attacks [Barrat et al., 2004, Guimerà et al., 2005].

Modular structure is an important topological property for a wide range of networks. In modular networks, nodes tend to form groups, or modules, composed of many strongly interconnected nodes; connections within the modules are dense,

whereas connections among the modules are more sparse [Girvan and Newman, 2001]. This implies that the majority of nodes in the network are preferentially connected to other nodes within the same module.

In contrast, nodes which form connections between the modules have been characterized mathematically, and are known as specialized hub nodes [Guimerà and Amaral, 2005]. Specialized hubs have an important role in maintaining efficient communication along the network, making their topological properties of great interest. The participation coefficient [Guimerà and Amaral, 2005] has been used to identify network hubs based on their connections with other nodes. This coefficient measures the diversity of a node's inter-modular connections and therefore depends on both the node's degree and its links to other modules. However, the participation coefficient is not able to identify nodes which play important roles in the overall network structure, in particular nodes which form key connections between modules. In the sections to follow, we propose a generalization of the participation coefficient, called the gateway coefficient, which depends not only on the node's individual properties but also on the network's modular structure. The gateway coefficient is able to rank nodes according to their participation in maintaining communication between modules, as well as within their own modules. We explore the gateway coefficient's behaviour in two very different but important example networks: the United States of America (U.S.) air transportation system and the human brain.

Since human mobility is central to the spread of communicable diseases, air transportation has a great impact on public health [McFarland, 1953]. It also has important economical and political implications [Britton, 1982, Button and Taylor, 2000]. For example, efficient route scheduling can reduce fuel consumption which will have positive impacts on the environment. In previous studies it has been shown that the air transportation system has a small-world topology and a scale-free degree distribution [Barrat et al., 2004]. Some studies [Guimerà et al., 2005] have also investigated node roles in such networks, based on the participation coefficient. In this study we explore the U.S international air transportation network's topological

features such as clustering, average path length, and degree distribution, as well as each airport's participation and gateway coefficients.

The second system analyzed in this paper is the network of functional connections in the human brain, as revealed by functional magnetic resonance imaging (fMRI). The topological properties of this network are well-studied, and show characteristic changes response to disorders affecting brain functions [Stam et al., 2009, Cho and Choi, 2010, Bullmore and Sporns, 2012]. Our main focus will be to identify regions characterized by high gateway coefficients; we predict that these regions have critical importance in the overall connectivity of the network.

5.2 Methods

5.2.1 Participation coefficient

Nodes can perform a wide variety of tasks in a network, from forming connections among modules, to strengthening the connections within them. An accurate characterization of node roles will deepen our understanding of the communication patterns of the network. For example, certain nodes have more connections compared to other nodes in the same module; such nodes are called hubs and are typically classified in terms of their within module degree z-score, defined as

$$z_i = \frac{k_{iS_i} - \overline{k}_{S_i}}{\sigma_{k_{S_i}}} \; .$$

Here S_i denotes the module to which node i belongs, k_{iS_i} is the number of connections from node i to module S_i, $\overline{k}_{S_i}$ is the average of k_{iS_i} over all the nodes in S_i, and $\sigma_{k_{S_i}}$ is its standard deviation [Guimerà and Amaral, 2005].

The participation coefficient P can also be used to further classify nodes. P is defined as

$$P_i = 1 - \sum_{S}^{N} \left(\frac{k_{iS}}{k_i} \right)^2$$

where N is the total number of modules, k_i is the degree of node i, and k_{iS} is the number of connections between node i and nodes in module S [Guimerà and Amaral, 2005]. We note that if node i has all of its neighbours within its module M then

$$P_i = 1 - \left(\frac{k_{i_M}}{k_i} \right)^2 = 0$$

whereas if its connections are uniformly distributed among all the network modules and N is large, then P tends to 1.

The role of a node is usually determined by both its participation coefficient P and its within module degree z-score. Guimera *et al.* proposed the thresholds shown in Figure 5.1 to classify nodes according to z and P. They classify nodes with $z > 2.5$ as hubs, and $z < 2.5$ as non-hubs. Within the hubs, they further classify nodes as connector or provincial hubs. If a node is mainly connected to nodes within its own module, it is called a provincial hub. If the node provides links between its own module and other modules, it is defined to be a connector hub.
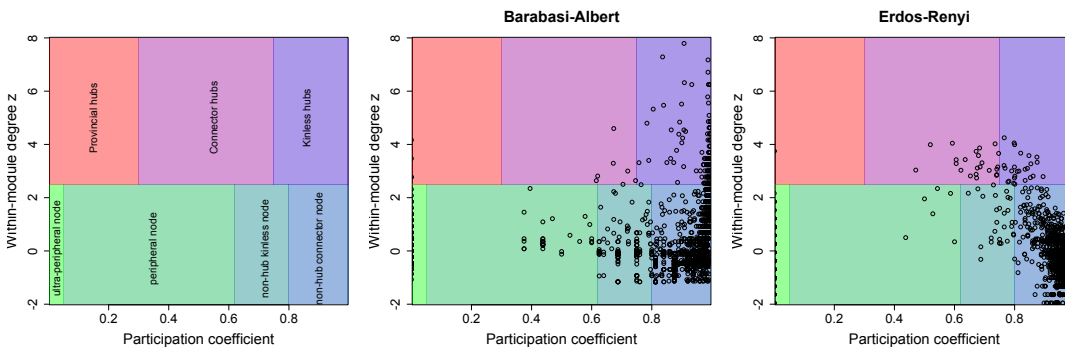

Figure 5.1: Proposed classification for hubs by Guimera et al [Guimerà and Amaral, 2005]. Examples of Barabasi-Albert and Erdös-Renyi graphs for 4000 nodes plotted in the $z - P$ space.

This classification can give insight into the general structure of the network. For example, most of the nodes in the Erdös-Renyi and Barabasi-Albert graphs shown in Figure 5.1 are non-hub connector nodes. The majority of hubs in a Barabasi-Albert graph are kinless hubs; whereas the random Erdös-Renyi graph contains both connector and kinless hubs. The participation coefficient has been used to infer important features of metabolic, air transportation and brain networks [Guimerà and Amaral, 2005]. For example, it has provided insight regarding traumatic brain injuries since lesions in provincial hubs have been found to have different effects than lesions in connector hubs [Sporns et al., 2007].

Despite these advantages, there are subtle differences among the nodes that are not reflected by either z or P. Figure 5.2 illustrates a toy network composed of four modules. We note that nodes 5 and 16 both belong to the same module, they share the same degree (3) and their links are distributed in the same manner (2 within their module, and one towards another module), therefore they have the same z-score and the same participation coefficient. However, their participation in the extra modular connectivity of the network is not the same. Node 5 provides the only connection between its own module A and module C. A disruption in node 5 will therefore disconnect modules A and C, whereas a disruption in node 16 will only reduce the number of extra modular links between modules A and B by one third.

There is another subtler difference between the participation of these two nodes in the network: we argue that connections to high centrality nodes are more important to the propagation of information than connections to low centrality nodes. The centrality of a node is a measure of its relative importance within the graph. The simplest centrality measure is degree. In the previous example, node 16 and node 5 are both connected to degree 3 and 5 nodes. However, in the third connection they differ: node 16 is connected to a degree 3 node (node 6), whereas node 5 is connected to a degree 6 node (node 1). Information will be more efficiently transmitted through a node of high degree centrality such as node 1.
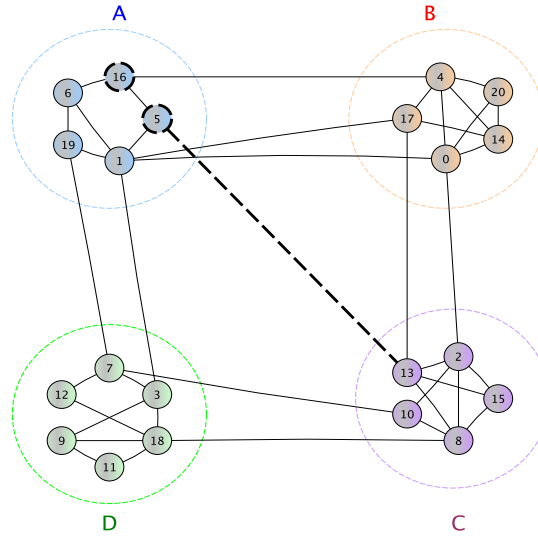
Figure 5.2: Example network. It consists of four modules denoted by A , B, C and D. Nodes 5 and 16 belong to the same module (A). Extra modular connections of nodes 5 and 16 are highlighted.

The path length L is an excellent measure of the overall connectivity of a network. The average path length for an undirected network is defined as

$$L = \sum_{i,j \in V} \frac{d(i,j)}{n(n-1)}$$

where V is the set of nodes in the network, $d(i,j)$ is the shortest path from node i to node j, and n is the number of nodes in the network. For weighted networks, a path length between nodes i and j is defined as the sum of the weights of the edges traversed; the shortest path $d(i,j)$ is the path with the smallest path length. Since L is averaged over all possible pairs of nodes, even very slight increases in L can imply that connectivity has been substantially reduced in some regions of the network. To illustrate, the average path length of the toy network is 2.46. If we remove node 16, it remains close to 2.46, whereas if we remove node 5 instead, it rises to 2.49. This increase in L reflects the fact that node 5 is a critical gateway between modules A and C. In the sections to follow, we propose a metric which will allow us to identify nodes that are important to overall network connectivity in this way.

5.2.2   Gateway Coefficient

To address these issues, we develop a new measure of a node's participation in the network in terms of the module's intra-connectivity, and the node's centrality. In this measure, each term of the participation coefficient is given a weight reflecting the "importance" of the connection. We refer to this modified participation coefficient as the gateway coefficient, defined as

$$G_i = 1 - \sum_{S}^{N} \left(\frac{k_{iS}}{k_i} \right)^2 (g_{iS})^2 \quad .$$

Thus we introduce a weight for each of the terms in the summation; this weight is defined as

$$g_{iS} = 1 - \overline{k_{iS}}\,\overline{c_{iS}}$$

where $\overline{k_{iS}}$ and $\overline{c_{iS}}$ will be defined as follows.

The quantity $\overline{k_{iS}}$ is defined as k_{iS} divided by the sum of k_{jS} for all nodes j in node i's module. Thus k_{iS} is normalized by the total number of extra modular connections between module M and module S, where M is the module to which node i belongs. The quantity $\overline{k_{iS}}$ therefore represents the fraction of the overall connections between module M and module S that belong to node i. This weight ranges between 0 and 1: it is zero if there are no connections from node i to module S, and it is 1 if all of the connections between modules M and S belong to node i.

Let V_{iS} denote the set of neighbours of node i within module S; c_{iS} is then defined as the sum of the centralities of the nodes in V_{iS}. Let c_n denote the sum of the centralities of the nodes in module n, c_n is calculated for all N modules in the network and the maximum value is used to normalize c_{iS}, yielding the following definition $\overline{c_{iS}} = c_{iS}/max(c_n)$. $\overline{c_{iS}}$ ranges between 0 and 1; it will approach zero if node i is only connected to low centrality or completely non-central nodes. The more central the neighbours of the node are, the larger $\overline{c_{iS}}$ will be.

Centrality measures the relative "importance" of a node; there are many ways in which this importance can be defined. Two of the most used measures in network analysis are degree centrality and betweenness centrality. Degree centrality refers to the degree of the node, and it is the simplest and most straightforward measure. Betweenness centrality is a more general measure based on the concept of the shortest path between two nodes. Betweenness quantifies the number of shortest paths that go through node i and it is defined as

$$c(i) = \sum_{j \neq i \neq k} \frac{\sigma_{jk}(i)}{\sigma_{jk}}$$

where σ_{jk} is the number of shortest paths from node j to node k, and $\sigma_{jk}(i)$ denotes the number of those paths that pass through node i. Either of these measures of centrality can be used in the definition of the gateway coefficient, yielding different metrics. We will denote these as G_d and G_b for degree and betweenness centrality formulations, respectively.

To illustrate the helpfulness of this new definition, we go back to our toy network. Let us use degree as the centrality measure. Table 5.1 shows the participation and gateway coefficient for nodes 5, 6, 12 and 16. We note that P gives the same degree of participation to nodes 5 and 16; in contrast, the gateway coefficient successfully identifies the differences discussed earlier giving rise to two different values. The gateway coefficient also allows us to rank the importance of nodes that do not have any extra modular connections (and therefore have a participation coefficient of zero). For example, node 6 has a higher gateway coefficient than node 12.

To further demonstrate the differences between the two coefficients, we removed high gateway or participation nodes and computed the average path length for Erdös-Renyi and Barabasi-Albert networks. After computing the gateway coefficient for all nodes in the network and arranging them in decreasing order, the node with the highest gateway coefficient was removed from the graph and the average path length was

node	P	$\overline{k_{iA}}$	$\overline{c_{iA}}$	$\overline{k_{iB}}$	$\overline{c_{iB}}$	$\overline{k_{iC}}$	$\overline{c_{iC}}$	$\overline{k_{iD}}$	$\overline{c_{iD}}$	G_d
5	0.444	0.333	0.428	-	-	1	0.238	-	-	0.608
16	0.444	0.333	0.286	0.333	0.238	-	-	-	-	0.542
6	0	0.5	0.571	-	-	-	-	-	-	0.489
12	0	-	-	-	-	-	-	0.25	0.428	0.202

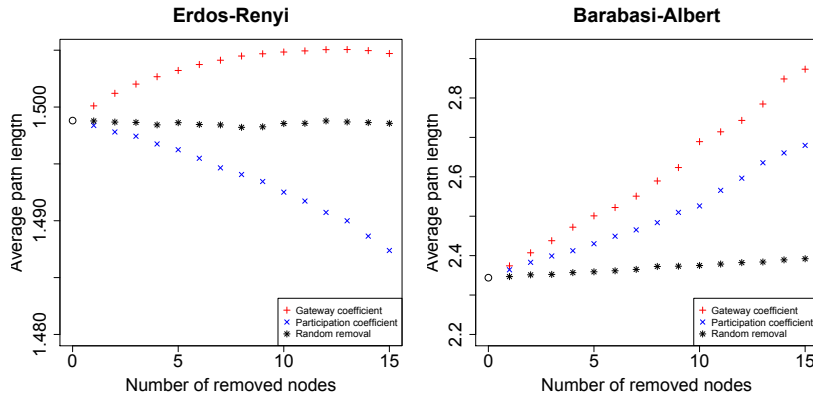Table 5.1: Participation coefficient, weights and gateway coefficient for nodes 5 and 16 of the toy network.

Figure 5.3: Sequential node removal for Erdös-Renyi (left) and Barabasi-Albert (right) graphs. Values averaged over 50 graphs with 100 nodes each. The Barabasi-Albert graphs had approx. 400 edges, and the Erdös-Renyi graphs had approximately 2000 edges. The x-axis shows both the number of removed nodes, and the rank of the removed node at that step. The y-axis shows the average path length of the resultant graph when removing high gateway coefficient nodes (red +); high participation coefficient nodes (blue ×); or random nodes (black ∗).

computed. This process was then repeated for the node with the 2nd highest gateway coefficient and so forth. The results are shown in Figure 5.3. We note that the removal of nodes with high gateway coefficients consistently resulted in longer average path lengths than those resulting from the removal of nodes with high participation coefficients. Longer path lengths suggest that the deletion of high gateway nodes is more disruptive to the network than the deletion of high participation nodes.

Since betweenness is directly related to path length, we also investigated the effects of removing high betweenness nodes from Erdös-Renyi networks. When the
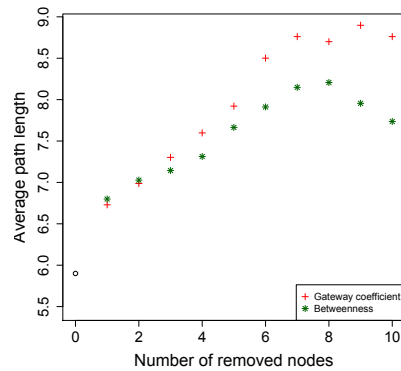
Figure 5.4: Sequential node removal of high betweenness and high gateway nodes for Erdös-Renyi graph. Values averaged over 30 graphs with 100 nodes and 100 edges each. The y-axis shows the average path length of the resultant graph when removing high gateway coefficient nodes (red +) or high betweenness nodes (green *

average degree is very high (close to 100), the sequential removal of high betweenness nodes has a similar effect on average path length as the removal of high gateway coefficient nodes (data not shown). However for networks with lower average degree, Figure 5.4 demonstrates that nodes with high gateway coefficients have a greater impact on average path length than high betweenness nodes. Although betweenness depends directly on path length, it does not take the modular structure of the network into account. Thus this result demonstrates that modularity is an important feature of the overall connectivity of the network, and that nodes with high gateway coefficients are critical to this connectivity, particularly in networks with low or moderate degree.

5.3 U.S. air transportation network

5.3.1 Data

We analyzed The U.S. Bureau of Transportation Statistics (BTS) database, which is composed of domestic and international data reported by air carriers. International flights are included only if either the origin or destination is in the United States. This database includes both the origin and destination information for each flight,

along with the airport coordinates.

We restricted our analysis to the month of January, 2012. During that period there were 19,706 nonstop domestic flights, and 5,897 international flights. Airports are represented as nodes in the network and directed edges represent scheduled flights between airports. Two different weights for the edges were considered. For the first analysis each edge is weighted by the number of passengers transported. This type of analysis can have epidemiological implications, since human mobility is of great importance in the spread of disease. For the second analysis, each edge is weighted by the number of flights between the origin and the destination airports; such flights may carry few passengers (or none at all). This analysis can have economical implications, since it offers insight into air travel routes and the resources needed to maintain them.

5.3.2   Data Analysis

Adjacency matrices were constructed and the resultant networks were directed and weighted. The modular analysis was based on an edge betweenness community structure algorithm proposed by Newman and Girvan [Newman and Girvan, 2004]: this approach was deemed appropriate since the centrality measure used for the analysis was the betweenness centrality.

The presence of U.S. cargo-only domestic flights in the flight-weighted network resulted in a very different behaviour than that of the passenger weighted network, particularly for Alaska. For this reason, domestic and international flight networks were analyzed separately. Alaska was the state with the highest number of domestic flights in the month of January, with 1387 in total, whereas the second highest number of flights was 377 from Florida. The large discrepancy between these numbers is due to the fact that air transportation is often the only way to reach certain areas in Alaska. In addition, a large fraction of Alaskan flights are cargo flights as mentioned earlier. Therefore it was expected that the edge betweenness modularity analysis

would reveal several sub-networks (modules) of highly interconnected airports within Alaska only.

Weighting by either passenger number or flight number, we computed both the clustering coefficient C (or the tendency to form clusters [Watts and Strogatz, 1998]) and average path length L of the network. For each weighting, we also constructed random networks with the same number of nodes and degree distribution. The small world index of the real-world network could then be computed as$(C/C_{rand})/(L/L_{rand})$, where C_{rand} and L_{rand} are the clustering coefficient and the average path length of the random networks [Watts and Strogatz, 1998].

The degree distribution was also computed and fitted to a scale-free [Barabási and Albert, 1999] and truncated scale-free topology [Amaral et al., 2000a]. We computed the degree and betweenness, as well as the participation and the gateway coefficient for each node in the network. Nodes were also classified by role according to the scheme proposed by Guimera *et al.* [Guimerà and Amaral, 2005].. Finally, we analyzed the change in the average path length when the airports with the highest gateway coefficients were removed from the network. Airports were sequentially removed from the network according to their gateway coefficient rank. The same procedure was applied to nodes with high participation coefficients and results were further compared.

5.3.3 Results

5.3.3.1 Network weighted by passengers

The air transportation network's average path length was close to 3. The average path length, as well as the clustering coefficient were found to be higher than those of random networks, implying that the network follows a small world topology. The degree distribution was also analyzed and it was found to be well described by a truncated scale-free topology.

The modularity analysis based on betweenness centrality revealed 5 main modules (containing 5 or more nodes). The Alaska module consists exclusively of airports within Alaska. The south-west central module includes airports in Texas and Lousiana. Airports in the western states Arizona, Nevada and Utah form the west module. Airports in the eastern half of the country, such as Florida, North Carolina, and Michigan form a module along with some airports in Alaska and a few international airports. The international module is the largest, and is comprised of many important airports world-wide including: Charles de Gaulle (France), Dubai International, Houston Intercontinental, John F. Kennedy International, Licenciado Benito Juarez International (Mexico), Narita International (Japan), Chicago O'Hare International, and Lester B. Pearson International (Canada).

The results are summarized in Table 5.2. The airport with highest degree was Atlanta Municipal airport, followed by Los Angeles International and Chicago O'Hare International airports; these airports had the highest number of ingoing and outgoing flights in the month of January 2012. Anchorage International airport was found to be the airport with the highest betweenness centrality, followed by Seattle International and John F. Kennedy International airports. These airports have the highest number of shortest paths passing through them, therefore acting as bridges along the shortest routes between airports. The participation coefficient identified Juneau, Anchorage and Fairbanks International airports as connector hubs. The airports with the highest gateway coefficient were Anchorage International, followed by Van Nuys and Juneau airport. Van Nuys and Juneau airports also showed high participation coefficients, however Anchorage International airport's participation coefficient was ranked in 11th place, below Detroit's airport. The high centrality found earlier for the Anchorage airport is therefore captured in part by the gateway coefficient. Figure 5.5 shows a plot of the flights to and from Anchorage International; colours indicate the module with which the flight connects.

A scatter plot of the participation and gateway coefficients (Figure 5.6) reveals several differences between these coefficients. As noted earlier, the gateway coefficient

	Passenger-weighted International	Flight-weighted Domestic	Flight-weighted International
Highest degree	Atlanta Municipal , GA	Birmingham, AL	Miami International, FL
Highest betweenness	Ted Stevens Anchorage International, AK	Ted Stevens Anchorage International, AK	John F. Kennedy International, NY
Highest gateway	Ted Stevens Anchorage International, AK	Ted Stevens Anchorage International, AK	Lester B. Pearson International (Canada)
Highest participation	Van Nuys, CA	Kodiak Airport, AK	Chubu Centrair International (Japan)
Average path length	3.222	3.314	3.233

Table 5.2: Highest degree and betweenness, gateway and participation coefficient airports for domestic and international networks, along with average path length.
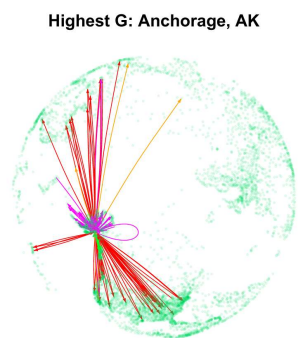

Figure 5.5: Flights from the airport with the highest gateway coefficient. The lines represent flights, and different colours represent different modules.

provides a ranking for airports classified as having a null participation coefficient. Airports on the red line have equal participation and gateway coefficients; however, there are a number of clear outliers with high gateway coefficients. The airports with the highest degree and betweenness, Atlanta and Anchorage airports respectively, showed high discrepancies between the two values. The gateway coefficient ranked these airports considerably higher than the participation coefficient.

Figure 5.6 also shows results for sequential node removal. We note that the removal of Anchorage airport, ranked first for the gateway coefficient and 11th for the participation coefficient, has a substantial impact on the average path length, whereas removing the highest ranked participation coefficient airports had little effect. It is

also worth noting that since L is averaged over all possible pairs of nodes, an increase from 3.2 to 3.8 in the average path length is substantial. The difference between the average path lengths after removal remained positive throughout 30 repetitions, indicating the average path length after removing high gateway nodes was consistently higher than the average path length after removing high participation nodes.
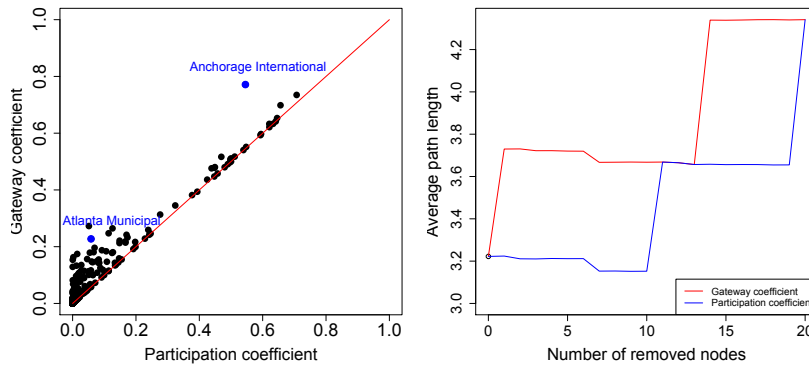

Figure 5.6: The left panel shows a scatter plot of the participation (x-axis) and gateway (y-axis) coefficients for the passenger-weighted based network. The right panel shows the average path length after sequential node removal for participation and gateway coefficients.

5.3.3.2 Networks weighted by flights

For flight-based networks, an average path length close to 3 was again found for both domestic and international networks, as well as a small world topology. Both the international and domestic networks were also found to follow a truncated scale-free topology.

For the international network, 5 modules with more than 10 airports were found. The Australasia and South-American-Caribbean modules consisted of airports in Asia and Australia, and of airports in South America and the Caribbean respectively as indicated by their names. Airports in the U.S. were mainly divided in three modules; the Eastern U.S and the Southern U.S modules were composed mainly of airports

within the U.S; whereas the International module consisted of airports in the Western U.S. along with the most important international airports.

Table 5.2 shows that the airport with highest degree was the Miami International, whereas the John F. Kennedy International in New York showed the highest betweenness centrality. The airport with the highest gateway coefficient was Pearson International airport in Toronto, Canada, whereas Chubu Centrair International in Nagoya, Japan had the highest participation coefficient. Following the Guimera *et al.* thresholds for the participation coefficient, the Pearson International airport in Toronto, Canada was identified as a connector hub and the Los Angeles international airport and the Chicago O'Hare airport were identified as provincial hubs.

A scatter plot of the participation and gateway coefficients (Figure 5.7) reveals airports ranked higher by the gateway coefficient than by the participation coefficient. The airport with the highest degree, Miami International, showed high discrepancies between these values; so did the airport with the highest gateway coefficient, Pearson International, which was ranked 16th by the participation coefficient. It is important to recall that this airport was also found to be the highest ranked connector hub. The gateway coefficient ranked these airports considerably higher than the participation coefficient.

Results for sequential node removal are shown in Figure 5.7. The removal of airports with the highest gateway coefficients has a substantially larger impact on the average path length than removing the highest ranked participation coefficient airports. Again, this finding suggests that the gateway coefficient offers a better representation of a node's involvement in the network's connectivity.

Table 5.2 also shows the results for the domestic flight network. The airport with the highest degree was found to be Birmingham airport in Alabama, and the airport with the highest betweenness centrality was Anchorage International in Alaska. Since the majority of flights in Alaska have both origin and destination within Alaska,
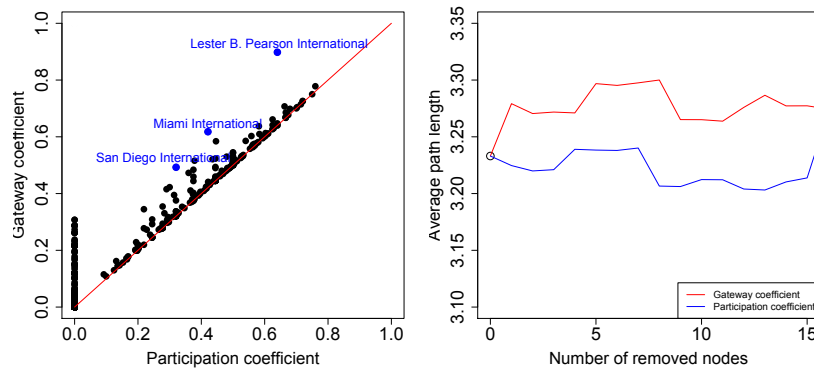
Figure 5.7: Left panel shows a scatter plot of the participation (x-axis) and gateway (y-axis) coefficients for the international flight based network. The right panel shows the average path length after sequential node removal for participation and gateway coefficients.

the participation coefficient was not able to indicate any major differences between Alaskan airports; however, a scatter plot of the participation and gateway coefficients (Figure 5.8) reveals the ability of the gateway coefficient to rank airports with null participation coefficient. Airports on the red line have equal participation and gateway coefficients; Anchorage and Juneau airports in Alaska are some of the clear outliers.
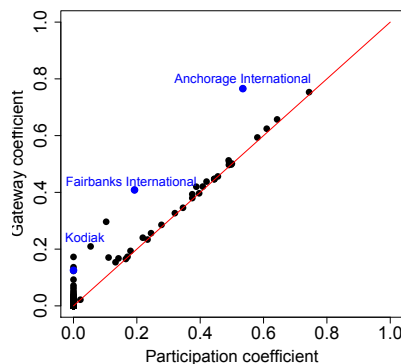

Figure 5.8: Scatter plot of the participation (x-axis) and gateway (y-axis) coefficients for the domestic flight-based network.

Results were also obtained for the domestic flight-based network with modules pre-assigned geographically by state (see Appendix C).

5.4   Functional neuroimaging network

5.4.0.3   Data

Full brain functional magnetic resonance imaging (fMRI) data was used for this analysis. For a complete description of the cognitive task and data acquisition see [Greening et al., 2011]. Briefly, subjects were scanned while performing an object discrimination task in which the participants were asked to select one object from a pair displayed against a computer screen, and subsequently received either positive or negative feedback depending on the object chosen; their Blood Oxygenation Level Dependent (BOLD) signal was collected resulting in a three dimensional time series that was later preprocessed and warped into standardized space. The network was analyzed with the use of Weighted Gene Co-Expression Network Analysis (WGCNA) software [Zhang and Horvath, 2005]. R (http://www.R-project.org) [R Development Core Team, 2008] was used to carry out all the calculations. This work was made possible by the facilities of the Shared Hierarchical Academic Research Computing Network (SHARCNET:www.sharcnet.ca) and Compute/Calcul Canada. All data were collected as approved by the Western University Human Research Ethics Board.

5.4.1   Data Analysis

After pre-processing the Pearson correlation coefficient r_{ij} between the time series of each pair of voxels was computed. Based on previous analyses [Ruiz-Vargas et al., tics], we computed the adjacency matrix A using the power adjacency function.

$$a_{ij} = |r_{ij}|^{\beta}.$$

In previous work we have demonstrated that a value of 6 for the parameter β yields a good compromise between retaining high network connectivity and reducing noise in

full brain fMRI data [Ruiz-Vargas et al., tics]. The degree of a node is defined as the row sum of the adjacency matrix. The resulting network is weighted and undirected.

Average linkage hierarchical clustering [Ravasz et al., 2002] was used to cluster similar nodes in a dendogram, whose branches determine clusters or modules. Modules are defined as groups of nodes with high topological overlap [Ravasz et al., 2002]. Finally the clusters were automatically detected using the tree cut method [Langfelder et al., 2008] which identifies modules based not only on absolute height in the dendogram, but also on their shape.

The data under analysis consisted of approximately 190000 voxels. Participation and gateway coefficients were computed for voxels with degree above the median. Since each voxel is assigned to a specific brain area according to the Talairach Tournoux atlas [Talairach and Tournoux, 1988], average participation and gateway coefficients were obtained by averaging the coefficients of all voxels within a specific brain area.

5.4.2   Results

A scatter plot of the participation and gateway coefficients is shown in Figure 5.9, where voxels on the red line have equal participation and gateway coefficients. Several voxels for which the two metrics differed substantially are highlighted.

The voxels with highest participation coefficient values include voxels within the cuneus, precuneus, and superior occipital gyrus; whereas voxels with the highest gateway coefficient values include voxels within the cuneus, precuneus, superior frontal and superior occipital gyrus. The two metrics differed most substantially for voxels in the frontal gyrus.
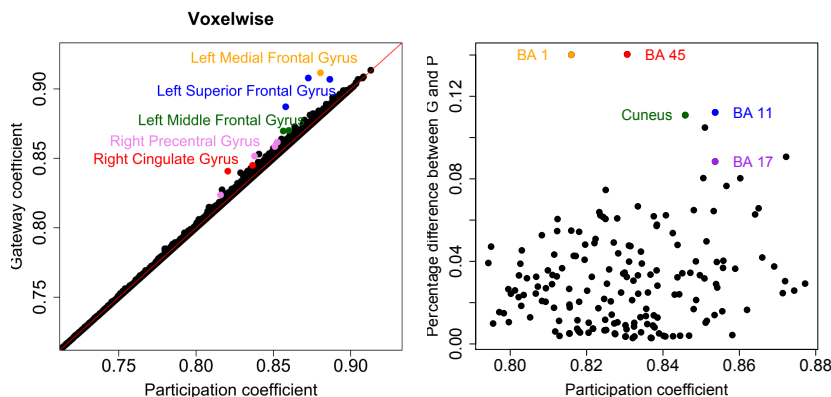
Figure 5.9: In the left panel: a scatter plot of the participation (x-axis) and gateway (y-axis) coefficients for the brain network voxelwise. In the right panel: the percentage difference between participation and gateway coefficients (y-axis) versus the participation coefficient averaged over each brain region. BA stands for Brodmann Area. Outliers are identified in both plots.

Even though the analysis showed clear differences between values for the individual voxels, prominent differences were not found for the grouped voxels (averaged values). However, as figure 5.9 shows, discrepancies between gateway and participation values occur frequently. In particular, the gateway coefficient exceeds the participation coefficient for Brodmann areas 45, 11 and 17, as well as for the cuneus. Such areas are thought to be involved in selection among competing options (BA45), decision making (BA11), and visual processing (BA17 and cuneus), roles highly involved in the task related to our data [Arroyo et al., 1997, Thompson-Schill et al., 1999, Kosslyn et al., 1999, Bechara, 2005].

The occipital and inferior temporal gyrus along with the lingual gyrus, areas greatly involved in visual processing, showed high participation and gateway coefficients. These results are in accord with the highly visual nature of the task under analysis. Other areas with high gateway coefficient are the right angular gyrus, which has been linked to spatiovisual attention [Chambers et al., 2004], and the posterior cingulate, which is central to the so-called "default mode network" [Raichle et al., 2001]. There were subtle differences between the coefficients: for instance, the gate-

way coefficient identified a higher participation of the middle occipital gyrus than the inferior temporal gyrus, whereas the participation coefficient showed the opposite. Figure 5.10 shows the brain areas that showed the highest involvement in the network's connectivity as exposed by the gateway coefficient.
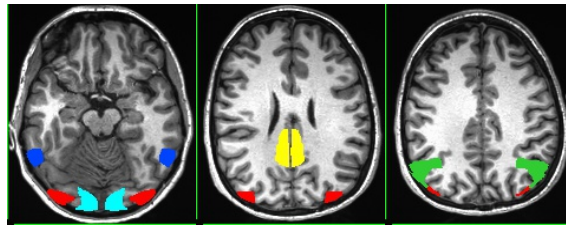

Figure 5.10: Brain areas with the highest involvement in the network's connectivity. Blue: Inferior temporal gyrus. Cyan: Lingual gyrus. Red: Occipital gyrus. Yellow: Posterior cingulate Green: angular gyrus.

5.5 Discussion

A new coefficient which quantifies a node's involvement in the intra and extra-modular connectivity of the network was introduced. The gateway coefficient yields intuitively appealing results when ranking the importance of nodes to network connectivity, as measured by average path length. One of the strengths of this new quantity is its ability to identify nodes with unique intermodular links. Such nodes are essential in preserving the communication between modules, and cannot be easily identified by previous topological quantities. The gateway coefficient can also recognize connectivity differences between nodes that only have connections within one module, taking into account the centrality of their connections. Overall the gateway coefficient offers an additional and useful tool in the accurate characterization of node roles.

We studied the U.S. air transportation system as a directed weighted network. Weights were analyzed in two manners to reflect different properties of the system. For both analyses a small-world topology was found, in accordance with previous studies [Barrat et al., 2004]. The degree distribution of both networks was found to

follow an exponentially truncated scale free behaviour. Physical constraints that limit the maximum number of flights and passengers an airport can hold [Amaral et al., 2000b] might explain the system's degree distribution, however further research is needed.

All networks showed large discrepancies between the gateway and participation coefficients for highly central (either by degree or betweenness, or both) nodes. The gateway coefficient consistently ranked these airports higher than the participation coefficient. Furthermore, an analysis of the domestic flight-based network revealed a huge subnetwork composed of flights within Alaska. It was mentioned earlier that this is due to the isolation of many areas that require flights as the principal method of transport. A lack of extra modular flights resulted in null participation coefficients for many Alaskan airports; however, the gateway coefficient successfully provided a ranking for these airports.

The average path length was studied as a measure of the impact of airport removal. Removing airports with high gateway coefficients resulted in larger path lengths and therefore a substantial disruption in the network. These results support our proposal of the gateway coefficient as an accurate measure of a node's involvement in the network's connectivity. Furthermore, our results were robust with respect to the centrality measure used (for degree and betweenness centrality).

The analysis was only made for the month of January for flights from or to the U.S. A broader analysis in the future could include a larger time span and world-wide data.

We also analyzed network data from fMRI studies of the human brain. The largest discrepancies between coefficients both voxel and areawise were found in brain areas highly related to the task being studied. These differences were more outstanding at the voxel level. Since the data used for this analysis was acquired during a visual task, brain areas involved in visual processing showed the highest gateway

coefficients. These results suggest that the gateway coefficient might be a tool to accurately identify brain areas with high involvement in the propagation of information during a specific task.

Bibliography

Amaral, L., Scala, A., Barthélémy, M., and Stanley, H. E. (2000a). Classes of small-world networks. *Proc Natl Acad Sci U S A*, 97(21):11149–11152.

Amaral, L. A., Scala, A., Barthelemy, M., and Stanley, H. E. (2000b). Classes of small-world networks. *Proc Natl Acad Sci U S A*, 97(21):11149–11152.

Arroyo, S., Lesser, R. P., Poon, W.-T., Robert, W., Webber, S., and Gordon, B. (1997). Neuronal generators of visual evoked potentials in humans: Visual processing in the human cortex. *Epilepsia*, 38(5):600–610.

Barabási, A.-L. and Albert, R. (1999). Emergence of scaling in random networks. *Science*, 286(5439):509–512.

Barrat, A., Barthélemy, M., Pastor-Satorras, R., and Vespignani, A. (2004). The architecture of complex weighted networks. *Proc Natl Acad Sci U S A*, 101(11):3747–3752.

Bartolomei, F., Bosma, I., Klein, M., Baayen, J., Reijneveld, J., Postma, T., Heimans, J., van Dijk, B., de Munck, J., de Jongh, A., Cover, K., and Stam, C. (2006). How do brain tumors alter functional connectivity? a magnetoencephalography study. *Ann Neurol*, 59(1):128–38.

Bassett, D., Bullmore, E., Verchinski, B., Mattay, V., Weinberger, D., and Meyer-Lindenberg, A. (2008). Hierarchical organization of human cortical networks in health and schizophrenia. *J Neurosci*, 28(37):9239–48.

Bechara, A. (2005). Decision making, impulse control and loss of willpower to resist drugs: a neurocognitive perspective. *Nat Neurosci*, 8(11):1458–1463.

Britton, S. G. (1982). The political economy of tourism in the third world. *Ann Tourism Res*, 9(3):331–358.

Bullmore, E. and Sporns, O. (2009). Complex brain networks: graph theoretical analysis of structural and functional systems. *Nat Rev Neurosci*, 10(3):186–98.

Bullmore, E. and Sporns, O. (2012). The economy of brain network organization. *Nat Rev Neurosci*, 13(5):336–349.

Button, K. and Taylor, S. (2000). International air transportation and economic development. *J Air Transp Manag*, 6(4):209–222.

Chambers, C. D., Payne, J. M., Stokes, M. G., and Mattingley, J. B. (2004). Fast and slow parietal pathways mediate spatial attention. *Nat Neurosci*, 7(3):217–218.

Cho, M. W. and Choi, M. Y. (2010). Brain networks: Graph theoretical analysis and development models. *Int J Imaging Syst Technol*, 20(2):108–116.

Girvan, M. and Newman, M. E. J. (2001). Community structure in social and biological networks. *Proc Natl Acad Sci U S A*.

Greening, S. G., Finger, E. C., and Mitchell, D. G. V. (2011). Parsing decision making processes in prefrontal cortex: Response inhibition, overcoming learned avoidance, and reversal learning. *NeuroImage*, 54(2):1432–1441.

Guimerà, R. and Amaral, L. (2005). Functional cartography of complex metabolic networks. *Nature*, 433:895–900.

Guimerà, R., Mossa, S., Turtschi, A., and Amaral, L. (2005). The worldwide air transportation network: Anomalous centrality, community structure, and cities' global roles. *Proc Natl Acad Sci U S A*, 102(22):7794.

Guimerà, R., Sales-Pardo, M., and Amaral, L. A. N. (2007). Module identification in bipartite and directed networks. cite arxiv:physics/0701151.

Kosslyn, S. M., Pascual-Leone, A., Felician, O., Camposano, S., Keenan, J., Ganis, G., Sukel, K., and Alpert, N. (1999). The role of area 17 in visual imagery: convergent evidence from PET and rTMS. *Science*, 284(5411):167–170.

Langfelder, P., Bin, Z., and Horvath, S. (2008). Defining clusters from a hierarchical cluster tree: The dynamic tree cut package for R. *Bioinformatics*, 24(5):719–720.

McFarland, R. A. (1953). Human factors in air transportation: occupational health and safety. *Human Factors in Air Transportation: Occupational Health and Safety*.

Newman, M. (2001). Scientific collaboration networks. i. network construction and fundamental results. *Phys Rev E*, 64:2001.

Newman, M. E. J. and Girvan, M. (2004). Finding and evaluating community structure in networks. *Phys Rev E*, 69(2):026113.

R Development Core Team (2008). *R: A Language and Environment for Statistical Computing*. R Foundation for Statistical Computing, Vienna, Austria. ISBN 3-900051-07-0.

Raichle, M. E., MacLeod, A. M., Snyder, A. Z., Powers, W. J., Gusnard, D. A., and Shulman, G. L. (2001). A default mode of brain function. *Proc Natl Acad Sci U S A*, 98(2):676–682.

Ravasz, E., Somera, A., Mongru, D., Oltvai, Z., and Barabási, A. (2002). Hierarchical organization of modularity in metabolic networks. *Science*, 297(5586):1551.

Ruiz-Vargas, E., Greening, S., Mitchell, D., and Wahl, L. (In review, SIAM J. Applied Mathematics). Topology of whole-brain fMRI networks: improving the truncated scale-free model.

Sporns, O., Honey, C. J., and Kötter, R. (2007). Identification and classification of hubs in brain networks. *PLoS ONE*, 2(10).

Stam, C., de Haan, W., Daffertshofer, A., Jones, B., Manshanden, I., van Cappellen van Walsum, A., Montez, T., Verbunt, J., de Munck, J., van Dijk, B.,

Berendse, H., and Scheltens, P. (2009). Graph theoretical analysis of magnetoencephalographic functional connectivity in alzheimer's disease. *Brain*, 132(Pt 1):213–24.

Strogatz, S. H. (2001). Exploring complex networks. *Nature*, 410(6825):268–276.

Talairach, J. and Tournoux, P. (1988). *Co-Planar stereotaxic atlas of the human brain: 3-D proportional system: An approach to cerebral imaging*. Thieme.

Thompson-Schill, S. L., D'Esposito, M., and Kan, I. P. (1999). Effects of repetition and competition on activity in left prefrontal cortex during word generation. *Neuron*, 23(3):513–522.

Watts, D. J. and Strogatz, S. H. (1998). Collective dynamics of 'small-world' networks. *Nature*, 393(6684):440–442.

Zhang, B. and Horvath, S. (2005). A general framework for weighted gene coexpression network analysis. *Stat Appl Genet Mol Biol*, 4(1):Article17.

Chapter 6

Conclusions and Future Work

6.1   Summary and conclusions

Real life networks have been much studied over the recent years; however, many of their underlying mechanisms are not yet understood. Topological properties that can give insight regarding the functionality of the system need to be properly character- ized. For instance, the degree distribution can provide information on the robustness and vulnerability of the human brain [Barabási et al., 2000]. This dissertation has attempted to overcome computational limitations to study in depth the degree dis- tribution of brain networks.

Expanding on the work of describing scale-free and truncated scale-free degree distributions, novel topologies were analyzed in Chapter 3; they proved to provide a better fit to brain networks that those used in previous studies (scale-free and truncated scale-free [Eguíluz et al., 2005, Achard et al., 2006, Iturria-Medina et al., 2008, Ferrarini et al., 2011]). The analysis of whole brain datasets without the im- position of restrictions on the voxels or the brain areas being studied, strengthens the reliability of our results.

Theoretically-based models of traumatic brain injuries have not been thoroughly studied even though they present many advantages: they are non-invasive and can provide critical information to decide the course of action after a TBI has occurred.

Even though the exact pathophysiology of a traumatic brain injury has not yet been established, cortical contusions and diffuse axonal degeneration are mechanisms

thought to be behind the dysfunctions associated with traumatic brain injuries [Levin et al., 1987, Maruta et al., 2010, Johnson et al., 2012]. We have provided several mathematical models for these mechanisms in Chapter 4 and Appendix B of this thesis, and investigated their effects on the brain's modular structure. The nature of our models allowed us to explore lesions with different locations and intensities. Our results explored the possibility of a restructuring of the modular connectivity's strength that may in part compensate for the disruption caused by the TBI. Furthermore, results from this study were in accordance with some of the known effects of a concussion.

Finally, Chapter (5) revisited a well-known network concept: the participation coefficient [Guimerà and Amaral, 2005, Guimerà et al., 2007]. We successfully introduced a novel coefficient, the gateway coefficient, that expands the scope of the participation coefficient, and efficiently ranks nodes according to their connectivity. We have illustrated the potential of this new coefficient through specific examples (air transportation and brain networks) and numerical simulations of toy networks.

Our results found high discrepancies between participation and gateway coefficients for airports with the highest degree and betweenness (for the air transportation network), and for brain areas highly involved in the task the patients had to perform (for the brain network).

Overall, the findings presented in this work are novel and can be used to provide important information on the structure and functionality of a system when modelled through network theory.

6.2   Future work

For future work, analysis of control and post-injury patient data is necessary to confirm the behaviour predicted by any mathematical model of traumatic brain injuries. The models proposed in this thesis may be modified, combined or extended to study other types of disorders. The models can also be used as a basis to study recovery

after traumatic brain injuries.

The gateway coefficient can be further used in other real life systems to explore the involvement and participation of their components.

Full brain datasets can be further studied to examine other types of topological quantities that will shed light on the functionality of the brain.

Bibliography

Achard, S., Salvador, R., Whitcher, B., Suckling, J., and Bullmore, E. (2006). A resilient, low-frequency, small-world human brain functional network with highly connected association cortical hubs. *J Neurosci*, 26(1):63–72.

Barabási, A.-L., Jeong, H., and Albert, R. (2000). Error and attack tolerance of complex networks. *Nature*, 406(6794):378–382.

Eguíluz, V. M., Chialvo, D. R., Cecchi, G. A., Baliki, M., and Apkarian, A. V. (2005). Scale-free brain functional networks. *Phys Rev Lett*, 94(1):018102.

Ferrarini, L., Veer, I. M., van Lew, B., Oei, N. Y. L., van Buchem, M. A., Reiber, J. H. C., Rombouts, S. A. R. B., and Milles, J. (2011). Non-parametric model selection for subject-specific topological organization of resting-state functional connectivity. *NeuroImage*, 56(3):1453–1462.

Guimerà, R. and Amaral, L. (2005). Functional cartography of complex metabolic networks. *Nature*, 433:895–900.

Guimerà, R., Sales-Pardo, M., and Amaral, L. A. N. (2007). Module identification in bipartite and directed networks. cite arxiv:physics/0701151.

Iturria-Medina, Y., Sotero, R. C., Canales-Rodríguez, E. J., Alemán-Gómez, Y., and Melie-García, L. (2008). Studying the human brain anatomical network via diffusion-weighted MRI and graph theory. *NeuroImage*, 40(3):1064–1076.

Johnson, V., Stewart, W., and Smith, D. (2012). Axonal pathology in traumatic brain injury. *Exp Neurol*.

Levin, H. S., Mattis, S., Ruff, R. M., Eisenberg, H. M., Marshall, L. F., Tabaddor, K., High Jr, W. M., and Frankowski, R. F. (1987). Neurobehavioral outcome following minor head injury: a three-center study. *J Neurosurg*, 66(2):234–243.

Maruta, J., Lee, S., Jacobs, E., and Ghajar, J. (2010). A unified science of concussion. *Ann N Y Acad Sci*, 1208.

Appendix A
Assortativity of brain networks

The degree distribution of a system is highly related to its assortatitvity, or the tendency of high-degree nodes to be connected to high-degree nodes. To further expand the findings of Chapter 3 we also studied the dependence of assortativity on the threshold used to define neighbourhoods within the network.

In order to define the node's neighbours a connectivity matrix is obtained and a threshold is typically applied. Different networks can arise from different threshold choices. For instance, a low threshold can result in a fully connected network that will hold all of the systems' information along with most of the experimental noise. Due to the size of the typical functional MRI data, dealing with a fully connected matrix imposes a big computational challenge. On the other hand, high thresholds will give rise to an increasingly sparse matrix, which is computationally more manageable but a lot of the network's information might be missing. Each study can impose its own threshold for the analysis, so it is important to ensure that the results are not exclusive to the subset of nodes defined by the threshold.

In order to analyze the assortativity of the network, the first step was to compute the average degree of the node's neighbours, and identify its dependence on the degree of the node. A definite assortative behaviour was found. Figure (A.1) shows that the average increases with k; as the threshold τ increases this behaviour becomes more evident.
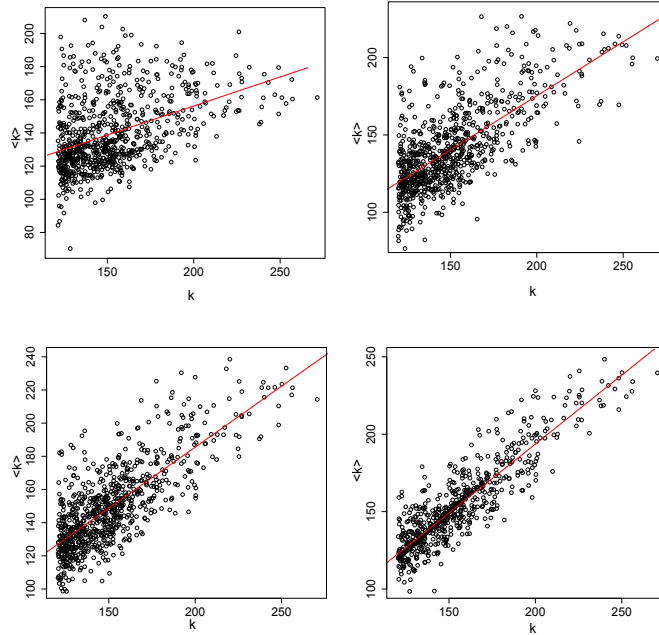
Figure A.1: Average neighbours degree plot. On the x axis the degree k of the highest connected voxels. On the y axis the average degree of the neighbours of the nodes that with such a k, in other words, the average neighbours degree. Plots for thresholds $\tau = 0.2, 0.4, 0.5, 0.7$, from left to right.

In addition, we computed the degree-dependent average nearest-neighbours degree for weighted networks k_{nn}^w , first proposed by Barrat *et al.*:

$$k_{nn,i}^w = \frac{1}{s_i} \sum_{j \in \Gamma(i)} w_{ij} k_j$$

where s_i is the vertex strength defined as the sum of weights of the nodes connected to i, w_{ij} is the weight of the connection between voxels i and j, k_j is the degree of voxel j, and $\Gamma(i)$ denotes the group of nearest neighbours of i. If the weighted degree-dependent nearest-neighbour degree $k_{nn}^w(k)$ increases with k, then the network is weighted assortative and therefore similar degree vertices tend to link together. The nearest neighbours of each node were defined as follows: two nodes were considered to be either connected if the magnitude of the correlation between them is above a certain threshold τ ranging from 0.1 to 1.0, getting the full spectrum of behaviour. The near-

est neighbour degree was computed multiple times for a subset of the data comprised by the most connected nodes, and for different thresholds, getting the full spectrum of behaviour. Figure (A.2) shows that k_{nn}^w is an increasing function of k, meaning the neighbours of high degree nodes have, on average, high degree themselves as well. An increase in the threshold defining neighbourhoods shows a significant decrease in the assortative behaviour of the network. This can be explained as an increase in the threshold significantly decreases the number of node's neighbours. However, a definite assortative behaviour was found for the whole τ spectrum, corroborating the generality of our findings. The hubs of the brain network at a voxel level follow an assortative behaviour.
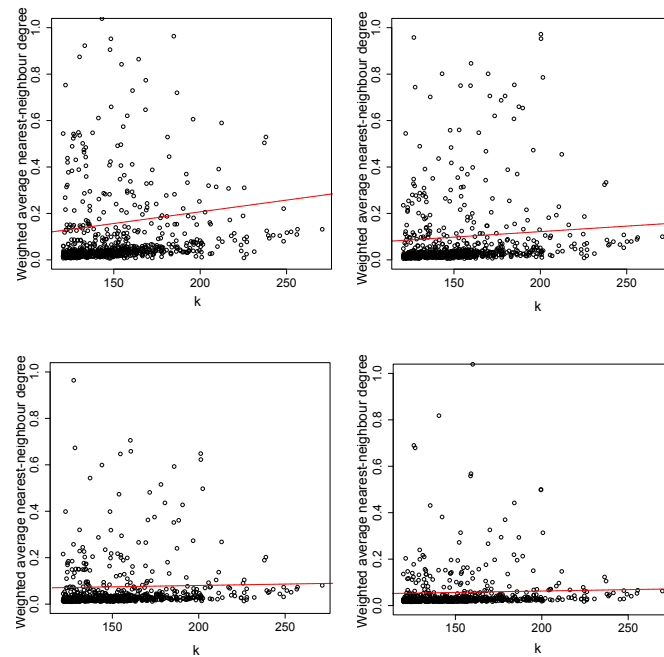

Figure A.2: Degree-dependent average nearest-neighbours degree vs node's degree k. On the x axis the degree k of the highest connected voxels, on the y axis, the degree-dependent average nearest-neighbours degree. Plots for thresholds $\tau = 0.3, 0.4, 0.5, 0.6$, from left to right.

Appendix B

Further injury models

B.1   Random weakening of nodes

Random weakening consists of randomly selecting a node from the network and weakening its connections. This procedure is done for a fraction of the nodes in the network.

In order to drastically weaken the chosen connection, the adjacency a_{ij} was raised to a power of $\alpha = 2$, this is equivalent to raising the entries of the correlation matrix to a power of 12 (since they had previously been raised to a power of $\beta = 6$ to reduce the noise).

$$\tilde{a}_{ij} = a_{ij}^{\alpha} = s_{ij}^{\beta\alpha} = |r_{ij}|^{12}$$

where $\tilde{a}_{ij}$ are the new entries of the adjacency matrix for the damaged edges.

Weakening was performed for all three subjects and three different fractions of weakened nodes, $1/10th$, $1/20th$ and $1/30th$, were considered. The results for one representative subject are discussed in detail below.

Weakening of 1/30th of the nodes proved to have little effect on the modular structure, preserving a large percentage of each module's pre-injury structure and causing no segmentations for any of the modules. However when 1/10th and 1/20th of the nodes were weakened, this again resulted in a segmentation of the first module as shown in Figure B.1.
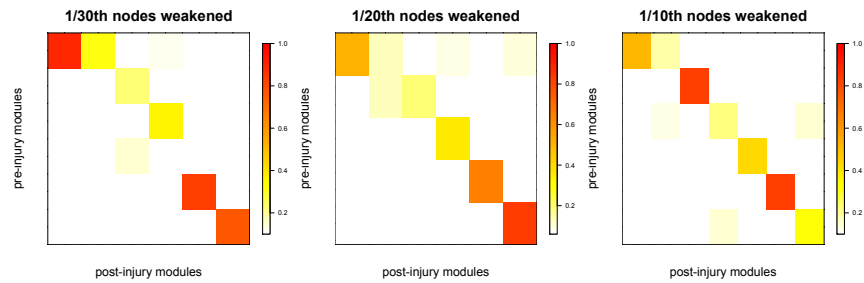
Figure B.1: Percentage identity colour plots. On the y axis we have the pre-injury modules from 1 to 6 top to bottom and on the x axis the post-injury modules. Darker colour indicates a higher percentage identity between the two modules. From left to right, the panels show colour plots for 1/30th of the nodes randomly weakened, 1/20th of the nodes randomly weakened, 1/10th of the nodes randomly weakened.

After performing the clustering analysis for both the pre-injury network, and the injured network, it was found that the largest module of the pre-injury network divided into two modules after weakening random nodes.

For example, after weakening 1/10th of the nodes, the first post-injury module retains 52% identity with the pre-injury structure and the second post-injury module retains 19% identity with the pre-injury structure. The sub-division of the pre-injury module can be visualized in Figure B.2.
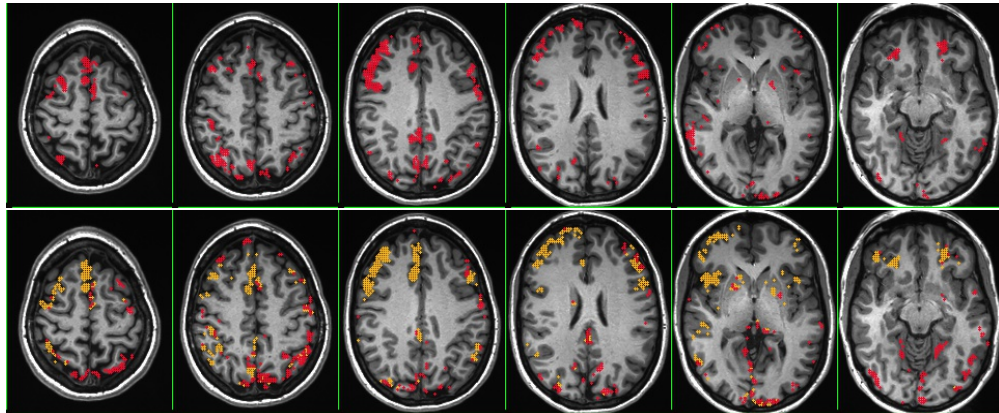
Figure B.2: Modular subdivision after random node weakening. The top panels show the largest pre-injury cluster for six different slices. The bottom panels show the same slices for the two modules recovered after the injury, in colours red and yellow.

Figure B.3b shows that the first post-injury module includes most of the pre-frontal cortical areas, mainly the right hemisphere. The left hemisphere areas start having more presence in the second post-injury cluster, as we can see in the left medial frontal gyrus (LMeFG), and the left superior frontal gyrus which is mainly contained in the second post-injury module. As we can see from Figure B.3d, random weakening of nodes had a similar effect on the prefrontal network, causing a division between the right and left hemisphere. The first post-injury module includes mainly the areas of the right hemisphere, such as the right precuneus (RP), right precentral gyrus (RPG) and the right cingulate gyrus (RCG); whereas the left precuneus (LP) and left precentral gyrus (LPG) are mainly included in the second post-injury module;.The effect of this injury seems to be that of dividing the left hemisphere from the right one in functionally separated modules.
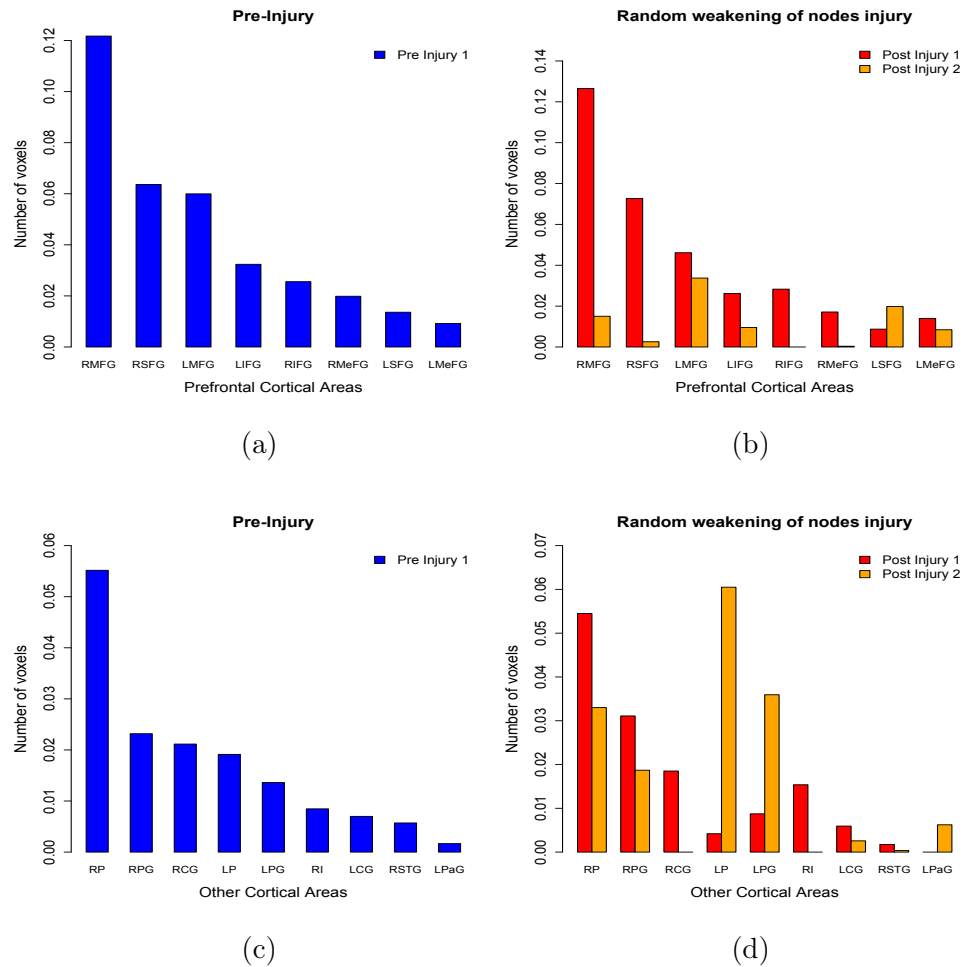
Figure B.3: Number of voxels per brain area. The left column panel shows the number of voxels per brain area divided by the total number of voxels in the largest pre-injury module (blue bars); whereas the panels in the second column show the number of voxels divided by the total for each of the main largest percentage identity post-injury modules for random node weakening.

For random weakening of the nodes, the overall network connectivity decreased by approximately 20% when 1/10th of the nodes where weakened, 10% for 1/20th and 5% for 1/30th, when compared to the pre-injury network. The intramodular and extramodular connectivities were also calculated and remained very similar to those of the pre-injury module for 1/20th and 1/30th of the nodes, whereas for 1/10th the intra-modular connectives of the segmented post-injury modules showed an increase.

B.2   Targeted attacks

Finally, we analyzed the particular case of targeted attacks. For this injury we chose as focal points voxels that were members of a specific module, and proceeded as before. As expected this type of injury caused the weakening, and in some cases, the division of the targeted module. For example when we specifically target the inferior frontal gyrus focal point with coordinates (-51,-39,6), we note significant damage in the modules that contain this area. Figure B.4 shows how the modules that included the targeted area (the first three pre-injury modules) show less percentage identity between the post-injury and pre-injury module, again we have a division of the module with the highest percentage of the targeted brain area, and the rest of the modules that did not include the targeted area remained almost intact. As mentioned above, this behaviour happens for all targeted attacks the authors tried, and the results were consistent, resulting in damage to the modules that contained the targeted area.
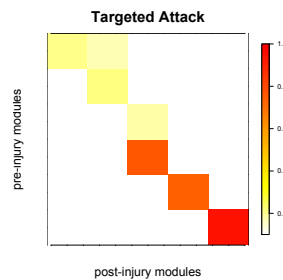

Figure B.4: Percentage identity colour plots for targeted attack. On the y axis we have the pre-injury modules from 1 to 6 top to bottom and on the x axis the post-injury modules. Darker colour indicates a higher percentage identity between the two modules.

Appendix C
Geographical partition for domestic
flight-based network results

A fourth network was considered in the analysis of air transportation networks in Chapter 5. The domestic flight-based network was also analyzed with a geographical partition, in which modules were pre-assigned by state.

Table C.1 shows the results. The airport with the highest degree, participation and gateway coefficients was found to be Birmingham airport in Alabama; whereas the airport with the highest betweenness centrality was Anchorage International in Alaska.

Figure C.1 shows a plot of the flights from the airport with the highest gateway coefficient; flights arriving to each module are assigned with different colours.

Figure C.2 shows a scatter plot of the participation and gateway coefficients. Once again, the airport with the highest betweenness centrality, Anchorage International, was the clear outlier; it showed the largest discrepancy between gateway and participation coefficient values.

	Domestic flight-weighted network
	geographical partition
Highest degree	Birmingham, AL
Highest betweenness	Ted Stevens Anchorage International, AK
Highest gateway	Birmingham, AL
Highest participation	Birmingham, AL

Table C.1: Highest degree and betweenness, gateway and participation coefficient airports for the domestic flight-based network, geographical partition.
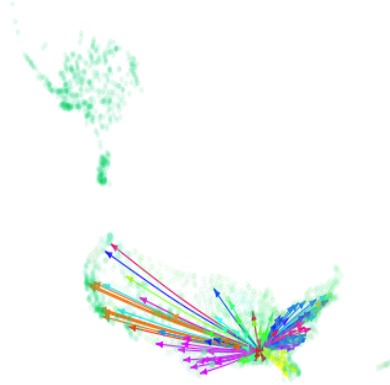
Figure C.1: Flights from the airport with the highest gateway coefficient. The lines represent flights, and different colours represent different modules.
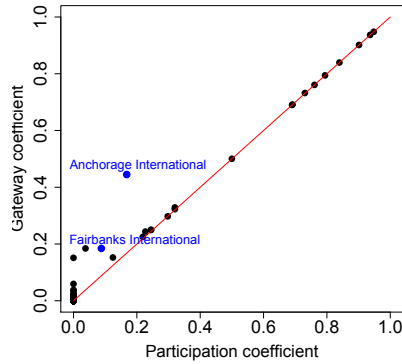

Figure C.2: Scatter plot of the participation (x-axis) and gateway (y-axis) coefficients for the domestic flight-based network.

Curriculum Vitae

Name:	Estefania Ruiz Vargas
Post-secondary Education and Degrees:	2009-2013 Ph.D. Applied Mathematics Western University London, Ontario, Canada 2006-2008 M.Sc. Physics Universidad Michoacana de San Nicolas de Hidalgo Morelia, Mexico 2002-2006 B.Sc. Physics and Mathematics Universidad Michoacana de San Nicolas de Hidalgo Morelia, Mexico
Honours and Awards	2009-2013 CONACyT Scholarship. Awarded by Consejo Nacional de Ciencia y Tecnologia to pursue a PhD at Western University 2006-2008 Graduation with Honours. Universidad Michoacana de San Nicolas de Hidalgo Morelia, Mexico 2006-2008 CONACyT Scholarship. Awarded by Consejo Nacional de Ciencia y Tecnologia to pursue a M.Sc 2002-2006 Graduation with Honours. Universidad Michoacana de San Nicolas de Hidalgo Morelia, Mexico

2002-2006 B.Sc.
Physics and Mathematics
Universidad Michoacana de San Nicolas de Hidalgo
Morelia, Mexico

Related Work   2009-2013. Teaching Assistant
Experience   Western University

Publications:

[J1] **E. Ruiz-Vargas**, S. G. Greening, D. G. V. MItchell, and L. M. Wahl, *Topology of whole-brain fMRI networks: improving the truncated scale-free model.* To be submitted.

[J2] **E. Ruiz-Vargas**, and L. M. Wahl, *The gateway coefficient: a novel metric for identifying critical inter- and intra-modular connections in modular networks.* To be submitted.

[J3] **E. Ruiz-Vargas**, and L. M. Wahl, *Network analysis of human fMRI data suggests modular restructuring after acquired brain injury.* To be submitted.